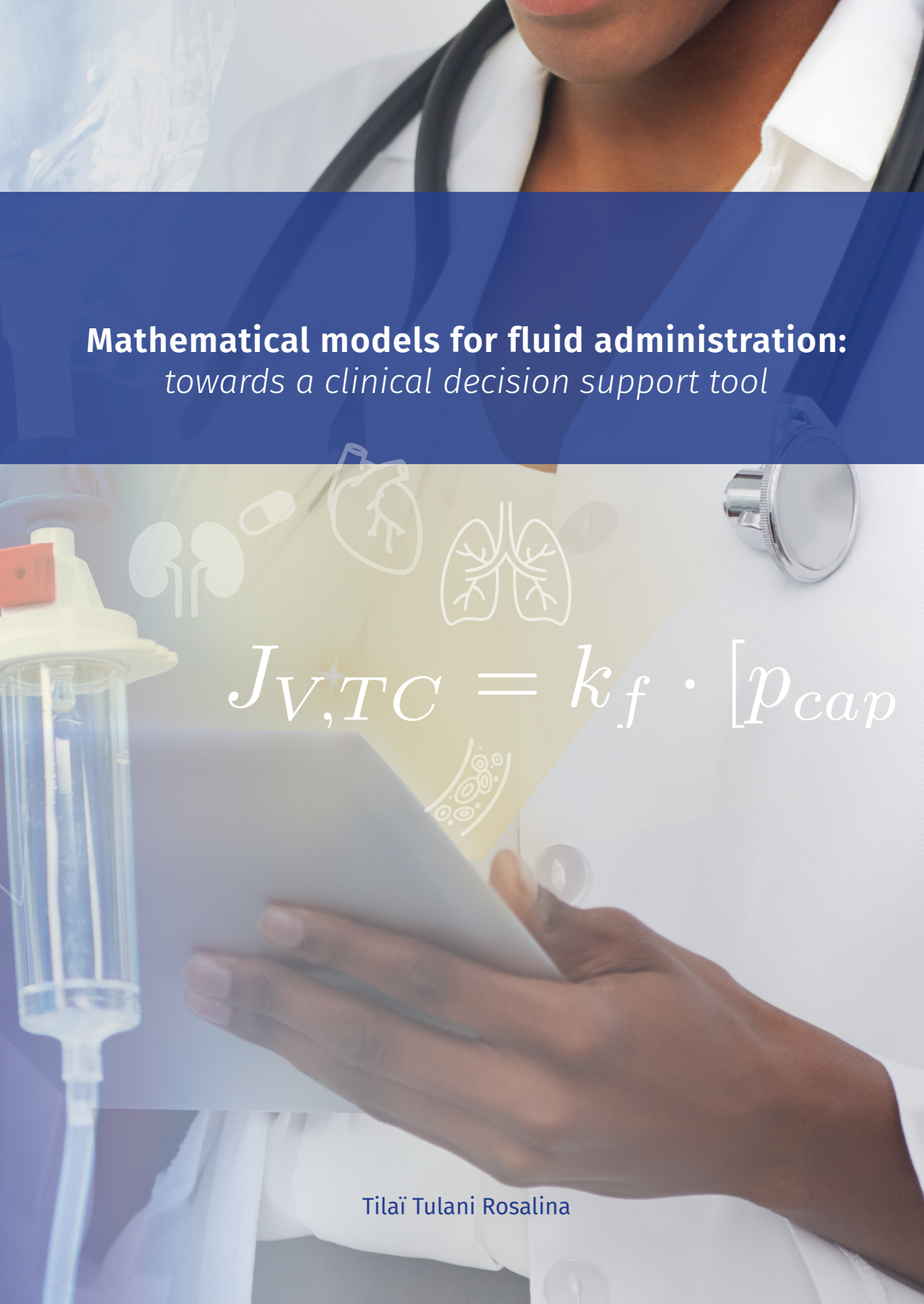


Mathematical models for fluid administration: *towards a clinical decision support tool*

Tilaï Tulani Rosalina

Mathematical models for fluid administration: towards a clinical decision support tool

Tilaï Tulani Rosalina

A catalogue record is available in the library of the Eindhoven University of Technology

ISBN 978-90-386-5003-6

Copyright © 2020, Tilaï Tulani Rosalina.
All Rights Reserved.

Cover design: Monique Rosalina, www.passaatdesign.com
Printed: Proefschrift Maken, www.proefschriftmaken.nl

The work in this thesis has been performed within the IMPULS II framework, in collaboration with Catharina Ziekenhuis Eindhoven & Philips Research.

Mathematical models for fluid administration: towards a clinical decision support tool

PROEFSCHRIFT

ter verkrijging van de graad van doctor aan de Technische Universiteit Eindhoven, op gezag van de rector magnificus prof.dr.ir. F.P.T. Baaijens, voor een commissie aangewezen door het College voor Promoties, in het openbaar te verdedigen op woensdag 18 Maart 2020 om 13:30 uur

door

Tilaï Tulani Rosalina
geboren te Utrecht.

Dit proefschrift is goedgekeurd door de promotoren en de samenstelling van de promotiecommissie is als volgt:

Voorzitter:	prof. dr. M. Merkx
Promotor:	prof. dr. ir. F.N. van de Vosse
Co-promotoren:	dr.ir. P.H.M. Bovendeerd
	dr. R.A. Bouwman
Leden:	prof. dr. C. Boer (Amsterdam UMC)
	dr. I. Vignon-Clémentel (INRIA)
	prof. dr. ir. J.W.M. Bergmans
	prof. dr. M.R.H.M. van Sambeek MD
	prof. dr. ir. N.A.W. van Riel
Adviseur:	dr. J.W.E.M. Sels (Maastricht UMC)

Het onderzoek dat in dit proefschrift wordt beschreven is uitgevoerd in overeenstemming met de TU/e Gedragscode Wetenschapsbeoefening.

This work is dedicated to my grandfather:
Otto '*Poetoe*' van de Kuilen Sr.,
florist by trade, *scientist* by nature.

Mathematical models for fluid administration: towards a clinical decision support tool - Summary -

Intravenous fluid administration is a common perioperative intervention, used to compensate for fluid loss through bleeding, evaporation and urine production. The challenge is to avoid complications related to hypovolemia, resulting in hypoxemia, and hypervolemia, causing edema, which possibly compromises organ perfusion. These complications are associated with slower patient recovery and 5% higher mortality rate.

Optimal intravenous fluid administration remains difficult due to high patient variability and a lack of sensitive patient-specific measurements of fluid status. Mathematical models may be used to gain more insight into the complex underlying physiology and eventually aid in determining patient-specific fluid administration protocols. Previously published fluid exchange models have not been introduced in the clinical work flow since they lack the opportunity to connect to clinically used indices of fluid status, such as pulse pressure variation (*ppv*) and stroke volume variation (*svv*). The aim of this thesis was to make a step towards a clinical decision support tool for fluid administration, by enhancing an existing model of fluid exchange with cardiovascular regulation, mechanical ventilation and drug administration, and formulating model output in terms of clinically measured signals.

First, we extended an existing fluid exchange model with a regulated model of cycle-averaged cardiovascular function. This combination allowed us to relate model outputs on fluid distribution in the body to standard clinical parameters, such as heart rate and arterial blood pressure. Model parameter settings were tuned to an experimental dataset, obtained in healthy volunteers subjected to intravenous infusion. The resulting model was found to correctly predict the experimentally observed response to intravenous infusion and bleeding in an independent volunteer study.

Clinically, the effect of fluid administration on hemodynamics (fluid responsiveness) can be tested by redistribution of blood through mechanical ventilation, quantified by *ppv* and *svv*. To predict these dynamic indices, we converted the model of cardiovascular hemodynamics from a cycle-averaged one into a dynamic one, and extended it with models of the pulmonary circulation and lung mechanics, to simulate the effect of spontaneous breathing and mechanical ventilation on hemodynamic function. Our results show that we can obtain realistic changes in *ppv*, *svv*, and change in cardiac index for mechanically ventilated, anesthetized patients after a fluid challenge. A preliminary sensitivity investigation showed that *ppv* and *svv* depend on intravascular volume, pericardial and

vascular properties, in decreasing order. In the future, the developed mathematical model may be used for interpretation of *ppv* and *svv* on the basis of underlying patient characteristics, potentially leading to a broader use of these indices in the clinical environment.

Moving towards a clinical application, we obtained a retrospective surgical dataset in collaboration with Catharina Hospital Eindhoven. To realistically simulate the clinical patient data, we extended our model with the effect of pharmacokinetic and -dynamic models for propofol, sevoflurane, phenylephrine, ephedrine and noradrenaline. In a pilot study, we compared model predictions on blood pressure and heart rate with retrospective measured data for three surgical patients. We concluded that, to model exact intraoperative blood pressure, all anesthetics, inotropes and vasopressors must be included in the model. However, to predict an average blood pressure during surgery and fluid distribution at the end of surgery, vasopressors and inotropes can be omitted.

Finally, since most fluid related complications occur on a time scale of multiple days, we tested our fluid exchange model in an ICU setting in a prospective study with Maastricht UMC+. We tested the predictive capabilities of the model for interstitial volume, and investigated the effects of the urine production and membrane permeability on the interstitial volume model predictions. Our results show that we can simulate the trends of fluid buildup after fluid administration with our current model. Additionally, we confirmed that the interstitial volume works as a buffer, taking up most of the excess administered fluid and thus allowing vascular volume to remain fairly constant. Interestingly, on the long term, this increase could be determined directly, as the net balance of fluid administration, bleeding, urine production and perspiration, while assuming a constant vascular volume.

In conclusion, we developed and evaluated a mathematical model predicting fluid responsiveness and redistribution in critically ill patients. This may serve as a strong basis for a clinical decision support model to guide intravenous fluid administration and thereby reduce hypervolemia-related complications.

Wiskundige modellen voor infuustoediening: richting klinische beslissingsondersteuning - Samenvatting -

Als patiënten een operatie ondergaan treedt er vochtverlies op door bloeding, verdamping en urineproductie. Om ondervulling te voorkomen word er door middel van een infuus vocht toegediend. Aan de ene kant kan ondervulling van het vaatstelsel leiden tot schadelijke gevolgen zoals zuurstoftekort. Aan de andere kant kan overvulling van het vaatstelsel leiden tot vochtopbouw in de weefsels. Als gevolg worden de vaten dichtgedrukt, wat de zuurstoftoevoer verminderd en dit kan uiteindelijk leiden tot een langzamer patiëntherstel en 5% hogere mortaliteit.

Het is moeilijk om de balans te vinden tussen onder- en overvulling omdat er een grote variabiliteit tussen patiënten is en er geen goede directe metingen voor de vochtbalans zijn. Het doel van dit onderzoek was het ontwikkelen van een wiskundig model, waarmee uiteindelijk de besluitvorming in de klinische praktijk ondersteund kan worden. Het model is gebaseerd op kennis van de fysica en fysiologie en geeft daarmee inzicht in de complexe onderliggende oorzaken van de problemen. Door het model te combineren met patiëntspecifieke metingen, kunnen er in de toekomst voorspellingen worden gemaakt over de vochtbalans van de patiënt. Uiteindelijk zal dit de arts extra informatie kunnen leveren, waardoor sommige complicaties kunnen worden voorkomen.

Als eerste stap om dit model te ontwikkelen hebben we een bestaand vloeistof uitwisselingsmodel uitgebreid met een simpel model voor de hartfunctie. Dit geeft de mogelijkheid om de model uitkomsten in termen van klinisch meetbare waarden, zoals gemiddelde bloeddruk en hartslag, te beschrijven. We hebben de modelwaarden bepaald op basis van een experimentele studie tijdens infuustoediening in gezonde vrijwilligers. Met deze waarden kon de gemeten reactie op bloeding en infuustoediening in een onafhankelijke vrijwilligersstudie goed worden voorspeld.

In de kliniek wordt het effect van infuusvocht op de bloedcirculatie vaak beoordeeld op basis van de variatie van de polsdruk en het slagvolume tijdens mechanische beademing, de zogenaamde pulse pressure variation (*ppv*) en stroke volume variation (*svv*). Om deze indices te kunnen berekenen, hebben we ons model uitgebreid met deelmodellen voor het kloppende hart, de longcirculatie en de longmechanica. Zodoende kunnen we het effect van spontane ademhaling en mechanische beademing op de bloedsomloop simuleren. Met dit model konden we de *ppv*, *svv* en verandering in hartminuutvolume bij beademde patiënten na een infuus toediening goed voorspellen.

Om de stap naar de klinische toepassing te maken hebben we in samenwerking met het Catharina Ziekenhuis Eindhoven retrospectief data verzameld, gemeten bij patënten tijdens de operatie. Om realistische operatie kamer data te kunnen simuleren hebben we het effect van medicijnen toegevoegd. De operatie van drie patiënten is gesimuleerd en daarna zijn de modelvoorspellingen ten aanzien van bloeddruk en hartslag vergeleken met de gemeten waarden. Uit deze studie kunnen we concluderen dat om het precieze verloop van bloeddruk te kunnen voorspellen, alle medicijnen moeten worden meegenomen in het model. Echter, om alleen een gemiddelde bloeddruk te voorspellen tijdens en aan het eind van de operatie zijn anesthesiemedicijnen voldoende. Dit maakt het model minder complex en vergt minder rekentijd.

Aangezien de meeste vloeistof-gerelateerde complicaties optreden na meerdere dagen is het model ook van belang op de intensive care. Daarom hebben we in samenwerking met Maastricht UMC+ een studie opgezet waarbij patiënten na een open-hart-operatie werden gevolgd. De toegediende hoeveelheid vloeistof en medicijnen, bloeddruk, hartslag en urine productie werden vastgelegd en gebruikt voor simulaties. Uit de resultaten blijkt dat met het huidige model de trend van vloeistof opbouw na infuus toediening kan worden voorspeld. Met onze bevindingen hebben we ook kunnen bevestigen dat het interstitium als opslagplaats werkt. Het grootste gedeelte van het overschot aan volume wordt hier opgeslagen, waardoor het bloedvolume vrijwel constant blijft. Op de lange termijn kan deze opslag zelfs worden afgeschat als de balans van infuustoe-diening, bloeding, urine productie en verdamping, met een constant aangenomen bloedvolume.

Samenvattend hebben we een wiskundig model ontwikkeld en getest wat het effect van vloeistof op de bloedsomloop en de vloeistofsverdeling in het lichaam kan voorspellen. Dit model kan de basis worden voor een klinisch model om beslissingen over infuustoediening te ondersteunen en uiteindelijk complicaties gerelateerd aan overvulling te verminderen.

Contents

Summary vi

Samenvatting viii

1 Background & aim of the thesis 1
- 1.1 General introduction . . . 2
- 1.2 Fluids are drugs . . . 3
- 1.3 Determining fluid responsiveness . . . 6
- 1.4 Determining fluid distribution . . . 8
- 1.5 Models for fluid administration . . . 8
- 1.6 Aim and thesis outline . . . 10

2 A mathematical model for intravenous fluid administration and fluid loss in healthy volunteers 19
- 2.1 Introduction . . . 21
- 2.2 Methods . . . 22
  - 2.2.1 Fluid exchange . . . 22
  - 2.2.2 Cardiovascular circulation . . . 25
  - 2.2.3 Cardiovascular regulation . . . 26
  - 2.2.4 Parameter estimation . . . 27
  - 2.2.5 Simulations performed . . . 28
- 2.3 Results . . . 30
  - 2.3.1 Simulation of the Watenpaugh experiment . . . 30
  - 2.3.2 Simulation of the Drobin experiment . . . 30
  - 2.3.3 Comparison to the 'Xie-like' model . . . 31
- 2.4 Discussion . . . 32
  - 2.4.1 Model setup . . . 33
  - 2.4.2 Results . . . 33
  - 2.4.3 Future work . . . 34
- 2.5 Conclusion . . . 34

3 A mathematical cardiorespiratory model to predict dynamic indices of fluid responsiveness **39**
3.1 Introduction . . . 41
3.2 Methods . . . 44
3.2.1 Cardiovascular model . . . 44
3.2.2 Lung mechanics model . . . 46
3.2.3 Parameter estimation . . . 48
3.2.4 Simulations performed . . . 51
3.3 Results . . . 53
3.3.1 Mechanical ventilation vs. spontaneous breathing in a healthy volunteer . . . 53
3.3.2 Mechanical ventilation in a patient . . . 53
3.3.3 Fluid challenges in a ventilated patient . . . 56
3.3.4 Sensitivity analysis . . . 56
3.4 Discussion . . . 57
3.4.1 Model setup . . . 58
3.4.2 Comparable models in literature . . . 59
3.4.3 Results . . . 59
3.4.4 Future work . . . 61
3.5 Conclusion . . . 61

4 Investigating the influence of drugs on the fluid distribution in surgical patients through a mathematical model **69**
4.1 Introduction . . . 71
4.2 Methods . . . 72
4.2.1 Cardiovascular fluid exchange model . . . 74
4.2.2 Pharmacokinetics . . . 75
4.2.3 Administration pathways . . . 75
4.2.4 Pharmacodynamics . . . 76
4.2.5 Parameter estimation . . . 77
4.2.6 Clinical data . . . 80
4.2.7 Simulations performed . . . 81
4.3 Results . . . 82
4.3.1 Patient A . . . 82
4.3.2 Patient B . . . 84
4.3.3 Patient C . . . 86
4.4 Discussion . . . 88
4.4.1 Model setup . . . 88
4.4.2 Data limitations . . . 89
4.4.3 Model results . . . 90
4.4.4 Model limitations . . . 92
4.4.5 Future work . . . 92
4.5 Conclusion . . . 93
4.6 Acknowledgements . . . 93

5 Implementing the fluid exchange model in the intensive care: a pilot study **99**
5.1 Introduction . . . 101
5.2 Methods . . . 102
5.2.1 Generic model . . . 102
5.2.2 Clinical data . . . 103
5.2.3 Parameter estimation . . . 103
5.2.4 Simulations performed . . . 105
5.3 Results . . . 105
5.3.1 Generic model simulations . . . 105
5.3.2 Model variations . . . 109
5.4 Discussion . . . 110
5.4.1 General considerations . . . 110
5.4.2 Results . . . 112
5.4.3 Future work . . . 113
5.5 Conclusion . . . 114

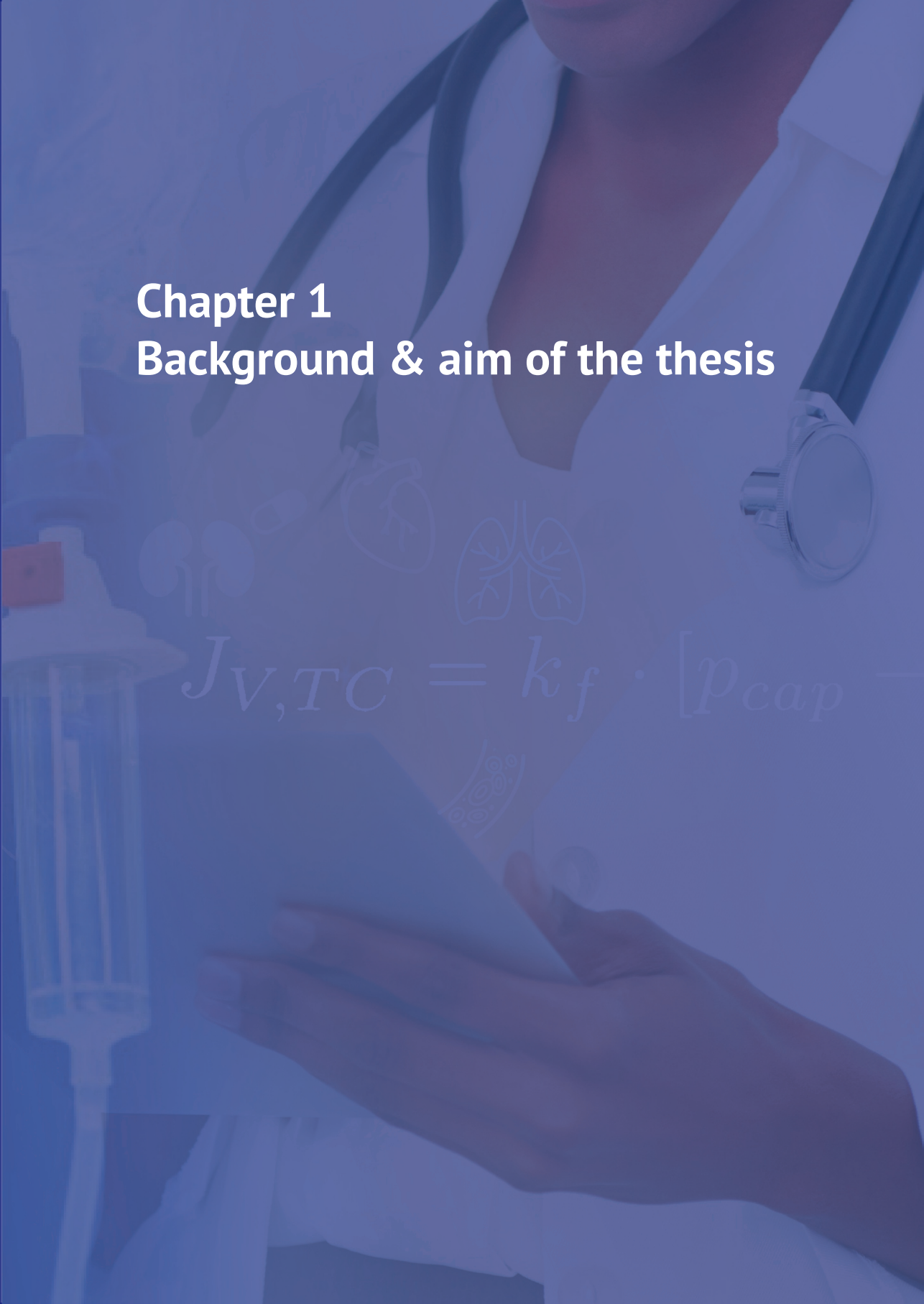
6 General discussion **123**
6.1 Finding the balance . . . 124
6.2 Main achievements . . . 124
6.3 Mathematical modeling perspectives . . . 126
6.4 Clinical perspectives . . . 128
6.4.1 Research tool . . . 128
6.4.2 Training tool . . . 129
6.4.3 Clinical-decision support tool . . . 129
6.5 Conclusion . . . 131

7 Epilogue **135**

Dankwoord **139**

Curriculum Vitae **143**

List of Publications **145**



Chapter 1
Background & aim of the thesis

1.1 General introduction

Each year more than 200 million liters of intravenous fluids (iv-fluids) are used in medical interventions in the United States alone (Chowdhury et al., 2012). These iv-fluids are administered to compensate fluid loss through bleeding, urine production and evaporation. The goal of administering these fluids is to maintain tissue perfusion, and thereby oxygen delivery in case of fluid losses (e.g., bleeding in case of trauma, surgery or other medical interventions). On the one hand, since a long time it is known that this approach reduces complications related to hypovolemia (Latta, 1832). A reduced circulating blood volume leads to a reduced venous return, and eventually hypotension. This triggers a hormonal response, promoting peripheral vasoconstriction, increasing cardiac contractility and inducing tachycardia. At a certain level these compensatory mechanisms, to maintain cardiac output and thereby tissue perfusion and oxygen delivery, will fail and the metabolic demands of various organ cannot be met. Eventually this leads to hypoxia with organ failure as result (Guyton et al., 2006).

On the other hand, more recently, it has been shown that high fluid buildup, due to excessive fluid administration, also causes negative effects on patient recovery (Holte et al., 2002; Prowle et al., 2010; Murphy et al., 2009; Schrier, 2010; Vincent et al., 2006). One of these negative effects is systemic edema buildup, leading to impaired tissue perfusion due to microvascular compression. This compression may cause increased peripheral resistance, inhibiting blood flow and oxygen delivery and eventually leads to disturbed wound healing and, in extreme cases, organ failure. Another negative effect may be lung edema, fluid buildup in the alveolar space, which leads to difficulty of breathing and impairment of oxygen uptake. These two extremes show that it is important to find a fluid administration protocol that avoids hypo-, and hypervolemia (Figure 1.1).

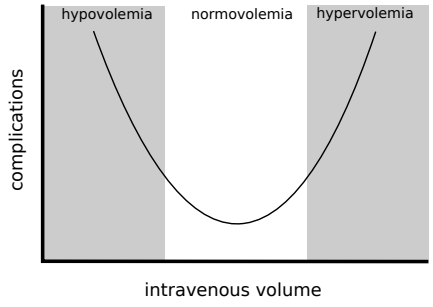


Figure 1.1: Schematic illustration of the relationship between intravenous volume and complication rate in hypo-, normo- and hypervolemia (Adapted from Roche et al. 2009).

The determination of the optimal amount of fluid to be administered is complicated, because it depends on the fluid balance which cannot be measured, and the associated complications occur in the long run. Fluid administration immediately increases intravascular volume, and improves hemodynamics. Unfortunately, these effects are temporary, leading to fluid build up on the long run and edema formation in the interstitial space. These difficulties result in wide variation of fluid administration protocols between practitioners. The global observational FENICE study by Cecconi et al. (2015) presents an overview of all different fluid administration guidelines, and how they are interpreted. The authors show that there is a lack of consensus on fluid administration protocols. Recently, an expert opinion panel from European Society of Intensive Care Medicine (Cecconi et al., 2019), noted that this could be explained since there are *'relevant gaps in the scientific evidence on fluid administration outside the ICU ...'* and the authors *'...recommend only basic interventions, based more on physiological rationales than high-quality randomized control trials'*. Hence, the expert panel recommends *only* continuing fluid administration by observation of a positive response in specific variables. In this thesis we aim to develop a mathematical model that can be used to investigate fluid administration protocols and eventually provide clinical decision support based on physics and physiology. Eventually this may lead to better prediction of patient response to fluid challenges, before administering any fluid.

1.2 Fluids are drugs

Fluid administration should be considered as carefully as any other drug administration procedure. When administering a drug, one must consider the type, quantity, and timing of administration (Gattas et al., 2013; Lira et al., 2014). There are broadly three types of intravenous fluids, namely blood products, crystalloids and colloids (Figure 1.2). Autologous blood products are the most intuitive replacement after hemorrhage. To make this possible during surgery, the cell saver method has been developed (Brzica et al., 1979; CellSaver^{TM}). This is a technique that 'recycles' the lost blood from a patient. Approximately 50% of the input is filtered and recycled and is then given back to the patient. Allogeneic blood transfusions can be used when no cell saver blood is available. Unfortunately, there is a scarcity of blood donors and there may be risks due to the immune response associated to administration of blood or blood components, which can be minimized by careful blood type crossmatching. These risks are lowest when administering autologous blood.

As an alternative, synthetic iv-fluids have been developed. Firstly, the mostly used type of fluids are crystalloids, such as 0.9% sodium chloride (saline) solution and Ringer's lactate. These are fluids that contain electrolytes in sterile water, to mimic the mineral content of human plasma. Whereas saline solution contains only sodium chloride, Ringer's Lactate is a more balanced solution,

which contains potassium, calcium and a small amount of lactate. Crystalloids are cheap and widely available. Water and small ions are easily transported over the transcapillary membrane. This translates to the notion that crystalloid solutions rapidly disappear towards the interstitium and only about 30% remains in the intravascular compartment (Hjelmqvist, 2000). This phenomenon is even larger in critically ill patients, especially during sepsis or other inflammatory diseases. These patients may have a high membrane permeability, leading to severe fluid buildup in the interstitial space. As a result, large volumes are often used, leading to risks associated with hypervolemia. Besides water, the administered fluid contains a high amount of salt. Since the renal circulation is mainly responsible of excretion of fluids and salts, there will be an increased renal functional demand. This may lead to acute kidney injury, especially in combination with a hormonal response to surgical injury, anaesthesia induced decrease in glomerular filtration rate, urine volume and ion excretion (Holte et al., 2002).

Secondly there are synthetic colloids such as hydroxyethyl starches (HES) or dextran solutions, which contain an additional component of a colloidal substance (e.g. albumin) that does not diffuse easily across the transcapillary membrane. Thus these colloids stay in the vascular compartment and cause a rapid and prolonged vascular pressure increase. The drawback is that they are less readily filtered in the kidney, thereby increasing the renal osmotic pressure. This can lead to adverse consequences such as acute kidney failure. To this end, these colloid solutions are now no longer recommended for patients with high risk of renal failure, like septic patients. Additionally, there are some concerns around toxicity of human albumin and other starches (Davidson, 2006; Schortgen et al., 2008). The functional outcome and usage of colloids is an espiacially widely controversial topic. Multiple global, multicenter trials have been set up in the past decade. The CHEST trial (Gattas et al., 2013) was a randomized control trial that investigated the mortality in 7000 patients who receives HES or saline during intensive care stay. The authors found no significant difference in 90-day mortality, however there was an increased rate of renal replacement therapy in the HES group.

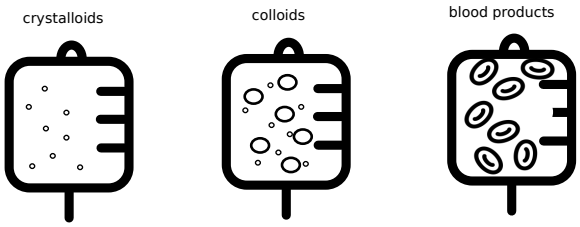


Figure 1.2: Schematic illustration of the three types of intravenous fluids, crystalloids, colloids and blood products, used in clinical practice.

Not only the type of fluid, but also determining the quantity and timing is a highly debated topic. The determination of the optimal amount of fluid to be administered is complicated, because it depends on the balance between intravascular and extravascular volume, which cannot be measured. Fluid administration is even more complex, because complications associated to edema occur at a time scale of hours and days. This makes it difficult to predict and assess the effect of a fluid bolus. It can take days to lose the increased volume, often quantified as an increased total body weight. This results in wide variation of fluid administration protocols between practitioners. This variation was quantified by e.g., Lilot et al. (2015) in a multicenter observational study. Here, it was shown that a patient weighing 75 kg undergoing a 4 hour procedure with 700 ml of fluid loss (400 ml blood loss and 300 ml urine production), will receive between 700 and 5400 ml of crystalloids, depending on the anesthesiologist. This variation clearly shows that there is no consensus on fluid administration protocols. The analysis showed that intra-operative hemodynamic and patient variables had less effect on the fluid administration protocol than the effect of personnel.

The reason for this variation is that fluid administration protocol are hard to standardize and objective measures to assess volume status (e.g., intravascular volume) at the bedside are currently lacking. This is important, since it is not enough to know the amount of fluid loss to predict the amount of fluid a patient should get. A reason for this is that the patient-specific necessity for fluid is not only determined by the in- and output of fluid, but also by patient characteristics. As mentioned, the effect of crystalloids is only temporary, as they move from intravascular to interstitial spaces inside the body. This fluid shift varies among patients. Contributing factors to these fluid shifts are anaesthesia and analgesia, which alter hemodynamic parameters (such as hydrostatic and osmotic pressure), stress factors and inflammation (leading to increased membrane permeability) (Holte et al., 2002; Brandstrup, 2006). This is especially evident for patients in septic shock. Here, the transcapillary fluid exchange is highly disturbed, possibly leading to high fluid buildup in the interstitial space.

Many clinical trials and meta-analyses have been set up, searching for the optimal fluid administration protocol. Typically, there are three types of fluid administration protocols, namely restrictive, liberal and goal-directed fluid administration protocols. However, there is no universal definition of each protocol, making comparison of different studies is difficult. In goal-directed studies, target values are defined for one or more hemodynamic variables. Fluid optimization is performed during the surgery so these targets are maintained during the procedure. Goal-directed therapy has the potential of accomplishing more consensus in fluid administration, if it is known which goals should be targeted and at which rate.

Over all, literature seems to indicate that less fluid brings better outcome. Still, some studies report contradicting findings. This can be explained because the boundaries of patient-specific optimal fluid volumes remain unclear, and, more importantly, a very frail patient group is often studied. There may be many factors contributing to their clinical outcome. Malbrain et al. (2014) show, through a meta-analysis and systematic review of literature data, that fluid overload is harmful and is associated with increased morbidity and mortality. Similarly, Brandstrup et al. (2003) showed that restricted fluid administration significantly reduced post-operative complications such as tissue healing complications and cardiopulmonary complications, compared to liberal protocols. There was even a 5 % lower mortality rate. On the other hand, the recent multicenter RELIEF trial (Myles et al., 2018) did not find better clinical outcome for patients receiving restrictive versus liberal fluid therapy. There was even a higher occurence of acute kidney injury found in the restrictive group.

1.3 Determining fluid responsiveness

There is a large inter-patient variability in the response to fluid administration, which makes evidence-based predictions difficult. Therefore, several strategies have been developed to determine if a patient is fluid responsive, i.e., if they will benefit from fluid administration, quantified by an increase in cardiac output (Pinsky et al., 2005; Cecconi et al., 2011). This section shows the current practice on determining fluid responsiveness through hemodynamic monitoring.

Physiologically, the relation between vascular fluid status and cardiac pump function relies on the Frank-Starling mechanism (Starling, 1918), relating stroke volume to preload (Figure 1.3). Patients on the steep part of this curve will exhibit an increase in cardiac output as a result of increased cardiac filling. For patients on the flat part of the Frank-Starling curve a change in preload does not significantly increase stroke volume (Weiss et al., 1979; Vincent et al., 2006; Cecconi et al., 2011), so they are not fluid responsive.

Administering fluid is the most intuitive way to determine fluid responsiveness (Vincent et al., 2006). Traditionally, a fluid bolus of 500 ml saline is administered rapidly, and hemodynamic outcomes such as arterial pressure, central venous pressure and cardiac output are monitored. If cardiac output increases, the patient is determined to be fluid responsive. Unfortunately, this method has major disadvantages. Firstly, determining the effectiveness requires a direct cardiac output measurement. Some cardiac output measurements are invasive and difficult and less invasive measurements are not always available, so often arterial blood pressure is taken as a surrogate measurement. Unfortunately, studies have shown that arterial (pulse) pressure alone is not sufficiently correlated to changes in cardiac output (Monnet et al., 2011; Pierrakos et al., 2012).

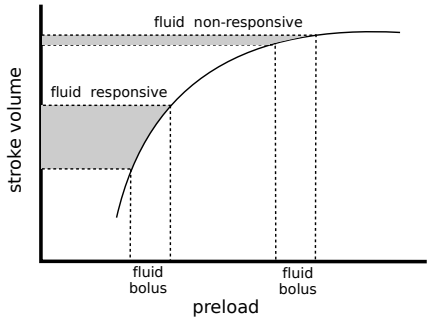


Figure 1.3: Schematic graph representing the Frank-Starling curve, relating preload (volume) to a change in stroke volume. A fluid responsive patient wil exhibit an increase in stroke volume after a fluid bolus, whereas fluid non-responsive patient show a very small increase in stroke volume (adapted from Michard et al. 2000).

Secondly, these fluid challenges carry the risk of volume overloading. Each fluid challenge that does not result in an increase of cardiac output, contributes to the hypervolemic state of the patient. Mini fluid challenges (100 ml of colloids), have been proposed as a solution, however very precise cardiac output monitoring is required here.

The insight that administering fluid boluses increases the risk of fluid overload has stimulated the use of scenarios in which cardiac filling is increased, without actually increasing the total amount of vascular volume (Michard et al., 2000). These scenarios rely on the redistribution of the available amount of volume, from the peripheral circulation to the heart. One option is a passive leg raise test. Raising the patient's legs creates a reversible preload challenge of around 300 ml of blood that can influence cardiac output (Jabot et al., 2009). Still, this method requires direct measurement of cardiac output (Monnet et al., 2016). Alternative static measurements, characterising cardiac output such as central venous pressure and global end diastolic volume, have been shown not to be indicative of volume status.

Another option is to make use of fluid redistribution in response to variations in intrathoracic pressure, as induced during mechanical ventilation. Here, cardiac filling increases with decreasing intrathoracic positive pressure and vice versa. The variation in filling is reflected in a variation of stroke volume and aortic pulse pressure, that can be assessed clinically. These changes are quantified with dynamic indices, e.g., the pulse pressure variation (*ppv*), systolic pressure variation (*spv*) and stroke volume variation (*svv*). Here, low values ($\leq$ 9 %) indicate fluid non-responsiveness, and high values ($\geq$ 13%) indicate fluid responsiveness, with the recommendation of intravascular filling (Daudel et al., 2010; Cecconi et al., 2015). These dynamic indices are highly promising measures to determine patient fluid responsiveness, with high sensitivity and specificity ($\geq$ 82 %). However, these indices are coupled to specific clinical constraints, such as a tidal volume 8 ml/kg, no open thorax, and no arrhythmia. Consequently, only 20% of intensive

care patients qualify for reliable pulse pressure variation analysis (Michard et al., 2000; Marik et al., 2009; Cannesson et al., 2011).

1.4 Determining fluid distribution

There is a more fundamental problem with these fluid challenges, namely, they only address the vascular fluid status. Thus the major risk factor, the shift of fluid from the intravascular to the interstitial space potentially causing edema, is not addressed.

There are some methodologies to measure or indicate volume overload. Bioimpedance spectroscopy (BIS) is a major emerging technique for direct determination of extracellular fluid volume and total body fluid volume. This method is based on a combination of electrical properties of materials and analytical models. Since 1990, this technique is also used to study in vivo human body composition. The high impedance of the cell membrane allows for distinguishing between fluid in and outside the tissue cells and can give an indication of fluid volume distribution (Matthie, 2008). For patients on hemodialysis, this technique has been shown to aid in better fluid management (Hu et al., 2012; Haapio et al., 2012; Hung et al., 2014). However, to show the benefits and applicability of using BIS in critical patients, more research is needed (Wabel et al., 2009; Dewitte et al., 2016; Yang et al., 2019).

Another option is to use double dilution indicator techniques. Here, a tracer substance is injected and after a sufficient amount of time the compartmental volume can be calculated. There are no specific tracers determine interstitial fluid, thus this can be deduced from the difference between subsequent measurements for plasma and extracellular fluid. The toxicity of these tracers and invasive technique make application in critical patients difficult. Other techniques that are frequently used for volume distribution in renal disease patients are the evaluation of biomarkers, ultrasonographic findings and body weight (Ekinci et al., 2018). However, none of these techniques are ready to be used for continuous fluid distribution determination.

1.5 Models for fluid administration

As discussed above, there are currently no specific and sensitive clinical direct measurements available to determine fluid responsiveness and distribution. Indirect measurements for fluid responsiveness are available, but there is not consensus on their usability and reliability. Whenever information cannot be measured, models can be used to combine indirect measures in order to obtain relevant information. Models, although not always mathematical, are already widely used in the clinical workflow. By coupling prior knowledge, available measurements,

experience and clinical background clinicians create a *mental* model of their patient every day. Nevertheless, *mathematical* models can be used to gain more insight into complex physiology, based on a full description of complex interactions that are relevant to the question. The output can be used to aid clinicians in their decision making process.

There are some examples of the introduction of such models in the clinical workflow. One example of such a model, which has gotten a FDA certification, is a model used in invasive cardiac catheterisation. This model determines the degree of stenosis in coronary arteries, virtually instead of invasively (Taylor et al., 2013; Douglas et al., 2016). Another example, is the prediction of useful locations for tissue ablation in patients suffering for right atrium fibrillation (Boyle et al., 2019), based on personalized mathematical modeling.

Currently, no model exists that is approved for guiding fluid administration in the clinic. Still, various models have been presented in literature that focus on fluid administration or (re-) distribution. These models can be roughly divided into three categories; models focussed on volume kinetics, vascular fluid responsiveness or fluid distribution. Volume kinetics is a method for calculating distribution and elimination of fluids based on repeated measurements of dilution. The basic model for volume kinetics (Drobin et al., 1999; Drobin et al., 2002; Hahn, 2010; Hahn, 2017; Saito et al., 2013) consists of two fluid compartments, namely the plasma and interstitial volume. There can be exchange between these compartments and elimination of fluid from the system by a clearance rate. This type of models have been used to analyze and simulate fluid distribution and expected volume expansion. This contributed to the quantification of the influence of stress, hypovolemia, anaesthesia and trauma (such as surgery or burns) on the internal distribution and elimination of fluids in patients. The drawback of this type of modeling is that this methodology requires many repeated hematocrit measurements (typically 25-40 over 4 hours). Clinical implementation of this type of model is not feasible with the invasive hematocrit techniques currently present in the clinical workflow.

Models that focus on vascular fluid responsiveness replace invasive fluid challenges such as described in Section 1.3. Messerges (2006), proposed a simple cardiovascular model, attempting to model systolic pressure variation (*spv*) as a measure of fluid responsiveness. However, the authors did not manage to fully simulate the clinical observations, most probably due to the complexity of the physical system, compared to the oversimplification of the model. This work was continued and extended with cardio- respiratory interactions and baroregulation, in the work published by Lansdorp et al. (2013) and Lansdorp et al. (2014). The focus of this study was to incorporate non-linearities of the heart model and the effects of ventilator settings (such as tidal volume) on dynamic variables (*ppv* and *svv*). The effects of ventilation and especially tidal volume variations are shown here. Another study that aims to develop a fluid responsiveness decision support tool is presented by Pironet (2016). They explore the total stressed volume as

an indicator of fluid responsiveness. Pironet presented a simple cardiovascular model suitable for intensive care unit applications. The aim of this study was to use readily available measurements to calculate the total stressed volume. Comparing the model results with conventional fluid responsiveness measurements gave good results. This kind of model can be used to predict dynamic fluid responsiveness indices (e.g., *ppv* and *svv*) as described previously. Smith (2004) and Starfinger (2008), also presented work on the development and testing of a cardiovascular model to simulate *ppv* and *svv* in critical care. Besides the modeling efforts, this group focusses on the development of an integral-based parameter identification method.

These fluid responsiveness models only focus on short-term effects, so they neglect fluid redistribution which occurs on a longer time scale (Section 1.4). Thus, the primary risk of hypervolemia (edema formation) cannot be predicted. Models focussing on long term fluid exchange models have been developed by Xie et al. (1995) and Gyenge et al. (1999) and Gyenge et al. (2003). The models include the transport of fluids and solids (proteins and ions) inside and between body compartments, based on the Starling's equation. According to this equation for transcapillary fluid exchange is driven by hydrostatic and osmotic pressures in the capillaries and interstitial space. Other groups (Chapple et al., 1993; Mazzoni et al., 1988; Carlson et al., 1996; Wolf et al., 1989; Wolf et al., 2011; Wolf, 2013) use a similar approach. Unfortunately, these models have a limited representation of the cardiovascular circulation and lack information on clinical parameters such as arterial pressure and heart rate. Since these parameters often guide fluid administration, it is hard to integrate these models in the clinical workflow.

1.6 Aim and thesis outline

To the best of our knowledge, the coupling of intravascular fluid responsiveness and longterm fluid distribution has not been made yet. This coupling is essential to provide clinical decision support regarding fluid responsiveness and administration protocols. In this thesis, we aim to make this coupling and move towards a clinical decision support model for fluid administration. We aim to develop a model that can eventually assist in prediction of fluid responsiveness and redistribution in critical patients based on clinically available information. The ultimate goal is to use this model to guid fluid administration and eventually, reduce hypervolemia related complications in perioperative care.

This can be achieved by integrating our model into the clinical workflow. Here, the key is to create a preoperative model based on patient measurements, and update this throughout and after surgery. This model can be used to test treatment options and provide extra information. Real-time data processing can be used to compare model output to measurements, and adapt the model parameters to improve future predictions. The same can be done for the postoperative

patient, combining the model with data and risk predictors such as early warning scores. This may allow for earlier detection of patient deterioration based on fluid overload. Finally, the goal is to have less fluid administration-related complications, and quicker patient recovery.

In the first part of this thesis we focus on developing the mathematical model. Firstly, we extend an existing fluid exchange model (Xie et al., 1995) with a regulated model of cardiovascular function (Jongen et al., 2016). This model is tested with healthy volunteer data. Predicted and measured changes in arterial pressure, heart rate and volume distributions, in response to fluid administration are compared **(Chapter 2)**. Next, to be able to predict clinically used dynamic indices for fluid responsiveness (*ppv* and *svv*) we extend our cardiovascular model with a pulmonary circulation and the one-fiber description for left and right ventricles. Also, to simulate the dynamic intrathoracic environment in ventilation, we add a lung mechanics model. This cardiorespiratory model is tested with literature data for spontaneously breathing healthy volunteers and mechanically ventilated aneasthetised patients **(Chapter 3)**.

In the second part we present two clinical pilot studies where we implement and test the model with clinical data. First, to get an indication on the effect of various medications on the fluid distribution in patients under surgery, we extend our model with pharmacokinetics and -dynamics descriptions for commonly used medications (anesthetics, inotropes and vasopressors). This model is tested on a small retrospective surgical dataset in collaboration with Catharina Hospital Eindhoven (**Chapter 4**). Second, we test our fluid exchange model in an intensive care setting. Here, we compare our prediction of measurable long term variables (such as urine production) to clinically observed values in a partly prospective intensive care unit dataset in collaboration with Maastricht University Medical Center. This pilot study provides us with insights in the patient variability and the effects of urine production and membrane permeability **(Chapter 5)**.

The thesis concludes with a general discussion **(Chapter 6)** where the findings are related to each other and put into a broader perspective.

Bibliography

Boyle, P. M. et al. (2019). "Computationally guided personalized targeted ablation of persistent atrial fibrillation". *Nature Biomedical Engineering*, pp. 1–10.

Brandstrup, B. (2006). "Fluid therapy for the surgical patient." *Best Practice & Research. Clinical Anaesthesiology* 20.2, pp. 265–283.

Brandstrup, B. et al. (2003). "Effects of intravenous fluid restriction on postoperative complications: comparison of two perioperative fluid regimens: a randomized assessor-blinded multicenter trial". *Annals of Surgery* 238.5, pp. 641–648.

Brzica, S. M. et al. (1979). "Autologous blood transfusion". *CRC Critical Reviews in Clinical Laboratory Sciences* 10.1, pp. 31–56.

Cannesson, M. et al. (2011). "Assessing the Diagnostic Accuracy of Pulse Pressure A "Gray Zone" Approach". *Anesthesiology* 115.2, pp. 231–241.

Carlson, D. E., Kligman, M. D., and Gann, D. S. (1996). "Impairment of blood volume restitution after large hemorrhage: a mathematical model". *The American Journal of Physiology* 270, R1163–R1177.

Cecconi, M, Singer, B, and Rhodes, A (2011). "The fluid challenge". *Annual Update in Intensive Care and Emergency Medicine 2011* 1, pp. 332–339.

Cecconi, M. et al. (2015). "Fluid challenges in intensive care: the FENICE study". *Intensive Care Medicine* 41.9, pp. 1529–1537.

Cecconi, M. et al. (2019). "Fluid administration for acute circulatory dysfunction using basic monitoring: narrative review and expert panel recommendations from an ESICM task force". *Intensive Care Medicine* 45.1, pp. 21–32.

Chapple, C. et al. (1993). "A model of human microvascular exchange: parameter estimation based on normals and nephrotics". *Computer Methods and Programs in Biomedicine* 41.1, pp. 33–54.

Chowdhury, A. H. et al. (2012). "A randomized, controlled, double-blind crossover study on the effects of 2-L infusions of 0.9% saline and plasma-lyte® 148 on renal blood flow velocity and renal cortical tissue perfusion in healthy volunteers". *Annals of Surgery* 256.1, pp. 18–24.

Daudel, F. et al. (2010). "Pulse pressure variation and stroke volume variation during increased intra-abdominal pressure: An experimental study". *Critical Care* 14.1, R122.

Davidson, I. (2006). "Renal impact of fluid management with colloids: a comparative review". *European Journal of Anaesthesiology* 23.9, pp. 721–738.
Dewitte, A. et al. (2016). "Bioelectrical impedance spectroscopy to estimate fluid balance in critically ill patients". *Journal of Clinical Monitoring and Computing* 30.2, pp. 227–233.
Douglas, P. S. et al. (2016). "1-year outcomes of FFRCT-guided care in patients with suspected coronary disease: the PLATFORM study". *Journal of the American College of Cardiology* 68.5, pp. 435–445.
Drobin, D. and Hahn, R. (1999). "Volume Kinetics of Ringer's Solution in Hypovolemic Volunteers". *Anesthesiology* 90, pp. 81–91.
Drobin, D. and Hahn, R. G. (2002). "Kinetics of Isotonic and Hypertonic Plasma Volume Expanders". *Anesthesiology* 96.6, pp. 1371–1380.
Ekinci, C. et al. (2018). "Effects of volume overload and current techniques for the assessment of fluid status in patients with renal disease". *Blood purification* 46.1, pp. 34–47.
Gattas, D. J. et al. (2013). "Fluid resuscitation with 6% hydroxyethyl starch (130/0.4 and 130/0.42) in acutely ill patients: systematic review of effects on mortality and treatment with renal replacement therapy". *Intensive Care Medicine* 39.4, pp. 558–568.
Guyton, A. and Hall, E. (2006). *Textbook of Medical Physiology*. 11th. Philadelphia: Elsevier Saunders.
Gyenge, C. C. et al. (1999). "Transport of fluid and solutes in the body I . Formulation of a mathematical model Transport of fluid and solutes in the body I . Formulation of a mathematical model". *American Journal of Physiology* 277.3, H1215–1227.
Gyenge, C. C. et al. (2003). "Preliminary model of fluid and solute distribution and transport during hemorrhage". *Annals of Biomedical Engineering* 31.7, pp. 823–839.
Haapio, M. et al. (2012). "Bioelectrical impedance analysis in the assessment of hydration status in peritoneal dialysis patients". *Peritoneal Dialysis-State-of-the-Art 2012*. Vol. 178. Karger Publishers, pp. 238–245.
Hahn, R. G. (2010). "Volume Kinetics for Infusion Fluids". *Anesthesiology* 113.2, pp. 470–481.
— (2017). "Arterial pressure and the rate of elimination of crystalloid fluid". *Anesthesia and Analgesia* 124.6, pp. 1824–1833.
Hjelmqvist, H (2000). "Colloids versus crystalloids". *Current Anaesthesia & Critical Care* 11.1, pp. 7–10.
Holte, K., Sharrock, N., and Kehlet, H. (2002). "Pathophysiology and clinical implications of perioperative fluid excess". *British Journal of Anaesthesia* 89.4, pp. 622–32.
Hu, Y. et al. (2012). "Decorated graphene sheets for label-free DNA impedance biosensing". *Biomaterials* 33.4, pp. 1097–1106.
Hung, S.-C. et al. (2014). "Volume overload correlates with cardiovascular risk factors in patients with chronic kidney disease". *Kidney International* 85.3, pp. 703–709.

Jabot, J. et al. (2009). "Passive leg raising for predicting fluid responsiveness: importance of the postural change". *Intensive Care Medicine* 35.1, pp. 85–90.
Jongen, G. J. et al. (2016). "A mathematical model to simulate the cardiotocogram during labor. Part A: Model setup and simulation of late decelerations". *Journal of Biomechanics* 49.12, pp. 2466–2473.
Lansdorp, B. et al. (2013). "A mathematical model for the prediction of fluid responsiveness". *Cardiovascular Engineering and Technology* 4.1, pp. 53–62.
Lansdorp, B. et al. (2014). "Mechanical ventilation-induced intrathoracic pressure distribution and heart-lung interactions". *Critical Care Medicine* 42.9, pp. 1983–1990.
Latta, T. (1832). "Malignant cholera". *Lancet* ii, pp. 45–274–7.
Lilot, M. et al. (2015). "Variability in practice and factors predictive of total crystalloid administration during abdominal surgery: Retrospective two-centre analysis". *British Journal of Anaesthesia* 114.5, pp. 767–776.
Lira, A. and Pinsky, M. R. (2014). "Choices in fluid type and volume during resuscitation: impact on patient outcomes". *Annals of Intensive Care* 4.1, p. 38.
Malbrain, M. L. et al. (2014). "Fluid overload, de-resuscitation, and outcomes in critically ill or injured patients: a systematic review with suggestions for clinical practice". *Anaesthesiology Intensive Therapy* 46.5, pp. 361–380.
Marik, P. E. et al. (2009). "Dynamic changes in arterial waveform derived variables and fluid responsiveness in mechanically ventilated patients: A systematic review of the literature". *Critical Care Medicine* 37.9, pp. 2642–2647.
Matthie, J. R. (2008). "Bioimpedance measurements of human body composition: critical analysis and outlook". *Expert review of medical devices* 5.2, pp. 239–261.
Mazzoni, M. C. et al. (1988). "Dynamic fluid redistribution in hyperosmotic resuscitation of hypovolemic hemorrhage." *American Journal of Physiology* 255, H629–H637.
Messerges, J. (2006). "Modeling systolic pressure variation due to positive pressure ventilation". *Annual International Conference of the IEEE Engineering in Medicine and Biology - Proceedings*, pp. 1806–1809.
Michard, F. and Teboul, J. L. (2000). "Using heart-lung interactions to assess fluid responsiveness during mechanical ventilation". *Critical Care* 4.5, pp. 282–289.
Monnet, X. et al. (2011). "Norepinephrine increases cardiac preload and reduces preload dependency assessed by passive leg raising in septic shock patients". *Critical Care Medicine* 39.4, pp. 689–694.
Monnet, X., Marik, P., and Teboul, J.-L. (2016). "Passive leg raising for predicting fluid responsiveness: a systematic review and meta-analysis". *Intensive Care Medicine* 42.12, pp. 1935–1947.
Murphy, C. V. et al. (2009). "The importance of fluid management in acute lung injury secondary to septic shock". *Chest* 136.1, pp. 102–109.
Myles, P. S. et al. (2018). "Restrictive versus liberal fluid therapy for major abdominal surgery". *New England Journal of Medicine* 378.24, pp. 2263–2274.

Pierrakos, C. et al. (2012). "Can changes in arterial pressure be used to detect changes in cardiac index during fluid challenge in patients with septic shock?" *Intensive Care Medicine* 38.3, pp. 422–428.
Pinsky, M. R. and Payen, D. (2005). "Functional hemodynamic monitoring". *Critical Care* 9.6, p. 566.
Pironet, A (2016). "Model-Based Prediction of the Response to Vascular Filling Therapy". PhD thesis. Universite de Liege.
Prowle, J. R. and Bellomo, R. (2010). "Fluid administration and the kidney". *Current Opinion in Critical Care* 16.4, pp. 332–336.
Roche, A. M., Miller, T. E., and Gan, T. J. (2009). "Goal-directed fluid management with trans-oesophageal Doppler". *Best Practice & Research Clinical Anaesthesiology* 23.3, pp. 327–334.
Saito, F. et al. (2013). "Interstitial fluid shifts to plasma compartment during blood donation". *Transfusion* 53.11, pp. 2744–2750.
Schortgen, F. et al. (2008). "The risk associated with hyperoncotic colloids in patients with shock". *Intensive care medicine* 34.12, p. 2157.
Schrier, R. W. (2010). "Fluid administration in critically ill patients with acute kidney injury". *Clinical Journal of the American Society of Nephrology* 5.4, pp. 733–739.
Smith, B. W. (2004). "Minimal Haemodynamic Modelling of the Heart & Circulation for Clinical Application". PhD thesis. University of Canterbury.
Starfinger, C. (2008). "Patient-Specific Modelling of the Cardiovascular System for Diagnosis and Therapy Assistance in Critical Care". PhD thesis. University of Canterbury.
Starling, E. H. (1918). *The Linacre lecture on the law of the heart*. Longmans, Green, & Company.
Taylor, C. A., Fonte, T. A., and Min, J. K. (2013). "Computational fluid dynamics applied to cardiac computed tomography for noninvasive quantification of fractional flow reserve: scientific basis". *Journal of the American College of Cardiology* 61.22, pp. 2233–2241.
Vincent, J.-L. and Weil, M. H. (2006). "Fluid challenge revisited". *Critical care medicine* 34.5, pp. 1333–1337.
Wabel, P. et al. (2009). "Importance of whole-body bioimpedance spectroscopy for the management of fluid balance". *Blood purification* 27.1, pp. 75–80.
Weiss, J. L. et al. (1979). "Evidence of Frank-Starling effect in man during severe semisupine exercise." *Circulation* 59.4, pp. 655–661.
Wolf, M. B. (2013). "Whole body acid-base and fluid-electrolyte balance: a mathematical model." *American Journal of Physiology - Renal Physiology* 305.8, F1118–31.
Wolf, M. and Watson, P. (1989). "Measurement of osmotic reflection coefficient for small molecules in cat hindlimbs". *American Journal of Physiology - Heart and Circulatory Physiology* 256.1, H282–H290.
Wolf, M. and Deland, E. (2011). "A mathematical model of blood-interstitial acid-base balance: application to dilution acidosis and acid-base status." *Journal of Applied Physiology* 110.4, pp. 988–1002.

Xie, S. et al. (1995). "A model of human microvascular exchange". *Microvascular Research* 49, pp. 141–162.
Yang, S.-F. et al. (2019). "Clinical Significance of Bioimpedance Spectroscopy in Critically Ill Patients". *Journal of Intensive Care Medicine* 34.6, pp. 495–502.

Chapter 2
A mathematical model for intravenous fluid administration and fluid loss in healthy volunteers

This chapter is based on: T. T. Rosalina, R.A. Bouwman, M.R. van Sambeek, F.N. van de Vosse, & P.H.M. Bovendeerd (2019). A mathematical model to investigate the effects of intravenous fluid administration and fluid loss. *Journal of Biomechanics*, vol. 88, pp. 4–11.

Abstract

The optimal fluid administration protocol for critically ill perioperative patients is hard to estimate due to the lack of tools to directly measure the patient fluid status. This results in the suboptimal clinical outcome of interventions. Previously developed predictive mathematical models focus on describing the fluid exchange over time but they lack clinical applicability, since they do not allow prediction of clinically measurable indices. The aim of this study is to make a first step towards a model predictive clinical decision support system for fluid administration, by extending the current fluid exchange models with a regulated cardiovascular circulation, to allow prediction of these indices. The parameters of the model were tuned to correctly reproduce experimentally measured changes in arterial pressure and heart rate, observed during infusion of normal saline in healthy volunteers. With the resulting tuned model, a different experiment including blood loss and infusion could be reproduced as well. These results show the potential of using this model as a basis for a decision support tool in a clinical setting.

2.1 Introduction

Intravenous fluid infusion, to compensate for perioperative fluid loss due to bleeding, perspiration and evaporation, is a common procedure to maintain arterial blood pressure and thereby tissue perfusion. However, part of the administered fluid will shift to the interstitial space, causing edema buildup that may eventually compress tissue microvasculature, disturb tissue perfusion and could lead to organ failure. Especially in the critically ill, these 'fluid shifts' can be large and unpredictable, due to changes in endothelial permeability and hydrostatic and osmotic pressure (Holte et al., 2002; Brandstrup, 2006). The optimal protocol for fluid administration depends on the intra- and extravascular fluid status of the patient. This fluid status is not directly measurable, and it cannot be easily deduced from indirect measurements. Additionally there is a large inter-patient variability, which makes evidence-based predictions difficult. Hence, it remains difficult to estimate the amount of fluid needed to compensate perioperative fluid loss. A patient specific mathematical model might be used to assist in determining the optimal fluid protocol.

In literature various mathematical models have been presented that focus on fluid administration and (re-) distribution. Some models describe fluid exchange between intra- and extravascular spaces using Starling's law, based on hydrostatic and osmotic pressures (Chapple et al., 1993; Xie et al., 1995; Gyenge et al., 1999; Gyenge et al., 2003; Mazzoni et al., 1988; Carlson et al., 1996; Wolf et al., 1989; Wolf et al., 2011; Wolf, 2013). Other models use a more phenomenological volume kinetics approach (Hahn et al., 1997; Svensen et al., 1999; Hahn, 2010; Hahn, 2017). Since the first type of models are based on laws of physics and physiology, they provide a stronger basis to predict the internal condition and the clinically observed information of a perioperative patient.

However, previously published models of this type have a limited representation of the cardiovascular circulation and lack information on arterial pressure and heart rate. Since arterial pressure is one of the important clinically available measurements used to guide fluid administration, it is hard to apply these models clinically.

We aim to develop a decision support model that can eventually assist in fluid administration to critically ill patients based on clinically available information such as arterial pressure and heart rate. In this study we extend a fluid exchange model (Xie et al., 1995) with a model of cardiovascular function (Jongen et al., 2016). Model parameters are partly taken from literature (Gyenge et al., 1999; Gyenge et al., 2003; Jongen et al., 2016), and partly determined from a fit to an experimental dataset of saline infusion (Watenpaugh et al., 1992). We evaluate our model by simulating another volunteer dataset of fluid administration in hypo- and normovolemia. Finally, we compare our model, with a regulated cardiovascular system, to the original fluid exchange model.

2.2 Methods

The model (Figure 2.1) combines submodels of cardiovascular hemodynamics, cardiovascular regulation, fluid exchange, and renal function.

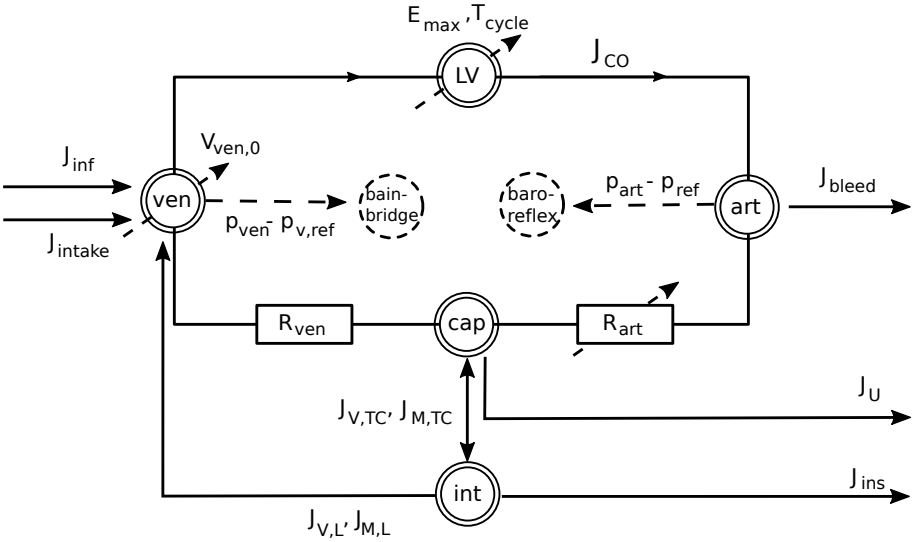


Figure 2.1: Schematic overview of the mathematical model: the left ventricle (*LV*) generates a blood flow (J_{CO}) that passes through the arteries (*art*), capillaries (*cap*) and veins (*ven*) facing a total resistance that is composed of an arterial and a venous part (R_{art} and R_{ven}). The baroregulation responds to the deviation of the mean arterial pressure (p_{art}) from a reference pressure (p_{ref}), and affects R_{art}, venous unstressed volume ($V_{ven,0}$), heart contractility (E_{max}) and cycle time (T_{cycle}). The Bainbridge reflex responds to the deviation of the mean venous pressure (p_{ven}) from the venous reference pressure ($p_{v,ref}$). The fluid exchange with the environment is determined by a basal fluid intake (J_{intake}), fluid infusion (J_{inf}), bleeding (J_{bleed}), urine production (J_U) and insensible losses (J_{ins}). The fluid exchange between the vascular compartment and the interstitium (*int*) consists of transcapillary fluid flow ($J_{V,TC}$) and lymphatic fluid ($J_{V,L}$). These fluid flows are related to corresponding protein flows, $J_{M,TC}$ and $J_{M,L}$, respectively.

2.2.1 Fluid exchange

The fluid exchange model is taken from Xie et al. (1995). It consists of a vascular and an interstitial compartment. The vascular compartment consists of plasma (with volume V_{PL} in ml), red blood cells (V_{RBC} in ml) and proteins (with mass M_{PL} in g), where the volume occupied by the proteins is neglected. The ratio of red blood cells to plasma is given by the hematocrit (H_{ct}):

$$H_{ct} = \frac{V_{RBC}}{(V_{RBC} + V_{PL})} \cdot 100. \tag{2.1}$$

The concentration of proteins in the plasma (c_{PL} in g/ml) is calculated as:

$$c_{PL} = \frac{M_{PL}}{V_{PL}}. \tag{2.2}$$

The interstitial compartment consists of fluid, with volume V_I, and proteins, with mass M_I. A part of this volume, the excluded volume ($V_{I,ex}$), is not available as a solvent for protein. This volume includes other macromolecules such as collagen and fibrin (Xie et al., 1995). Therefore we distinguish between interstitial protein concentration (c_I), and available interstitial protein concentration (c_{IA}):

$$c_I = \frac{M_I}{V_I}, \qquad c_{IA} = \frac{M_I}{(V_I - V_{I,ex})}. \tag{2.3}$$

The exchange of fluid between compartments satisfies the mass balance:

$$\frac{dV_{PL}}{dt} = J_{intake} + J_{inf} - J_{V,TC} + J_{V,L} - J_U - J_{V,\,bleed} \tag{2.4}$$

$$\frac{dV_I}{dt} = J_{V,TC} - J_{V,L} - J_{ins}. \tag{2.5}$$

Here, J_{intake} is the basal intake in normovolemia in ml/s, J_{inf} is the infused fluid flow in ml/s, $J_{V,TC}$ is the transcapillary fluid flow in ml/s, $J_{V,L}$ is the lymph flow in ml/s, J_U is the urine flow in ml/s, $J_{V,\,bleed}$ is the plasma loss due to haemorrhage (J_{bleed}) in ml/s and J_{ins} is the insensible fluid loss in ml/s. It holds that:

$$J_{V,bleed} = J_{bleed} \cdot (1 - H_{ct}). \tag{2.6}$$

The transcapillary fluid exchange ($J_{V,TC}$) is described by the Starling hypothesis:

$$J_{V,TC} = k_f \cdot [p_{cap} - p_I - \sigma(\pi_{cap} - \pi_I)]. \tag{2.7}$$

Here, k_f is the membrane permeability constant in ml/mmHg·s, p is the hydrostatic pressure in mmHg, π is the protein osmotic pressure in mmHg, with subscripts *cap* for the capillaries and *I* for the interstitium, and σ is the unitless reflection coefficient. The capillary pressure is computed from the cardiovascular model, which will be described in section 2.2. The interstitial pressure is calculated by empirical equations taken from Chapple et al. (1993), depending on the state of hydration:

$$p_I = \begin{cases} p_{I,N} + \frac{(V_I - V_{I,N})}{C_{under}} & V_I \leq V_{I,N} \\ p_{I,N} + \frac{(V_I - V_{I,N})}{C_{int}} & V_{I,N} < V_I < V_{I,over} \\ p_{I,over} + \frac{(V_I - V_{I,over})}{C_{over}} & V_I \geq V_{I,over} \end{cases}. \tag{2.8}$$

Here, $p_{I,N}$ is the interstitial pressure in normovolemia ($V_{I,N}$) and $p_{I,over}$ is the interstitial pressure at the threshold for hypervolemia ($V_{I,over}$). In the normovolemic range ($V_{I,N} < V_I < V_{I,over}$), p_I is determined by the normal interstitial compliance (C_{int}). The compliances C_{over} and C_{under} determine p_I in hyper-, and hypovolemia, respectively.

Finally, the osmotic pressure is based on the protein concentrations as follows:

$$\pi_{cap} = k_{prot} \cdot c_{PL}, \qquad \pi_I = k_{prot} \cdot c_I, \tag{2.9}$$

where k_{prot} is an empirical proportionality coefficient.

The lymph flow ($J_{V,L}$), which causes water to be constantly transported back into the intravascular space, depends on the interstitial pressure (Chapple et al., 1993):

$$J_{V,L} = \begin{cases} 0 & p_I < p_{I,ex} \\ J_{L,N} \cdot \left[\frac{p_I - p_{I,ex}}{p_{I,N} - p_{I,ex}}\right] & p_{I,ex} < p_I < p_{I,N}. \\ J_{L,N} + LS \cdot (p_I - p_{I,N}) & p_I > p_{I,N} \end{cases} \tag{2.10}$$

Here $J_{L,N}$ is the normal lymph flow, $p_{I,ex}$ is the pressure corresponding to the volume $V_{I,ex}$ and LS is the combination of a tissue permeability (L) and surface area (S) in ml/mmHg·s.

The elimination of fluids in steady state occurs through insensible losses (J_{ins}), assumed to be constant, and urine production (J_U). J_U is assumed to be linearly related to plasma volume (Gyenge et al., 2003):

$$J_U = \begin{cases} J_{U,N} + k_{UD} \cdot \frac{V_{PL} - V_{PL,N}}{V_{PL,N}} & V_{PL} \leq V_{PL,N} \\ J_{U,N} + k_{UE} \cdot \frac{V_{PL} - V_{PL,N}}{V_{PL,N}} & V_{PL} > V_{PL,N} \end{cases}. \tag{2.11}$$

Here $J_{U,N}$ is the normal urine production at normal plasma volume ($V_{PL,N}$) and $k_{U,D}$ and $k_{U,E}$ govern the change in urine production at depleted and elevated plasma volumes, respectively.

We assume that protein flows (in g/s) are only associated with the transcapillary protein flow ($J_{M,TC}$), lymph protein flow ($J_{M,L}$) and bleeding ($J_{V,\,bleed}$). Thus the follwing mass balances hold:

$$\frac{dM_{PL}}{dt} = -J_{M,TC} + J_{M,L} - J_{V,\,bleed} \cdot c_{PL} \tag{2.12}$$

$$\frac{dM_I}{dt} = J_{M,TC} - J_{M,L}. \tag{2.13}$$

The transcapillary protein flow ($J_{M,TC}$) is based on Kedem et al. (1958):

$$J_{M,TC} = J_{V,TC} \cdot (1-\sigma) \cdot \left[\frac{c_{PL} - c_{IA} \exp\left(\frac{-J_{V,TC}(1-\sigma)}{PS}\right)}{1 - \exp\left(\frac{-J_{V,TC}(1-\sigma)}{PS}\right)} \right], \tag{2.14}$$

with P= D_M/h, the protein permeability (D_M is the protein diffusion constant, and h is the membrane thickness) and the surface area S, commonly treated as one parameter PS, (protein permeability-surface area product of the capillary).

The lymphatic flow of protein ($J_{M,L}$) is considered to occur through convection only:

$$J_{M,L} = J_L \cdot c_I \tag{2.15}$$

Finally, to account for bleeding, the following mass balance for red blood cells holds:

$$\frac{dV_{RBC}}{dt} = J_{bleed} \cdot H_{ct}. \tag{2.16}$$

2.2.2 Cardiovascular circulation

To determine the capillary pressure (p_{cap}), used in (2.7), we implemented a cardiovascular model of the cycle-averaged systemic circulation (Jongen et al., 2016).

The model for the left ventricle is based on Hoppensteadt et al. (2002). Cardiac output (J_{CO}) is defined as:

$$J_{CO} = \frac{V_{stroke}}{T_{cycle}}. \tag{2.17}$$

Here the stroke volume (V_{stroke}) is determined by end diastolic volume (V_{ed}) and end ejection volume (V_{ee}), which in turn depends on the filling (p_{ed}) and ejection pressure (p_{ee}) of the heart. T_{cycle} is cardiac cycle time. We consider a linear pressure-volume relation for diastole and end ejection (Suga et al., 1973):

$$p_{ed} = E_{pas}(V_{ed} - V_{lv,0}); \qquad p_{ee} = E_{max}(V_{ee} - V_{lv,0}) \tag{2.18}$$

with E_{max} the maximal elastance and E_{pas} the passive elastance of the left ventricle and $V_{lv,0}$ in the left ventricle volume intercept.

For the systemic nodes, the following constitutive equations hold for the mean arterial pressure (p_{art}) and venous pressure (p_{ven}):

$$p_{art} = \frac{V_{art} - V_{art,0}}{C_{art}}; \qquad p_{ven} = \frac{V_{ven} - V_{ven,0}}{C_{ven}}. \tag{2.19}$$

Here V_{art} is the arterial blood volume, $V_{art,0}$, is the arterial unstressed volume, C_{art} is the arterial compliance, V_{ven} is the venous volume, $V_{ven,0}$ is the unstressed

venous volume and C_{ven} is the venous compliance. Since we assume a cycle-averaged system, without pulsatility and valves, we can assume $p_{ee} = p_{art}$ and $p_{ed} = p_{ven}$. Therefore the cardiac output can be calculated as follows:

$$J_{CO} = \frac{1}{T_{cycle}} \cdot \left(\frac{p_{ven}}{E_{pas}} - \frac{p_{art}}{E_{max}}\right). \tag{2.20}$$

At the same time it holds that:

$$J_{CO} = \frac{p_{art} - p_{ven}}{R_{art} + R_{ven}}, \tag{2.21}$$

with R_{art} and R_{ven} the arterial and venous capillary resistances in mmHg/ml, respectively.

Combining (2.19), (2.20) and (2.21) we can determine the arterial and venous pressures analytically:

$$p_{art} = \frac{k_v}{k_a C_v + k_v C_a}(V_{tot} - V_{art,0} - V_{ven,0} - V_{lv,0}); \qquad p_{ven} = p_{art} \cdot \frac{k_a}{k_v}. \tag{2.22}$$

with:

$$\begin{aligned} C_a &= C_{art} + \frac{1}{2E_{max}}; \qquad C_v = C_{ven} + \frac{1}{2E_{pas}}; \\ k_a &= \frac{1}{R_{art}} + \frac{f_H}{E_{pas}}; \qquad k_v = \frac{1}{R_{ven}} + \frac{f_H}{E_{max}}, \end{aligned} \tag{2.23}$$

and

$$f_H = \frac{1}{T_{cycle}}. \tag{2.24}$$

Finally, the capillary pressure that is used in (2.7) is calculated by:

$$p_{cap} = p_{ven} + J_{CO} \cdot R_{ven}. \tag{2.25}$$

2.2.3 Cardiovascular regulation

Cardiovascular regulation is modelled by two pathways: baroregulation and the Bainbridge reflex. We model the baroregulation based on Wesseling et al. (1985) and Jongen et al. (2016). A change in arterial pressure leads to a response of four cardiovascular effectors; the cardiac contractility (E_{max}), cycle time (T_{cycle}), pre-capillary peripheral resistance (R_{art}) and venous unstressed volume ($V_{ven,0}$). Due to our large timescale, the model has been simplified by neglecting the effector time delays and low pass filters in the original model.

The change in arterial pressure is transformed into a normalised receptor signal $-1 \leq b(t) \leq 1$, through a sigmoidal receptor function:

$$b(t) = \frac{2}{1 + \exp(-k \cdot (p_{art}(t) - p_{ref}))} - 1, \tag{2.26}$$

where k controls the sensitivity of the receptor and p_{ref} is the reference mean arterial pressure.

This is translated into the receptor signal after passing through a low pass filter:

$$\frac{dr(t)}{dt} = \frac{1}{\tau_r}(b(t) - r(t)), \tag{2.27}$$

where τ_r is the low pass filter receptor time constant. The change in E_{max}, R_{art} and $V_{ven,0}$ is calculated by effector specific gains k_E, k_R and k_V:

$$\begin{aligned} E_{max}(t) &= E_{max,0} \cdot (1 + k_E \cdot r(t)); \\ R_{art}(t) &= R_{art,0} \cdot (1 + k_R \cdot r(t)); \\ V_{ven0}(t) &= V_{ven0,0} \cdot (1 + k_V \cdot r(t)), \end{aligned} \tag{2.28}$$

where $E_{max,0}$, $R_{art,0}$ and $V_{ven0,0}$ represent the steady state values for the effectors.

The change in T_{cycle} is also affected by the Bainbridge reflex, i.e. the positive chronotropic response of the heart to stretch-activated channels in the atria. In hypervolemia the atria are stretched and this results in extra stimulation of the sino-atrial node, thereby increasing the heart rate. To account for this increase in heart rate we have added a receptor signal (r_a), calculated by a normalised change in venous pressure p_{ven}, with respect to a reference value ($p_{v,ref}$) taken as a substitute for right atrium pressure:

$$r_a(t) = \frac{p_{ven}(t) - p_{v,ref}}{p_{v,ref}}. \tag{2.29}$$

The cycle time is finally calculated by:

$$T_{cycle}(t) = T_{cycle,0} \cdot (1 + k_T \cdot r(t) + k_{Ta} \cdot r_a(t)). \tag{2.30}$$

where k_T is the baroregulation effector gain and k_{Ta} is the bainbridge effector gain.

2.2.4 Parameter estimation

The cardiovascular system was tuned to yield normal steady state hemodynamics for a 70 kg subject, characterised by

Most regulation parameters are based on estimations of Wesseling et al. (1985). For the regulation, p_{ref} is set to normal arterial pressure (93 mmHg) and $p_{v,ref}$ is set

to normal venous pressure (5 mmHg). To simulate the response of the model to perturbations we fitted the cardiovascular model output (Δp_{art}, ΔHR and ΔR_{art}) to a dataset from literature (Watenpaugh et al., 1992). In this experimental study the effect of infusion of 30 ml/kg of normal saline, with an infusion rate of 100 ml/min was analysed in seven male volunteers of 78 kg. By manual fitting of k_R and k_{Ta}, the responses of the change in resistance and change in heart rate were tuned to available experimental data. To obtain correct changes in total arterial pressure, the rest of the effect was tuned by fitting k_V.

Settings for many parameters in the fluid exchange model are taken from Xie et al. (1995). Settings for parameters $J_{L,N}$, PS and J_{intake} were computed, to satisfy steady state conditions. Hence, (2.4), (2.5), (2.12) and (2.14), are assumed to be equal to zero. In normal conditions we assume no intravenous infusion ($J_{inf} = 0$) or bleeding ($J_{bleed} = 0$). Hence, for the sum of the plasma and the interstitial volume it holds that:

$$J_{intake} = J_{ins} + J_{U,N} \tag{2.31}$$

After setting protein concentrations to values taken from Gyenge et al. (1999), we can determine $J_{L,N}$ and PS analytically, by combining (2.10) and (2.14) with:

$$J_{intake} - J_{V,TC} + J_{V,L} - J_U = 0, \tag{2.32}$$

and:

$$J_{M,TC} - J_{M,L} = 0. \tag{2.33}$$

The fluid distribution results during infusion (ΔV_{PL}, ΔV_I and ΔV_U), were fitted to the experimental results by changing k_f and k_{UE}. All model parameter values are listed in Table 2.1.

2.2.5 Simulations performed

The model was implemented in MATLAB R2014b. Differential equations are solved by an Euler forward integration scheme with a time step of 0.1 s. First, the simulations for parameter estimations as described in section 2.4 were performed. Secondly, to demonstrate the predictive value of the model on an independent dataset, we simulated an experiment presented by Drobin et al. (1999) without additional fitting. There, the authors infused 25 ml/kg in 10 healthy volunteers (with mean bodyweight of 76 kg), being normovolemic or hypovolemic (after induced haemorrhage of 900 ml in 15 minutes). Experimental and model computed changes of the plasma volume and total urine production at the end of the experiment could be directly compared.

Lastly, we compared our fluid exchange model, with the more complex regulated cardiovascular system, to the fluid exchange model as described in Xie et al. (1995). To this end, we simplified our cardiovascular circulation model to a 'Xie-like' model by replacing E_{max} and E_{pas} by a single elastance value E_{LV},

Symbol	*Value*	*Unit*	*Equation*	*Reference*
C_{art}	2.6	ml/mmHg	2.22	Calculated*
C_{ven}	$2.5 \cdot 10^{2}$	ml/mmHg	2.22	Calculated*
C_{int}	2.0	ml/mmHg	2.8	Xie et al., 1995
C_{under}	0.6	ml/mmHg	2.8	Xie et al., 1995
C_{over}	0.1	ml/mmHg	2.8	Xie et al., 1995
E_{max}	1.7	mmHg/ml	2.18	Calculated*
E_{pas}	$4.4 \cdot 10^{-2}$	mmHg/ml	2.18	Calculated*
$J_{L,N}$	$8.6 \cdot 10^{-3}$	ml/s	2.10	Calculated in steady state
J_{ins}	$1.3 \cdot 10^{-2}$	ml/s	2.4	Watenpaugh et al., 1992
$J_{U,N}$	$1.7 \cdot 10^{-2}$	ml/s	2.11	Xie et al., 1995
k_f	0.2	ml/mmHg·s	2.7	Watenpaugh et al., 1992
k_{prot}	0.4	mmHg · ml/g	2.9	Gyenge et al., 2003
k_{UE}	$3.5 \cdot 10^{-4}$	ml/s	2.11	Gyenge et al., 2003
k_{UD}	$4.6 \cdot 10^{-5}$	ml/s	2.11	Gyenge et al., 2003
k	$7.5 \cdot 10^{-2}$	1/mmHg	2.26	Wesseling et al., 1985
k_T	0.6	-	2.30	Wesseling et al., 1985
k_{Ta}	-2.2	-	2.30	Watenpaugh et al., 1992
k_E	-0.2	-	2.28	Wesseling et al., 1985
k_R	-0.7	-	2.28	Watenpaugh et al., 1992
k_V	0.9	-	2.28	Watenpaugh et al., 1992
LS	$1.2 \cdot 10^{-2}$	ml/mmHg·s	2.10	Xie et al., 1995
PS	$6.9 \cdot 10^{-3}$	ml/s	2.14	Calculated in steady state
$p_{I,ex}$	-0.1	mmHg	2.10	Xie et al., 1995
$p_{I,N}$	-0.7	mmHg	2.8, 2.10	Xie et al., 1995
$p_{I,over}$	1.8	mmHg	2.8	Xie et al., 1995
p_{ref}	93	mmHg	2.26	Normal hemodynamics
$p_{v,ref}$	5.0	mmHg	2.26	Normal hemodynamics
$M_{PL,0}$	224.0	g	2.2	Xie et al., 1995
$M_{I,0}$	250.3	g	2.3	Xie et al., 1995
R_{art}	908.0	mmHg s/ml	2.22	Calculated*
R_{ven}	62.7	mmHg s/ml	2.22	Calculated*
τ_r	1.0	s	2.28	Wesseling et al., 1985
T_{cycle}	0.8	s	2.20, 2.22, 2.23 2.28, 2.30	Normal hemodynamics
$V_{art,0}$	746.6	ml	2.22	Calculated*
$V_{I,N}$	8400	ml	2.3, 2.8	Xie et al., 1995
$V_{I,EX}$	2100	ml	2.3, 2.10	Xie et al., 1995
$V_{lv,0}$	0	ml	2.22	Normal hemodynamics
$V_{ven,0}$	2433	ml	2.22	Calculated*
$V_{PL,N}$	3200	ml	2.1, 2.11	Xie et al., 1995
$V_{RBC,0}$	1800	ml	2.1	Xie et al., 1995
σ	0.99	-	2.7, 2.14	Xie et al., 1995

Table 2.1: Parameter settings, units and references used for a reference human of 70 kg, with *Calculated based on normal hemodynamics as explained in section 2.4. Here, subscript 0 indicates the initial value. Parameters k_f, k_{UE}, k_R, k_V and k_{Ta} are fitted on Watenpaugh et al., 1992.

such that the total compliance of the circulation model was identical to the one used by Xie et al. Due to this simplification we also had to exclude the baroregulation. To solely evaluate the role of the baroreflex, we performed additional simulations with our extended model without baroregulation.

2.3 Results

2.3.1 Simulation of the Watenpaugh experiment

To reproduce the experimental data, obtained by Watenpaugh et al. (1992), we manually fitted k_f, k_{UE}, k_R, k_V and k_{Ta}, presented in Table 2.1. Computed results match the experimental results, demonstrating that the model was fitted to the experiment successfully. The changes in volume (per kg body mass), heart rate and arterial pressure in the model and experiment are shown in Figure 2.2. During infusion, p_{art} and HR increase with a maximal value of 9 mmHg and 15 bpm, respectively. Maximal p_{ven} is 5.8 mmHg post-infusion. The simulated change in HR can be attributed to a decrease of 10 bpm and increase of 25 bpm, as a result of the baroregulation and Bainbridge reflex. At the end of infusion, the change in plasma and interstitial volume is 11.4 ml/kg and 21.5 ml/kg, respectively. After infusion p_{cap} and p_{art} return towards normal values. However, at 180 minutes post infusion HR (+3 bpm), and plasma volume (+ 2.4 ml/kg) are still elevated. Eventually, 14.3 ml/kg urine is produced at the end of the experiment. Interstitial volume decreases more gradually than plasma volume and is still elevated by 11 ml/kg at the end of simulation, which is reflected in an elevated urine production of 11.8 ml/kg compared to a normal production of 2.6 ml/kg.

2.3.2 Simulation of the Drobin experiment

In Figure 2.3, the simulated and experimental (Drobin et al., 1999), changes in volume distribution in hypo- and normovolemia are shown. As in the experiment changes are reported with respect to the start of infusion, set at t = 0 for both scenarios. In the normovolemic simulation, infusion causes a maximal change in plasma volume of 8.4 ml/kg, which corresponds to the measured plasma dilution. For hypovolemia the change in plasma volume (+10.3 ml/kg) also corresponds to the experimental results. The differences in p_{cap} show the effect of pre-infusion haemorrhage. The difference between hypo- and normovolemia results is most pronounced in the simulated urine production. Cumulative urine production at 180 minutes post infusion is reported to be 12.3 $\pm$ 1 ml/kg and 9.7 $\pm$ 2 ml in normo-, and hypovolemia, respectively. The model captures this in the normovolemic case (11.4 ml/kg), but not in the hypovolemic case (3.6 ml/kg). This results in an elevated interstitial volume in the latter case.

2.3.3 Comparison to the 'Xie-like' model

To further evaluate our extended model, we simulated the Watenpaugh experiment with our reduced 'Xie-like' model, resembling the model by Xie et al. (1995) (Figure 2.2). This model does not include p_{art} and HR. As compared to our extended model, it does predict an increased maximum rise in p_{cap} (15.1 vs. 13.1 mmHg). Consequently, more fluid is transported from the plasma into the interstitium and urine production is reduced at the end of the experiment by 2 ml/kg.

Finally, the effect of regulation was evaluated by simulating the Watenpaugh experiment without baroregulation (Figure 2). This results in an increased p_{art} (38 mmHg vs. 9 mmHg post infusion) and no changes in HR. Results for changes in capillary pressure, plasma and interstitial volume, and urine production are similar to those of the 'Xie-like' model.

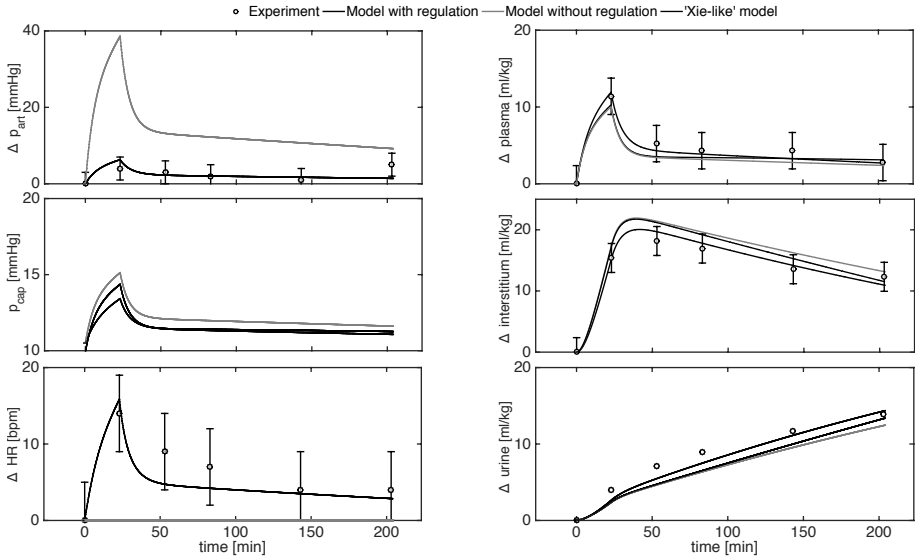


Figure 2.2: Simulation of the experiment of Watenpaugh et al. (1992), with 30 ml/kg saline infusion from t = 0 to t = 23 minutes; experimental results are shown in symbols; simulation results are shown in solid lines, for the model with regulation, without regulation and the 'Xie-like' model. Left: change in mean arterial pressure (Δp_{art} in mmHg), absolute capillary pressure (p_{cap} in mmHg) and change in heart rate (ΔHR in bpm). Right: scaled changes in plasma (ΔV_{PL} in ml/kg), interstitial (ΔV_I in ml/kg) and urine volume (ΔV_U in ml/kg).

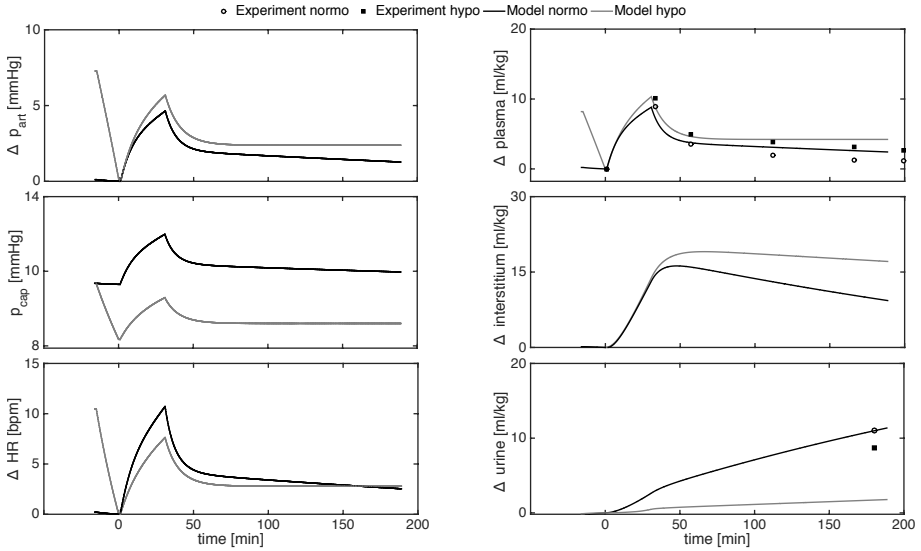


Figure 2.3: Simulation of the experiment by Drobin et al. (1999); results of 25 ml/kg saline infusion in a normovolemic and hypovolemic state. Left: the change in mean arterial pressure (Δp_{art} in mmHg), absolute capillary pressure (p_{cap} in mmHg), change in heart rate (ΔHR in bpm). Right: scaled changes in plasma (ΔV_{PL} in ml/kg), interstitial (ΔV_I in ml/kg) and urine volume (ΔV_U in ml/kg). Experimental data (from Drobin et al., 1999) are shown with symbols.

2.4 Discussion

Optimisation of perioperative fluid administration remains difficult due to high patient variability and the lack of tools to directly measure patient fluid status. Mathematical models have the potential of improving fluid administration protocols. Previously developed mathematical models focussed on describing the fluid exchange over time but they lacked clinically measurable indices such as heart rate and arterial blood pressure. The aim of our study was to make a first step towards a clinically applicable fluid administration support model, by combining existing fluid exchange models (Xie et al., 1995; Gyenge et al., 2003) with a cardiovascular circulation model that includes baroregulation (Jongen et al., 2016) and the Bainbridge reflex. To the best of our knowledge this is the first time that such a coupling of short- and long term effects (cardiovascular regulation and fluid exchange, respectively) has been made.

Our model was used to study the effects of fluid infusion and blood loss in healthy volunteers. We could fit the model to predict the fluid exchange in one experiment (Watenpaugh et al., 1992) and subsequently reproduce results from another experiment (Drobin et al., 1999) without further tuning. The Watenpaugh experiment was also simulated in our model without regulation, and in a 'Xie-like' model. Here, the increase in interstitial volume is approximately 10 % lower in the extended model. We conclude that differences between our model and the 'Xie-like' model are mainly due to the addition of the (short term) regulation.

2.4.1 Model setup

To achieve our goal of clinical decision support, the right balance between model complexity and accuracy must be made. The current goal was to study long term effects of fluid infusion on volume distribution in volunteers and their hemodynamic response in terms of mean arterial pressure and heart rate. Therefore, we chose to use a model for cycle-averaged hemodynamics without beat-to-beat information, which reduces the amount of parameters that needs to be estimated. We implemented the traditional Starling equation (2.7) to model whole-body transcapillary transport. Experiments (Michel et al., 1987) have shown that there is a distinction between transport in normal capillaries, where reabsorption of fluid seems absent, and fenestrated capillaries, where reabsorption is present. In recent years there has been an adaptation of the Starling equation, to better capture fluid exchange in capillaries (Adamson et al., 2004). However, we adopted the traditional Starling approach, since in our lumped parameter approach spatial variations, and hence variations in capillary type, are not taken into account. Lastly, we assumed urine production solely based on plasma volume, thereby omitting the effects of hormone regulation pathways such as the RAAS mechanism.

2.4.2 Results

The three fitted parameters in the fluid exchange model (k_f, $J_{L,N}$ and PS) can be compared to previously presented values (Gyenge et al., 1999; Tatara et al., 2007). k_f is the determining factor for the maximum plasma expansion during infusion, and determines the persisting level after infusion. Our fitted value is 0.15 ml/mmHg·s, which is high compared to 0.03 ml/mmHg·s, reported in Gyenge et al. (1999) and 0.08 ml/mmHg·s in Tatara et al. (2007). But it is still within the range reported in literature (0.008 - 0.34 ml/mmHg·s, Chapple et al. (1993)). PS and $J_{L,N}$ were derived from the condition of homeostatic equilibrium, i.e. from the condition of equal fluid intake and loss over time. Our calculated value for $J_{L,N}$ (0.009 ml/s) is low compared to literature values (0.02 - 0.04 ml/s, Reddy, 1986). PS is hard to estimate from literature, however this parameter is closely correlated to the estimation of σ (0.8 - 0.99$[-]$, Chapple et al. 1993). Ultimately, the transcapillary transport is not characterised by the individual values of these parameters, but by their combination (2.14), as expressed by the Péclet number: $Pe = (1 - \sigma)J_{V,TC}/PS$. Comparing our results ($\sigma = 0.99$, $Pe = 0.0106$) to Gyenge et al. (1999) ($\sigma = 0.99$, $Pe = 0.0103$) and Tatara et al. (2007) ($\sigma = 0.875$, $Pe = 0.046$), shows the same order of magnitude. Thus, the Péclet number and therefore the combination of σ and PS is supported by literature.

Cardiovascular regulation is described by baroregulation and the Bainbridge reflex. In this study the venous pressure ($p_{v,ref}$) is taken as a substitute for atrial pressure. This simplification is inherent to our choice of a simplified heart model.

The change in *HR* by +15 bpm due to an increase of $p_{v,ref}$ by 1 mmHg, predicted by the model is supported by literature. Experimental data reported in Kohl et al. (1999) show an increase in the same order of magnitude (+8 bpm).

The predictive value of the model is demonstrated, since results of Drobin et al. (1999) are captured quite well with the same fitted parameters. Notably, there is an underestimation of urine production in the hypovolemic simulation (3.6 ml/kg vs 9.7 ml/kg). The urine production during hypovolemia is governed by parameter k_{UD} in (2.11), adopted from Gyenge et al. (2003), since this could not by fitted from the Watenpaugh dataset. Fitting of k_{UD} to the Drobin dataset proved to be impossible due to the fact that $J_{U,N}$ is four times smaller than the experimental J_U. However, Gupta et al. (2016) reported a hypovolemic urine production of 1.5 ml/kg, demonstrating considerable variation in between experimental data.

2.4.3 Future work

Our final goal is to develop a decision support model that can eventually assist in fluid administration to critically ill patients. It is known that fluid exchange in the perioperative period is altered. Perioperative medication for anaesthesia, analgesia and hemodynamic support affect (baro) regulation and renal function, which influences capillary fluid exchange. Additionally there can be effects of surgical inflammation causing capillary leakage (Brandstrup, 2006). In our model this can be accounted for in parameters related to membrane permeability (e.g. σ and k_f in 2.7). Moreover, patients may suffer from comorbidities such as cardiac dysfunction, renal insufficiency and chronic hypertension. Therefore, in future work we need to extend the cardiac and renal model, to allow for realistic simulation of these pathologies.

For eventual use in a specific patient, suitable parameter values have to be found using data assimilation techniques. To gain more insight into the possibilities for parameter fixing and prioritisation, a structured sensitivity analysis (Eck et al., 2015) should also be performed. Additionally this could indicate which submodels should be explored further.

2.5 Conclusion

To conclude, we combined a simple model for cardiovascular hemodynamics with an existing model for fluid exchange for healthy volunteers enabling coupling of readily available clinical measurements to a fluid exchange model. This is the first step towards our general aim to develop a patient-specific decision support model to guide fluid administration.

Bibliography

Adamson, R. H. et al. (2004). "Oncotic pressures opposing filtration across non-fenestrated rat microvessels". *Journal of Physiology* 557.3, pp. 889–907.

Brandstrup, B. (2006). "Fluid therapy for the surgical patient." *Best Practice & Research. Clinical Anaesthesiology* 20.2, pp. 265–283.

Carlson, D. E., Kligman, M. D., and Gann, D. S. (1996). "Impairment of blood volume restitution after large hemorrhage: a mathematical model". *The American Journal of Physiology* 270, R1163–R1177.

Chapple, C. et al. (1993). "A model of human microvascular exchange: parameter estimation based on normals and nephrotics". *Computer Methods and Programs in Biomedicine* 41.1, pp. 33–54.

Drobin, D. and Hahn, R. (1999). "Volume Kinetics of Ringer's Solution in Hypovolemic Volunteers". *Anesthesiology* 90, pp. 81–91.

Eck, V. G., Donders, W. P., and Sturdy, J. (2015). "A guide to uncertainty quantification and sensitivity analysis for cardiovascular applications". *International Journal for Numerical Methods in Biomedical Engineering*, e02755.

Gupta, R. and Gan, T. (2016). "Peri-operative fluid management to enhance recovery". *Anaesthesia* 71, pp. 40–45.

Gyenge, C. C. et al. (1999). "Transport of fluid and solutes in the body I . Formulation of a mathematical model Transport of fluid and solutes in the body I . Formulation of a mathematical model". *American Journal of Physiology* 277.3, H1215–1227.

Gyenge, C. C. et al. (2003). "Preliminary model of fluid and solute distribution and transport during hemorrhage". *Annals of Biomedical Engineering* 31.7, pp. 823–839.

Hahn, R. G. and Svensén, C. (1997). "Plasma dilution and the rate of infusion of Ringer's solution". *British Journal of Anaesthesia* 79.1, pp. 64–67.

Hahn, R. G. (2010). "Volume Kinetics for Infusion Fluids". *Anesthesiology* 113.2, pp. 470–481.

— (2017). "Arterial pressure and the rate of elimination of crystalloid fluid". *Anesthesia and Analgesia* 124.6, pp. 1824–1833.

Holte, K., Sharrock, N., and Kehlet, H. (2002). "Pathophysiology and clinical implications of perioperative fluid excess". *British Journal of Anaesthesia* 89.4, pp. 622–32.

Hoppensteadt, F. and Peskin, C. (2002). *Modeling and Simulation in Medicine and the Life Sciences*. Springer-Verlag New York.

Jongen, G. J. et al. (2016). "A mathematical model to simulate the cardiotocogram during labor. Part A: Model setup and simulation of late decelerations". *Journal of Biomechanics* 49.12, pp. 2466–2473.

Kedem, O. and Katchalsky, A. (1958). "Thermodynamic analysis of the permeability of biological membranes to non-electrolytes". *Biochimica et Biophysica Acta* 27, pp. 229–246.

Kohl, P., Hunter, P., and Noble, D. (1999). "Stretch-induced changes in heart rate and rhythm: clinical observations, experiments and mathematical models." *Progress in Biophysics and Molecular Biology*, pp. 91–138.

Mazzoni, M. C. et al. (1988). "Dynamic fluid redistribution in hyperosmotic resuscitation of hypovolemic hemorrhage." *American Journal of Physiology* 255, H629–H637.

Michel, B. Y.C. C. and Phillips, M. E. (1987). "Steady state fluid filtration at different vapillary pressures in perfused frog mesenteric capillaries". *Journal of Physiology* 76.388, pp. 421–435.

Reddy, N. (1986). "Lymph circulation: physiology, pharmacology, and biomechanics". *Critical Reviews in Biomedical Engineering* 14, pp. 45–91.

Suga, H., Sagawa, K., and Shoukas, A. A. (1973). "Load independence of the instantaneous pressure-volume ratio of the canine left ventricle and effects of epinephrine and heart rate on the ratio." *Circulation Research* 32.3, pp. 314–322.

Svensen, C et al. (1999). "Stability of the interstitial matrix after crystalloid fluid loading studied by volume kinetic analysis." *British Journal of Anaesthesia* 82.4, pp. 496–502.

Tatara, T., Tsunetoh, T., and Tashiro, C. (2007). "Crystalloid infusion rate during fluid resuscitation from acute haemorrhage". *British Journal of Anaesthesia* 99.2, pp. 212–217.

Watenpaugh, D. E. et al. (1992). "Role of atrial natriuretic peptide in systemic responses to acute isotonic volume expansion". *Journal of Applied Physiology* 73.4, pp. 1218–1226.

Wesseling, K. and Settels, J. (1985). *Psychophysiology of cardiovascular control: Models, methods and Data*. Vol. 26. Plenum Press, New York.

Wolf, M. B. (2013). "Whole body acid-base and fluid-electrolyte balance: a mathematical model." *American Journal of Physiology - Renal Physiology* 305.8, F1118–31.

Wolf, M. and Watson, P. (1989). "Measurement of osmotic reflection coefficient for small molecules in cat hindlimbs". *American Journal of Physiology - Heart and Circulatory Physiology* 256.1, H282–H290.

Wolf, M. and Deland, E. (2011). "A mathematical model of blood-interstitial acid-base balance: application to dilution acidosis and acid-base status." *Journal of Applied Physiology* 110.4, pp. 988–1002.
Xie, S. et al. (1995). "A model of human microvascular exchange". *Microvascular Research* 49, pp. 141–162.

Chapter 3
A mathematical cardiorespiratory model to predict dynamic indices of fluid responsiveness

This chapter is based on: T. T. Rosalina, R.A. Bouwman, M.R. van Sambeek, K.D. Lau, F.N. van de Vosse, & P.H.M. Bovendeerd. A mathematical cardiorespiratory model to predict dynamic indices of fluid responsiveness. *Submitted to: Journal of Medical Engineering & Physics*.

Abstract

Optimal fluid administration during and after surgery is of great importance, especially in critical patients, since hypo- and hypervolemia are both associated with complications. Optimization of fluid administration is challenging, because direct measurements of fluid status are not available and there is much debate on indirect clinical parameters. Pulse pressure variation (*ppv*) and stroke volume variation (*svv*) are dynamic indices that can be used for indirect estimation of the effectiveness of fluid administration. Unfortunately, specific constraints prevent the regular acquisition of *ppv* and *svv* in a clinical setting. To investigate dependence of *ppv* and *svv* on vascular filling status and cardiac and vascular properties, we developed a mathematical cardiorespiratory model based on physics and physiology to predict *ppv* and *svv* and investigate their relationship to vascular volume and cardiac and vascular properties. Our model consists of a closed loop representation of the cardiovascular circulation where intrathoracic compartments are influenced by a dynamic pleural pressure, which is calculated in a dedicated, coupled lung mechanics model. We simulated changes in alveolar volume and hemodynamic responses for mechanically ventilated anesthetized patients, during fluid administration at varying total blood volumes. Calculated *ppv*, *svv* and change in cardiac index were comparable to experimentally reported values. Interestingly, *ppv* and *svv* were found to depend differently on vascular, and pericardial properties. The results show the potential of the model to analyse potential broader use of *pvv* and *svv* in critical care.

3.1 Introduction

In the operating room and the intensive care unit, intravenous fluid administration is necessary to compensate for perioperative fluid loss due to bleeding, urine excretion, perspiration, and evaporation. However, it remains difficult to estimate the amount of fluid needed to compensate for these losses, especially in septic patients, where a large part of the administered fluid quickly moves to the interstitial space. Key to fluid administration is to avoid complications due to underfilling or overfilling. Infusion of too little fluid will not adequately restore tissue perfusion pressure, whereas too much fluid may cause a buildup of excess fluid in the extravascular space. The latter compresses the microcirculation and thereby compromises tissue perfusion (Holte et al., 2002; Brandstrup, 2006). Unfortunately, fluid distribution cannot be measured directly. Therefore, clinicians need to rely upon indirect measurements to determine fluid responsiveness.

Physiologically, the relationship between vascular fluid volume and cardiac pump function is described by the Frank-Starling mechanism. This states that an increase in cardiac filling leads to an increase in cardiac output, up to a certain filling level (Frank, 1895; Starling et al., 1926). One option to test a patient's location on the Starling curve is to give a fluid bolus and to measure the change in cardiac output (Latta, 1832; Cecconi et al., 2011). The drawback is that patients who are already on the flat part of the Starling curve are exposed to hypervolemia. Alternatively, cardiac filling may be increased without actually increasing the total amount of vascular volume (Michard et al., 2000). These scenarios rely on the redistribution of the available amount of blood volume (V_{bl}), from the periphery to the heart, e.g., in a passive leg raise test by raising the legs of a patient by 45°, or by placing the patient in a Trendelenburg position. Another option is to make use of fluid redistribution in response to variations in intrathoracic pressure, as induced during mechanical ventilation. Here, cardiac filling increases with decreasing intrathoracic pressure and vice versa. This change in filling is reflected in a variation of stroke volume and aortic pulse pressure (Figure 3.1), which can be assessed clinically. These changes are quantified with dynamic indices pulse pressure variation (*ppv*) and stroke volume variation (*svv*). A high *ppv* or *svv* ($\geq$ 13%) indicates fluid responsiveness, with the recommendation of intravascular filling (Daudel et al., 2010; Cecconi et al., 2015). A low *ppv* or *svv* ($\leq$ 9%) indicates fluid non-responsiveness, where intravascular filling is not expected to increase cardiac output.

As shown in literature (Michard et al., 2000; Marik et al., 2009), *ppv* and *svv* are promising measures to determine patient fluid responsiveness, with high sensitivity and specificity (> 82 %). However, these indices are coupled to specific clinical constraints, such as a tidal volume $\geq$ 8 ml/kg, no open thorax, and no arrhythmia (Cannesson et al., 2011). Consequently, only 20% of intensive care patients qualify for reliable pulse pressure variation and stroke volume variation analysis (Cannesson et al., 2011; Michard et al., 2015).

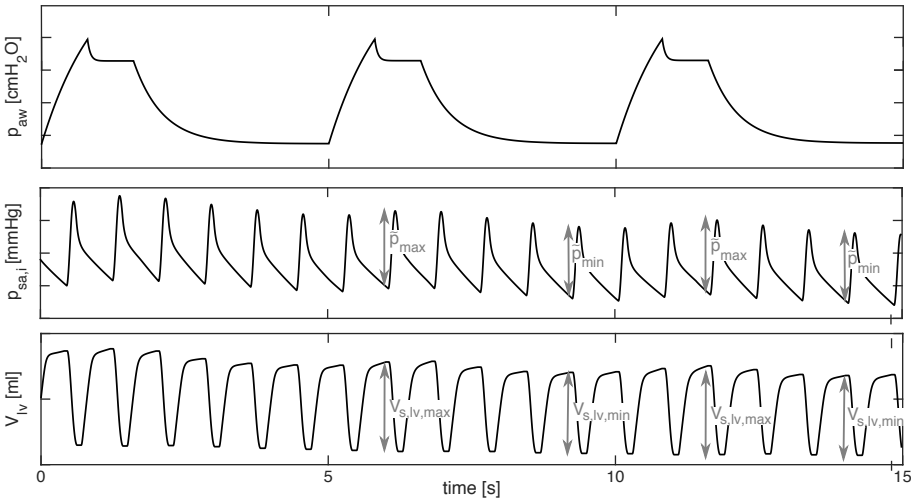


Figure 3.1: Explanation of the calculation of pulse pressure variation (*ppv*) and stroke volume variation (*svv*) in three ventilation cycles, based on results from the model simulations. Here, p_{aw} is the induced airway pressure, $p_{sa,i}$ is the intrathoracic arterial pressure, $\tilde{p}_{max}$ and $\tilde{p}_{min}$ are the maximal and minimal pulse pressure, V_{lv} is the left ventricle volume and $V_{s,lv,max}$ and $V_{s,lv,min}$ are maximum and minimum left ventricle stroke volumes. Since the first cycle of ventilation produces a transient increase in V_{lv}, we computed *ppv* and *svv* during the subsequent breathing cycles, using (3.22) and (3.23).

We hypothesize that a more extensive clinical use of *ppv* and *svv* can be obtained by investigating the relationship between patient characteristics and *ppv* and *svv* through a mathematical model. Such a model can provide quantitative insight in the current clinical constraints, potentially leading to a more extensive and equally reliable clinical use of the dynamic indices.

In this study we present a mathematical model of the cardiorespiratory system to study the dependence of *ppv* and *svv* on vascular volume, and cardiac and vascular properties. Firstly, we set up a lumped parameter model of the cardiovascular circulation, coupled to a lung mechanics model. Secondly, we simulate mechanical ventilation in anesthetized patients, and compare predicted alveolar volume to measured values for Innes et al. (1993). Thirdly, we investigate the sensitivity of *ppv* and *svv* to the amount of total blood volume varying in a range of 4000 to 5500 ml. Lastly, we investigate the sensitivity of *ppv* and *svv* to settings for the arterial, venous, and pericardial pressure-volume relationships.

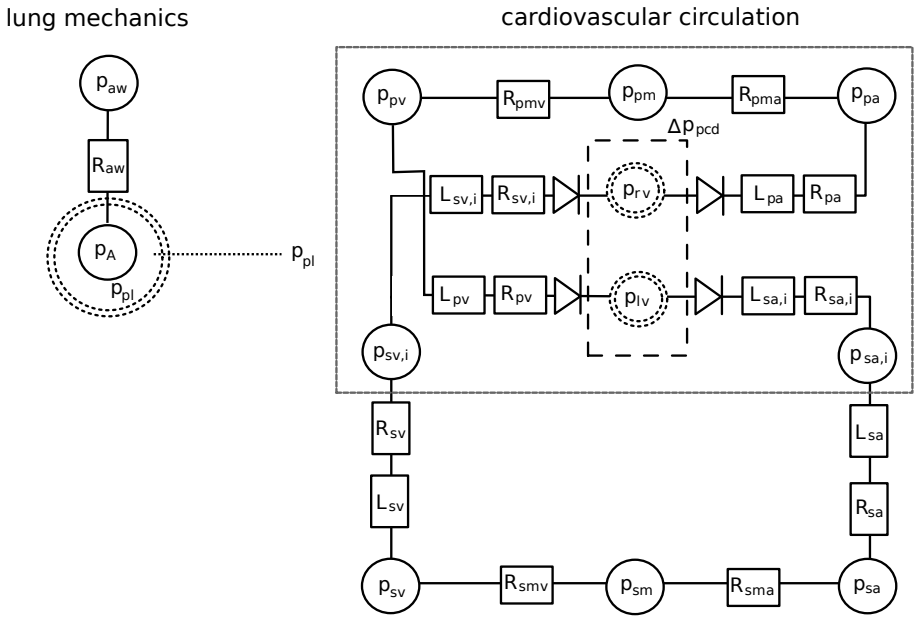


Figure 3.2: Schematic representation of the cardiorespiratory model. In the lung mechanics model (left) the mouth opening, with airway pressure p_{aw}, is connected to the alveoli, with pressure p_A, through the airway resistance R_{aw}. The dashed box around p_A represents the pleural pressure (p_{pl}). In the cardiovascular model (right), the circular elements represent compartments for storage of blood, p_{lv} and p_{rv} are the pressure in the left and right ventricle, $p_{sa,i}$ and p_{sa} are the intrathoracic and extrathoracic systemic arterial pressure, p_{sm} is the systemic microcirculation pressure, $p_{sv,i}$ and p_{sv} are the intrathoracic and extrathoracic systemic venous pressures, p_{pa} is the pulmonary arterial pressure, p_{pm} is the pulmonary microcirculation pressure, p_{pv} is the pulmonary venous pressure. The dashed box around the *lv* and *rv* represents the pericardium, that induces a transmural pericardial pressure Δp_{pcd}. The solid boxes represent segments for transport of blood. R_{sa} and R_{sv} are the systemic arterial and venous resistances, $R_{sa,i}$ and $R_{sv,i}$ are the intrathoracic arterial and venous resistances, R_{sma} and R_{smv} are the systemic microcirculation arterial and venous resistances, R_{pa} and R_{pv} are the pulmonary arterial and venous resistances, R_{pma} and R_{pmv} are the pulmonary microcirculation arterial and venous resistances, L_{sa} and L_{sv} are the systemic arterial and venous inertances, $L_{sa,i}$ and $L_{sv,i}$ are the intrathoracic arterial and venous inertances, L_{pa} and L_{pv} are pulmonary arterial and venous inertances.

3.2 Methods

A schematic overview of the combined cardiovascular and lung mechanics model is shown in Figure 3.2. In the lumped parameter description of the cardiovascular circulation we represent the storage of blood in vessels and cardiac ventricles through 'volume-storing' compartments, and transport in vessels through segments connecting these compartments. This transport is driven by the difference in absolute pressure between these compartments. In general, the absolute compartmental pressure, p, is given by:

$$p = \Delta p + \Delta p_{pcd} + p_{pl}. \tag{3.1}$$

Here, Δp is the transmural pressure drop over the ventricular or vascular wall, Δp_{pcd} is the transmural pericardial pressure drop, and p_{pl} is the pleural pressure. Here, Δp_{pcd} applies for the left and right ventricle only. Similarly, p_{pl} applies only for intrathoracic circulation compartments. The extrathoracic compartments are subject to zero external pressure.

3.2.1 Cardiovascular model

Cardiac compartments

Left and right ventricles of the heart are described with the one-fiber model (Bovendeerd et al., 2006). The one-fiber model relates local myocardial tissue behaviour (stress and strain) to global cardiac behaviour (volume and pressure), according to:

$$\Delta p = \frac{1}{3}(\sigma_{a,f} + \sigma_{p,f} - 2 \cdot \sigma_r) \cdot \ln\left(1 + \frac{V_w}{V}\right) \tag{3.2}$$

Here, Δp is the transmural cavity pressure drop in the ventricle, $\sigma_{a,f}$ is the active fiber stress, $\sigma_{p,f}$ is the passive fiber stress, σ_r is the passive radial tissue stress, V is the cavity volume and V_w is the corresponding wall volume. The relationships for $\sigma_{a,f}$, $\sigma_{p,f}$ and σ_r, are taken from literature (Bovendeerd et al., 2006), and are summarized in the Appendix. This cardiac model captures physiological behaviour such as the Starling mechanism, illustrated in Figure 3.3A, through the stroke volume - preload effect.

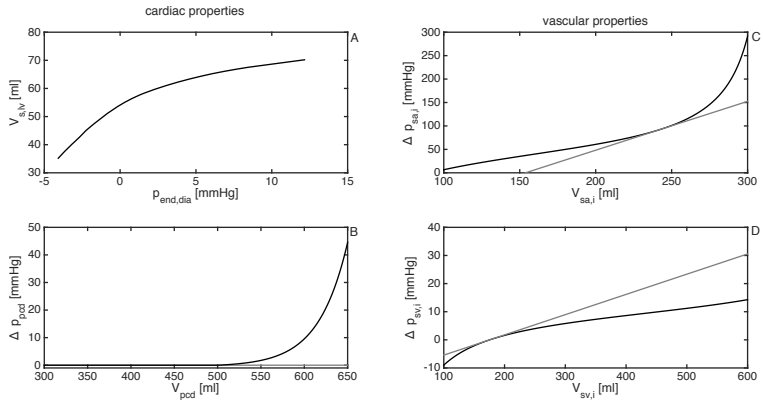


Figure 3.3: Cardiac and vascular properties used in the reference (black) and linearized (gray) model. Panel (A) shows the left ventricle properties, where $V_{s,lv}$ is left ventricle stroke volume and $p_{end,dia}$ is left ventricular end diastolic pressure. Panel (B) shows pericardial properties, where Δp_{pcd} and V_{pcd} are the pericardial pressure and volume, respectively. Panel (C) shows arterial properties where $\Delta p_{sa,i}$ and $V_{sa,i}$ are intrathoracic arterial pressure and volume, respectively, and panel (D) shows venous properties, where $\Delta p_{sv,i}$ and $V_{sv,i}$ are intrathoracic venous pressure and volume, respectively.

The ventricles are contained within the pericardium, that induces a pressure drop (Δp_{pcd}), depending on pericardial properties and volume (V_{pcd}) (Smith et al., 2004):

$$\Delta p_{pcd} = \begin{cases} 0 & V_{pcd} \leq V_{0,pcd} \\ p_{pcd,0} \cdot (e^{\lambda(V_{pcd} - V_{0,pcd})} - 1) & V_{pcd} > V_{0,pcd}. \end{cases} \tag{3.3}$$

$$V_{pcd} = V_{lv} + V_{w,lv} + V_{rv} + V_{w,rv}. \tag{3.4}$$

Here, $p_{pcd,0}$ is a pressure constant, λ is the stiffness parameter, V_{lv} and V_{rv} are the left and right ventricle cavity volume, respectively, $V_{w,lv}$ and $V_{w,rv}$ are the corresponding wall volumes, and $V_{0,pcd}$ is the pericardial unstressed volume. A visual representation of the non-linear pericardial behaviour is shown in Figure 3.3B.

Vascular compartments

The intrathoracic large vessels (aorta and vena cava) have been shown to exhibit a non-linear pressure-volume relationship (Langewouters et al., 1984; Shapiro, 1977). We describe the transmural pressure (Δp) of the large intrathoracic arteries and veins through the inverted arctan model (Langewouters et al., 1984):

$$\Delta p = p_0 - p_1 \cdot \tan\left(\pi \cdot (\frac{1}{2} - \frac{V}{V_{max}})\right) \qquad \text{with } V_{min} \leq V \leq V_{max} \tag{3.5}$$

Here, V is the vascular volume and p_0, p_1, V_{min} and V_{max} are fitting variables. This relationship describes the stiffening of the large systemic arteries at high volumes and collapse of the vena cava at low volumes, shown in Figure 3.3C & D, respectively.

In the remaining large extrathoracic vessels, the systemic microcirculation and the pulmonary circulation, we assume a linear pressure-volume relationship:

$$\Delta p = \frac{(V - V_0)}{C}, \tag{3.6}$$

where V is the vascular volume, V_0 is the unstressed volume, and C is the compliance.

Vascular segments

The pressure drop between compartments induces a flow q, that is determined by the resistance (R) and the inertance (L) of a segment:

$$\Delta p = R \cdot q + L\frac{dq}{dt}. \tag{3.7}$$

Inertia is included in the segments adjacent to the four cardiac valves (Figure 4.1) (Cox et al., 2009). Valve opening is pressure driven, while valve closure occurs when the flow through the valve becomes negative. Additionally, since the vena cava is collapsable (Backer et al., 2014) we assume the resistance to be related to the volume through (Albanese et al., 2015):

$$R_{sv,i} = k_r \cdot \left(\frac{V_{max,sv,i}}{V_{sv,i}}\right)^2 + R_{sv,i,0}. \tag{3.8}$$

Here k_r is a scaling factor, $V_{max,sv}$ is the maximum volume and $R_{sv,i,0}$ is an offset parameter.

Finally, the change in volume in each compartment is based on conservation of mass:

$$\frac{dV}{dt} = q_{in} - q_{out}, \tag{3.9}$$

where q_{in} is the inflow and q_{out} is the outflow of blood into each volume compartment.

3.2.2 Lung mechanics model

To determine the pleural pressure (p_{pl}) acting on the intrathoracic compartments, we used a simplified version of a lung mechanics model from literature (Albanese et al., 2015). The model contains the alveoli, contained within the chest wall. An airway resistance R_{aw} connects the alveoli to the mouth, represented by a

prescribed pressure p_{aw}, see Figure 4.1. The absolute pressures in the pleura (p_{pl}) and alveoli (p_A) are determined by:

$$p_{pl} = E_{cw} \cdot (V_{cw} - V_{0,cw}) \tag{3.10}$$

$$p_A = p_{pl} + E_A \cdot (V_A - V_{0,A}). \tag{3.11}$$

Here, E_{cw} is the time-dependent chest wall elastance, V_{cw} is the chest wall volume, $V_{0,cw}$ is the corresponding time-dependent unstressed volume. Similarly, E_A is the constant alveolar elastance, V_A is the alveolar volume and $V_{0,A}$ is the corresponding constant unstressed volume.

The time-varying elastance (E_{cw}) and unstressed volume ($V_{0,cw}$) of the chest wall represent spontaneous breathing:

$$E_{cw}(t) = E_{cw,pas} + a(t) \cdot (E_{cw,max} - E_{cw,pas}) \tag{3.12}$$

$$V_{0,cw}(t) = V_{0,cw,pas} + a(t) \cdot (V_{0,cw,max} - V_{0,cw,pas}). \tag{3.13}$$

where $E_{cw,pas}$ and $E_{cw,max}$ are the passive and maximal chest wall elastance, respectively, and $V_{0,cw,pas}$ and $V_{0,cw,max}$ are the passive and maximal chest wall unstressed volume, respectively. The activation function ($0 \leq a(t) < 1$) represents the effect of the respiratory muscles, modelled by a normalised, dimensionless generic respiration function (Albanese et al., 2015):

$$a(t) = \begin{cases} \frac{1}{T_i \cdot T_e} \cdot (-t^2 + T \cdot t) & 0 \leq t \leq T_i \\ \frac{1}{1-\exp(-T_e/\tau)} \cdot \left(\exp(\frac{T_i - t}{\tau}) - \exp(\frac{-T_e}{\tau}) \right) & T_i < t < T \end{cases} \tag{3.14}$$

Here, T is the respiratory period based on respiration rate RR ($T = 60/RR$), and $T = T_i + T_e$ where T_i and T_e represent the inspiratory and expiratory time, respectively, and τ is the time constant of the exponential expiratory profile.

During mechanical ventilation respiratory muscles are assumed to be passive, hence $a(t) = 0$. In this case the driving force for inspiration is a positive airway pressure (p_{aw}):

$$p_{aw} = \begin{cases} p_{end,exp} + (p_{v,max} - p_{end,exp}) \cdot \frac{1-\exp(-t/\tau_{i,v})}{1-\exp(-T_{i,v}/\tau_{i,v})} & 0 \leq t < T_{i,v} \\ p_{v,max} + (p_{i,h} - p_{v,max}) \cdot \frac{1-\exp(-(t-T_{i,v})/\tau_{i,h})}{1-\exp(-T_{i,h}/\tau_{i,h})} & T_{i,v} \leq t < T_{i,h} \\ p_{i,h} + (p_{end,exp} - p_{i,h}) \cdot \frac{1-\exp(-(t-T_{i,h})/\tau_e)}{1-\exp(-T_e/\tau_e)} & T_{i,h} \leq t < T_e. \end{cases} \tag{3.15}$$

Figure 3.1 shows the visual representation of (3.15). From a starting level at end expiratory pressure ($p_{end,exp}$), p_{aw} increases to maximal ventilation pressure ($p_{v,max}$) at the moment $T_{i,v}$ of end inspiration, drops to a holding pressure ($p_{i,h}$)

at the moment $T_{i,h}$ of end of breath holding, and drops to $p_{end,exp}$ again at the moment T_e of end expiration. Time constants $\tau_{i,v}$, $\tau_{i,h}$ and τ_e determine the rate of change during each phase.

Finally, the change in alveolar and chest wall volume is based on the air flow:

$$\frac{dV_A}{dt} = \frac{dV_{cw}}{dt} = q_{aw}, \tag{3.16}$$

where the flow of air (q_{aw}) depends on the difference between the airway pressure (p_{aw}) and alveolar pressure (p_A), and airway resistance (R_{aw}):

$$q_{aw} = \frac{p_{aw} - p_A}{R_{aw}}. \tag{3.17}$$

3.2.3 Parameter estimation

Cardiovascular parameters

All model parameters are presented in Table 3.1. They represent a normal hemodynamic state for a 70 kg person, characterised by a normovolemic blood volume of 5000 ml, mean arterial pressure ($p_{sa,i}$) of 92.9 mmHg, mean capillary pressure (p_{sm}) of 11 mmHg, mean venous pressure ($p_{sv,i}$) of 5 mmHg, ejection fraction of 67 % and a cardiac output of 5000 ml/min during spontaneous breathing.

The wall and cavity volume of the left and right ventricles were taken from Cox et al. (2009). The material parameters for the left and right ventricles in the one fiber model were taken to be equal and are adopted from Bovendeerd et al. (2006). Pericardial properties are taken from Smith et al. (2004). The systemic circulation contains 90% of the blood volume, distributed over the arteries (17.5%, 25% of which intrathoracic), capillaries (5 %) and veins (77.5%, 5% of which intrathoracic) (Albanese et al., 2015). The total unstressed volume is 70% of the blood volume (Feihl et al., 2009) and distributed accordingly. Pulmonary circulation contains 10% of the blood volume, with (unstressed) volumes distributed over arteries, capillaries and veins in the same way as in the systemic circulation. Inertances were taken from Cox et al. (2009) and divided over intra- and extrathoracic compartmens similar to the above mentioned quantities.

The parameters for the intrathoracic arteries in (3.5) were taken from Langewouters et al. (1984). For the intrathoracic vena cava, we tuned (3.5) to the original collapsible tube law (Shapiro, 1977), with the bending stiffness (K_p) taken from Müller et al. (2014) for tibial veins. The linear compliance and resistance parameters of the systemic vessels were tuned to satisfy the above mentioned pressures and cardiac output. Pulmonary resistances are calculated as a fraction (20 %) of systemic values (Shoukas, 1975). Pulmonary compliances were tuned to obtain realistic mean pulmonary pressures; p_{pa} is about 20 mmHg, p_{pm} is about 11 mmHg and p_{pv} is about 10 mmHg.

Table 3.1: Cardiovascular parameter settings, units and references used in the reference scenario of the model.

Symbol	*Value*	*Unit*	*Equation*	*Reference*
A_{BS}	1.75	m^2	3.24	Belloni et al. (2008)
C_{pa}	7.31	ml/mmHg	3.6	Calculated
C_{pm}	10.41	ml/mmHg	3.6	Calculated
C_{pv}	0.55	ml/mmHg	3.6	Calculated
C_{sa}	2.88	ml/mmHg	3.6	Calculated
C_{sm}	0.14	ml/mmHg	3.6	Calculated
C_{sv}	106.45	ml/mmHg	3.6	Calculated
k_r	1	-	3.8	Albanese et al. (2015)
L_{pa}	90	$mmHg \cdot ms^2/ml$	3.7	Cox et al. (2009)
L_{pv}	90	$mmHg \cdot ms^2/ml$	3.7	Cox et al. (2009)
L_{sa}	67.5	$mmHg \cdot ms^2/ml$	3.7	Cox et al. (2009)
$L_{sa,i}$	22.5	$mmHg \cdot ms^2/ml$	3.7	Cox et al. (2009)
L_{sv}	85.5	$mmHg \cdot ms^2/ml$	3.7	Cox et al. (2009)
$L_{sv,i}$	4.5	$mmHg \cdot ms^2/ml$	3.7	Cox et al. (2009)
$p_{0,sa}$	40	mmHg	3.5	Langewouters et al. (1984)
$p_{0,sv}$	9.5	mmHg	3.5	Albanese et al. (2015)
$p_{1,sa}$	50	mmHg	3.5	Langewouters et al. (1984)
$p_{1,sv}$	7	mmHg	3.5	Albanese et al. (2015)
$p_{pcd,0}$	0.50	mmHg	3.3	Smith et al. (2004)
R_{pa}	16.5	$mmHg \cdot ms/ml$	3.7	Calculated
R_{pma}	169.6	$mmHg \cdot ms/ml$	3.7	Calculated
R_{pmv}	23.1	$mmHg \cdot ms/ml$	3.7	Calculated
R_{pv}	15.2	$mmHg \cdot ms/ml$	3.7	Calculated
R_{sa}	150	$mmHg \cdot ms/ml$	3.7	Calculated
$R_{sa,i}$	50	$mmHg \cdot ms/ml$	3.7	Calculated
R_{sma}	1039.6	$mmHg \cdot ms/ml$	3.7	Calculated
R_{smv}	4.9	$mmHg \cdot ms/ml$	3.7	Calculated
R_{sv}	3.5	$mmHg \cdot ms/ml$	3.7	Calculated
$R_{sv,i,0}$	25	$mmHg \cdot ms/ml$	3.8	Albanese et al. (2015)
$V_{0,pa}$	112.50	ml	3.6	Calculated
$V_{0,pcd}$	500	ml	3.3	Calculated
$V_{0,pm}$	19.38	ml	3.6	Calculated
$V_{0,pv}$	368.13	ml	3.6	Calculated
$V_{0,sa}$	157.7	ml	3.6	Calculated
$V_{0,sm}$	27.56	ml	3.6	Calculated
$V_{0,sv}$	2257.5	ml	3.6	Calculated
$V_{min,sa,i}$	100	ml	3.5	Calculated
$V_{max,sa,i}$	320	ml	3.5	Langewouters et al. (1984)
$V_{min,sv,i}$	100	ml	3.5	Calculated
$V_{max,sv,i}$	668	ml	3.5, 3.8	Calculated
$V_{w,lv}$	200	ml	3.2, 3.4	Cox et al. (2009)
$V_{w,rv}$	100	ml	3.2, 3.4	Cox et al. (2009)
λ	0.03	-	3.3	Smith et al. (2004)

Table 3.1: Lung mechanics parameter settings, units and references used in the model — continued

Symbol	*Value*	*Unit*	*Equation*	*Reference*
E_A	0.05	cmH_2O/ml	3.11	Albanese et al. (2015)
$p_{0,pl}$	-5	cmH_2O	3.18, 3.19	Albanese et al. (2015)
R_{aw}	1.7	$cmH_2O \cdot ms/ml$	3.17	Albanese et al. (2015)
$V_{0,A}$	1400	ml	3.11	Albanese et al. (2015)
V_{FRC}	2400	ml	3.11	Albanese et al. (2015)
τ	555	ms	3.14	Albanese et al. (2015)
$\tau_{i,v}$	1000	ms	3.15	Innes et al. (1993)
$\tau_{i,h}$	50	ms	3.15	Innes et al. (1993)
τ_e	500	ms	3.15	Innes et al. (1993)

Lung mechanics parameters

In the lung mechanics model, R_{aw} and E_A were calculated by lumping resistances and compliances from the model by Albanese et al. (2015). Other parameters were calculated using data from literature (Innes et al., 1993), measured during mechanical ventilation and spontaneous breathing in healthy volunteers and patients. We selected one volunteer and one patient for our model simulations.

For mechanical ventilation, we considered the passive equilibrium state of the alveoli and the chest wall, characterised by patient-specific properties $V_{0,A}$ and $V_{0,cw}$. At end expiration of normal breathing (p_A = 0), V_A equals the functional residual capacity (V_{FRC}) and pleural pressure equals $p_{0,pl}$. From (3.11) we can determine $V_{0,A}$ with:

$$V_{0,A} = V_{FRC} + \frac{p_{0,pl}}{E_A}. \tag{3.18}$$

Here, V_{FRC} and $p_{0,pl}$ are taken from literature (Albanese et al., 2015). In this passive equilibrium state it holds that $E_{cw} = E_{cw,pas}$, and $V_{0,cw} = V_{0,cw,pas}$. Then (3.10) and (3.11) can be combined to determine the relation between $p_{0,pl}$, $V_{0,A}$ and $V_{0,cw,pas}$:

$$V_{0,cw,pas} = V_{0,A} - p_{0,pl} \cdot (\frac{1}{E_{cw,pas}} + \frac{1}{E_A}) \tag{3.19}$$

where we consider that $V_A = V_{cw}$.

To determine the passive chest wall elastance ($E_{cw,pas}$) in mechanical ventilation, we note that in the passive state the total lung elastance (E_L) equals:

$$E_L = E_A + E_{cw,pas}. \tag{3.20}$$

Here, we take E_A from literature (Albanese et al., 2015), and determine E_L from measurements of tidal volume (V_T) and peak airway pressure ($p_{v,max}$), obtained during mechanical ventilation (Innes et al., 1993):

$$E_L = \frac{p_{v,max}}{V_T}. \tag{3.21}$$

Combining (3.20) and (3.21) we can calculate $E_{cw,pas}$.

For spontaneous breathing, (3.12) and (3.13) are driven by additional patient-specific properties, $E_{cw,max}$ and $V_{cw,max}$. In our simulations, these parameters were manually tuned until simulated V_T visually matched experimental V_T during spontaneous breathing (Innes et al., 1993).

3.2.4 Simulations performed

The model was implemented in MATLAB 2014b. Differential equations were solved by forward Euler integration with a time step of 1 ms. All simulations started with 25 cardiac cycles without ventilation or breathing, in order to achieve a hemodynamic steady state.

Firstly, to evaluate the tuning of the lung mechanics model, we simulated one volunteer experiment from literature (Innes et al., 1993) during spontaneous breathing and mechanical ventilation. For mechanical ventilation p_{aw} was imposed by tuning (3.15) to the experimental data. ΔV_A was qualitatively compared with experimental data.

Secondly, we simulated one anesthetized patient from the same study (Innes et al., 1993), during mechanical ventilation. We used measured lung elastance (E_L), maximal airway pressure (p_{aw}), and tidal volume (V_T) reported for this patient. ΔV_A was qualitatively compared to experimental data, and the effect of mechanical ventilation on the circulation was evaluated by calculating *ppv* and *svv*.

Specifically, *ppv* is calculated as follows (Michard et al., 2000):

$$ppv = \frac{\tilde{p}_{max} - \tilde{p}_{min}}{(\tilde{p}_{max} + \tilde{p}_{min})/2} \cdot 100. \tag{3.22}$$

Here, $\tilde{p}_{max}$ and $\tilde{p}_{min}$ are the maximum and minimum intrathoracic arterial pulse pressure during one breathing cycle. The pulse pressure is obtained from the systolic and diastolic pressure in the intrathoracic arterial compartment during one heart beat.

For *svv* the same principle is used:

$$svv = \frac{V_{s,lv,max} - V_{s,lv,min}}{(V_{s,lv,max} + V_{s,lv,min})/2} \cdot 100. \tag{3.23}$$

Here, $V_{s,lv,max}$ and $V_{s,lv,min}$ are the maximum and minimum left ventricle stroke volume during one breathing cycle, respectively. Since the ventilation cycle time does not correspond to an integer number of cardiac cycle times, *ppv* and *svv* values vary slightly between consecutive breathing cycles in a hemodynamically stable situation. Therefore, similar to clinical practice the mean value of 3 subsequent ventilation cycles was used. We simulated 23 consecutive, 3 cycle intervals

to quantify mean and standard deviation of *ppv* and *svv*. Each simulation was repeated for (mild) hypo- (4500 ml) and hypervolemic (5500 ml) states.

Thirdly, we investigated the relationship of *ppv* and *svv* to total blood volume V_{bl} in detail by simulating the experimental protocol of (Belloni et al., 2008). In this study, *ppv*, *svv*, and change in cardiac index (ΔCI) were measured within 5 minutes before and after a fluid challenge of 7 ml/kg hydroxyethyl starch. We simulated this by performing a fluid challenge of 7 ml/kg of 0.9 % saline in our standard 70 kg patient (490 ml), with mechanical ventilation as in the previous simulation, for initial blood volumes varying from 4000 to 5500 ml.

To compare with experiments, we calculated the dynamic indices and cardiac index before fluid challenge as ppv_{t0}, svv_{t0} and CI_{t0}. Cardiac index (CI) was calculated as follows:

$$CI = \frac{HR \cdot V_{s,lv}}{A_{BS}}, \tag{3.24}$$

where HR is the heart rate in bpm, $V_{s,lv}$ is left ventricle stroke volume in [ml] and A_{BS} is the body surface area in m^2. Index values after the fluid challenge are denoted by ppv_{t5}, svv_{t5} and CI_{t5}. The relative variation in cardiac index (ΔCI in %) is calculated as:

$$\Delta CI = \frac{CI_{t5} - CI_{t0}}{CI_{t0}}. \tag{3.25}$$

Lastly, we performed a preliminary sensitivity analysis of *ppv* and *svv* to specific model properties considered relevant in literature (Michard et al., 2000; Kubitz et al., 2006; Feissel et al., 2004; Wyffels et al., 2010). To examine the effect of the pericardium, we performed a simulation with the pericardium removed ($\Delta p_{pcd} = 0$). To investigate the non-linear effect of arterial stiffening we linearized (3.5) about the working point in the simulation of normal hemodynamics, characterised by $V_{ref,sa,i}$ (240 ml) and $\Delta p_{ref,sa,i}$ (92.9 mmHg). To investigate the effect of venous collapse, we linearized (3.5) around $V_{ref,sv,i}$ (175 ml), and $\Delta p_{ref,sv,i}$ (0 mmHg) for the intrathoracic vena cava:

$$\Delta p_{lin} = \Delta p_{ref} + \left.\frac{dp}{dV}\right|_{V_{ref}} \cdot (V - V_{ref}), \tag{3.26}$$

This results in linearized functions for $\Delta p_{sa,i}$, $\Delta p_{sv,i}$ shown in Figure 3.3. Simulations based on the experimental protocol by Belloni et al. (2008), were repeated with one model variation at a time. Qualitative differences in the trends in the dynamic indices were analyzed.

3.3 Results

3.3.1 Mechanical ventilation vs. spontaneous breathing in a healthy volunteer

Figure 3.4 shows measured (Innes et al., 1993) and simulated lung mechanics data for a healthy volunteer during spontaneous breathing and mechanical ventilation. Measured and calculated patient-specific parameters are shown in Table 3.2.

Figure 3.4A shows that measured airway pressure (p_{aw}) sampled over multiple spontaneous breathing cycles by Innes et al. (1993), is about zero. In the model, p_{aw} was set to zero, and inspiration is driven by the activation function (3.14). Settings of patient-specific parameters (E_L, $E_{cw,pas}$,$V_{0,cw,pas}$) were obtained from simulation of mechanical ventilation for the same subject. Additionally, $E_{cw,max}$ and $V_{cw,max}$ were tuned to a tidal volume of about 1500 ml (Figure 3.4B). This spontaneous breathing results in a variation of p_{pl} from -5 to -12 cmH_2O in each breath (Figure 3.4A).

Figure 3.4C shows that measured airway pressure (p_{aw}), sampled over multiple mechanical ventilation cycles by Innes et al. (1993) is not cyclic. In our model we assumed a continuous pressure course from 0 to 18 cmH_2O as input. Figure 3.4D shows measured and simulated change in alveolar volume (ΔV_A). This change can be quantified by a tidal volume (V_T) of about 1500 ml, which corresponds to experimental data. The imposed airway pressure results in an increase in p_{pl} from -5 to +4 cmH_2O (shown in Figure 3.4C in gray).

3.3.2 Mechanical ventilation in a patient

Figures 3.5E-H show measured (Innes et al., 1993) and simulated lung mechanics data for an anesthetized patient for normal blood volume of 5000 ml. Since we are interested in *ppv* and *svv*, we show three cycles of mechanical ventilation. Measured and calculated patient-specific parameters are shown in Table 3.2. Measured airway pressure (p_{aw}) is sampled by Innes et al. (1993) over multiple ventilation cycles.

We approximate the non-cyclic pressure course from the experiment by a cyclic input for the model. This imposed airway pressure p_{aw} results in an increase in p_{pl} from -5 to +9 mmHg (shown in Figure 3.5E in gray). Figure 3.5F shows that measured and simulated change in alveolar volume (ΔV_A) equals about 620 ml.

Maximum and minimum pulse pressure in the systemic arteries equal 37 and 34.4 mmHg, respectively (Table 3.3). Averaged over 23 consecutive intervals of 3 cycles, we find a *ppv* of 7.2 $\pm$ 0.3 %. Ventilation affects variation of right ventricular volume (V_{rv}) more than that of left ventricular volume (V_{lv}).

Table 3.2: Results for subject- specific parameter calculation and fitting used in the healthy volunteer and anesthetized patient simulations.

Output	*Volunteers* ventilation	breathing	*Patient*	*Unit*	*Derivation*
$E_{cw,pas}$	0.033	0.033	0.018	cmH_2O/ml	(3.21)
$E_{cw,max}$	-	0.0059	-	cmH_2O/ml	Innes et al. (1993)
E_L	0.011	0.011	0.0233	cmH_2O/ml	Innes et al. (1993)
$p_{end,exp}$	0	-	3.2	cmH_2O	Innes et al. (1993)
$p_{i,h}$	17.7	-	16.4	cmH_2O	Innes et al. (1993)
$p_{v,max}$	18.9	0	19.7	cmH_2O	Innes et al. (1993)
RR	12	12	12	bpm	Innes et al. (1993)
T_i	1700	2222	1600	ms	Innes et al. (1993)
$T_{i,v}$	1400	-	800	ms	Innes et al. (1993)
$T_{i,h}$	1700	-	1600	ms	Innes et al. (1993)
T_e	3300	2778	3400	ms	Innes et al. (1993)
$V_{0,cw,pas}$	3525	3525	2674	ml	(3.19)
$V_{0,cw,max}$	-	4252	-	ml	Innes et al. (1993)

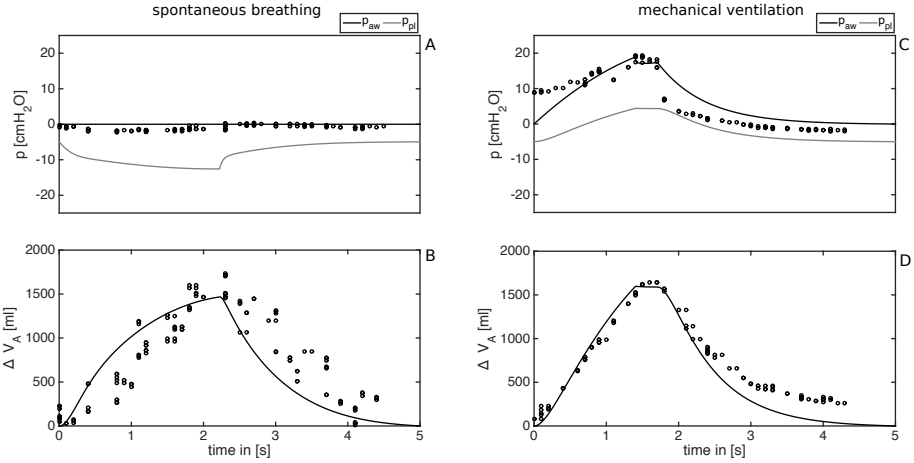


Figure 3.4: Healthy volunteer results of the experiment by (Innes et al., 1993); simulation results are shown in solid lines; experimental results are shown in symbols. Panel (A) shows lung pressure; airway pressure (p_{aw} in black) and pleural pressure (p_{pl} in gray) and panel (B) shows change in alveolar volume (ΔV_A), during mechanical ventilation. The same variables are shown in panel (C) and (D), for spontaneous breathing.

Table 3.3: Minimum and maximum right ventricular ($V_{s,rv}$) and left ventricular ($V_{s,lv}$) stroke volumes and intrathoracic pulse pressure ($\tilde{p}$), and dynamic indices *svv* and *ppv* (mean $\pm$ sd).

Output		*4500 ml*	*5000 ml*	*5500 ml*
		min max	min max	min max
$V_{s,rv}$	[ml]	25 62	40 72	52 74
$V_{s,lv}$	[ml]	43 49	54 61	61 68
svv	[%]	14.4 ± 0.2	12.1 ± 0.1	11.7 ± 0.3
$\tilde{p}$	[mmHg]	20.8 24	34.4 37	45 48
ppv	[%]	14.2 ± 0.5	7.2 ± 0.3	4.9 ± 0.3

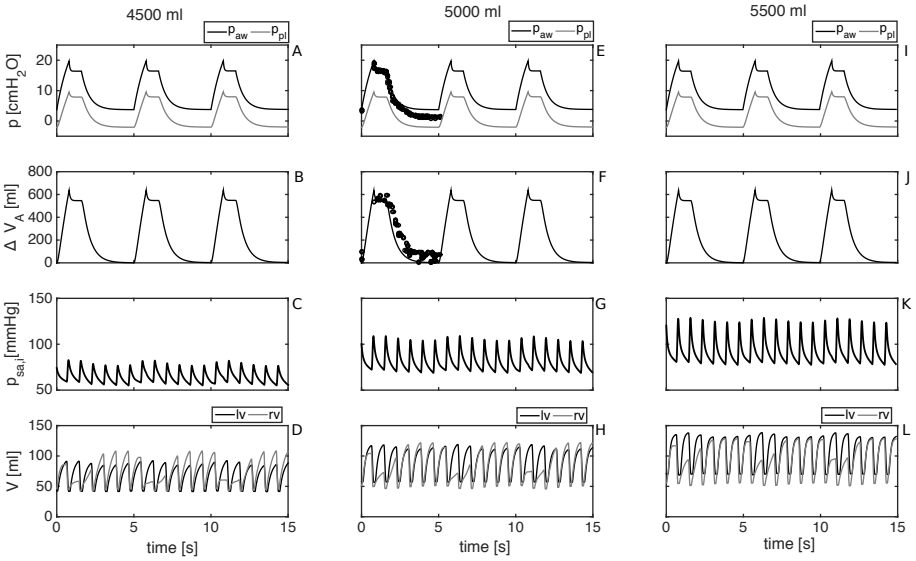


Figure 3.5: Anaesthetized patient results during 3 cycles of mechanical ventilation; simulation results are shown in solid lines; experimental results (Innes et al., 1993) are shown in symbols. Panel (A) shows lung mechanics pressure; airway pressure (p_{aw} in black) and pleural pressure (p_{pl} in gray), (B) shows change in alveolar volume (ΔV_A), (C) shows intrathoracic arterial pressure ($p_{sa,i}$), and (D) shows left ventricle volume (V_{lv} in black) and right ventricle volume (V_{rv} in gray) for V_{bl} of 4500 ml. Similarly, panel (E-H) show these variables for V_{bl} of 5000 ml and panel (I-L) for V_{bl} of 5500 ml.

Right ventricular stroke volume ($V_{s,rv}$) varies from 40 to 72 ml, with the lowest value at maximal inspiration. $V_{s,lv}$ is affected less (54 to 61 ml) and with a phase lag with respect to the right ventricle, leading to a *svv* of 12.1 $\pm$ 0.1 %.

Next, we turn to the simulation results in hypovolemia (4500 ml, Figure 3.5A-D) and hypervolemia (5500 ml, Figure 3.5I-L). Lung mechanics outputs (p_{aw}, p_{pl} and ΔV_A) are not affected by changes in V_{bl}. Cardiovascular outputs are highly affected. Pressures and pulse pressures are reduced in hypovolemia (Figure 3.5C), but *ppv* increases to 14.2 $\pm$ 0.5 % (Table 3.3). *svv* increases also to 14.4 $\pm$ 0.2 %. Hypervolemia (5500) results in higher pressures and pulse pressures (Figure 3.5K), and decreased *ppv* of 4.9 $\pm$ 0.3 % and *svv* of 11.7 $\pm$ 0.3 % (Table 3.3).

3.3.3 Fluid challenges in a ventilated patient

In Figure 3.6, the solid black lines show the effect of variation in blood volume on *ppv* and *svv* for the reference model. Here, *ppv* decreases from 27% at 4000 ml to 5.5% at 5500 ml (Figure 3.6A). *svv* decreases from 18.5 % at 4000 ml to 12.7 % at 4750 ml, after which it stabilizes around 12% (Figure 3.6B).

Figures 3.6C and 3.6D show the effect of fluid loading on the change of cardiac index (ΔCI), as a function of *ppv* before fluid loading (ppv_{t0}) or *svv* before fluid loading (svv_{t0}). In the experiment (Belloni et al., 2008), ΔCI increases from about 15% at a ppv_{t0} of 2% to about 45% at a ppv_{t0} of 30% (Figure 3.6C). And it increases from about 15% at a svv_{t0} of 10% to about 45% at a svv_{t0} of 20% to 30% (Figure 3.6D). In the reference model, the relationship between ΔCI and *ppv* is similar to the experimental one. The model predicted relation between ΔCI for *svv* agrees fairly well with the experimental data for svv_{t0} larger than 12% (Figure 3.6D). In the model, values of svv_{t0} stabilize at 12%, where ΔCI varies from 5% to 15%.

3.3.4 Sensitivity analysis

Figure 3.6 also shows the effect of model variations. Linear arterial properties flatten the trend of *ppv* values over the full volume range (Figure 3.6A, dashed black) but do not affect *svv* (Figure 3.6B, dashed black). Linear venous properties only reduce *ppv* with 1% in the lower V_{bl} range (Figure 3.6A, dashed gray) but do not affect *svv* either (Figure 3.6B, dashed gray). Removal of the pericardium results in lower *ppv* for blood volumes exceeding 4750 ml (Figure 3.6A, solid gray). Now, *svv* decreases with increasing blood volume over the whole volume range, as opposed to the situation in the reference simulation, where it stabilized above 4750 ml.

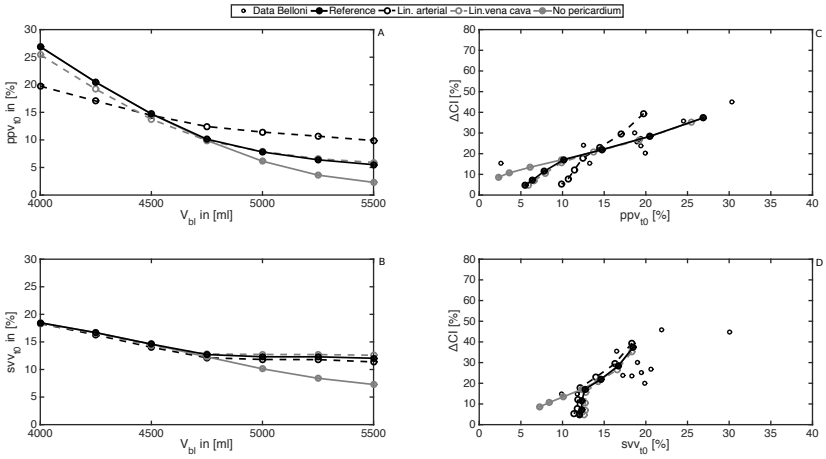


Figure 3.6: Effect of variation of blood volume (V_{bl}) and cardiovascular properties on *ppv*, *svv* and ΔCI in anesthetized patients. The effect of change in blood volume on ppv_{t0} (panel A) and svv_{t0} (panel B) are shown. The relationship between change in cardiac index (ΔCI) and *ppv* before fluid challenge (ppv_{t0} in panel C) and *svv* (svv_{t0} in panel D). Experimental results in (C) & (D) are shown with open circles. Panels (A)-(D) show model results with reference parameters (straight black), without pericardial constraints (straight gray), linearized arterial properties (dashed black) and linearized venous properties (dashed gray). For clarity of the figure standard deviations of *ppv* and *svv* are not shown.

3.4 Discussion

Clinicians use dynamic indices (*ppv* and *svv*), determined during mechanical ventilation, to assess the filling status of the circulation without the risk of fluid overloading. The aim of this study was to develop and test a mathematical model to investigate the dependence of *ppv* and *svv* on vascular volume, and cardiac and vascular properties. Eventually this may lead to better understanding of the principles of *ppv* and *svv*, and potentially a broader use of these indices in the clinic.

Our results show that we can obtain realistic changes in pleural pressure and alveolar volume in healthy volunteers and anesthetized patients during spontaneous breathing and mechanical ventilation. Also, we can obtain realistic changes in *ppv*, *svv*, and change in cardiac index for mechanically ventilated, anesthetized patients after a fluid challenge. Thirdly, the results show that *ppv* and *svv* depend on intravascular volume and pericardial and vascular properties, in decreasing order.

3.4.1 Model setup

We chose to model the cardiorespiratory system using a lumped parameter approach. The relatively low amount of model parameters to be estimated and low computational power facilitate the eventual implementation of the model into a clinical decision support tool that may assist in fluid administration in critically ill patients to avoid hypo- and hypervolemia (Rosalina et al., 2019). We took $p_{sa,i}$ as representative for the arterial blood pressure that is measured in the clinic. Pulse wave propagation models could be used to allow for more spatial variation of both arterial properties and locations of where pressures can be extracted from the mode, and to account for pulse wave reflections. However, our choice seems to be justified by the observation that computed *ppv* and *svv* are comparable to experimental data (Belloni et al., 2008). The model parameters were tuned to an arterial blood pressure of approximately 80/120 mmHg in spontaneous breathing. During mechanical ventilation, the pulse pressure and mean arterial pressure decrease due to positive intrathoracic pressure. In reality, this may be compensated by baroregulation, e.g., with a higher heart rate. In our model baroregulation is not included, so this may affect the pulse pressure slightly. We did not include baroregulation in this model. Under normal circumstances, short term (baro-) regulation controls arterial blood pressure. For patients under anesthesia, we assumed that baroregulation is fully deactivated. In the healthy volunteers, blood pressure remains around it's working level. Therefore baroregulation is not expected to affect the trends in *ppv* and *svv* simulation results.

The cardiovascular model consists of a pulmonary and systemic circulation. We added a nonlinear pressure-volume relationship for the large vessels, to account for arterial stiffening and venous collapse (Michard et al., 2000; Feissel et al., 2004), which have been hypothesized to be essential for *ppv* and *svv* (Feissel et al., 2004; Wyffels et al., 2010). Since volume variation in the rest of the vessels is relatively small, we assume that these pressure-volume relations can be modeled to be linear around their reference point. Left and right ventricles of the heart are described with the one-fiber model (Bovendeerd et al., 2006). The one-fiber model can describe the nonlinear relation between preload and stroke volume in the Frank-Starling curve of the heart (shown in Figure 3.3), as opposed to our previously used linear, cycle-averaged heart model (Rosalina et al., 2019).

The simplification of the lung mechanics model presented in literature (Albanese et al., 2015; Chiew et al., 2011) still allows for the realistic computation of the pleural pressure and reduces the number of parameters to be estimated. We added a time-varying elastance model that allows for the simulation of spontaneous breathing and mechanical ventilation with the same model parameters. The variation of E_A and $V_{0,A}$ is lumped into the chest wall time-varying elastance model. However, some groups (Chiew et al., 2014) vary this separately by adding a separate time-varying elastance model for the alveoli.

Ventricular interaction has been shown to affect *ppv* and *svv* (Kubitz et al., 2006; Sun et al., 1997). Literature shows that pericardial constraints account for 20 % of the total ventricular interaction, whereas septal interaction accounts for only 2 % (Sun et al., 1997). The latter is, therefore, not taken into account in this study. This decision may limit the applicability of the model in patients with right ventricular failure and septal bowing.

3.4.2 Comparable models in literature

Similar models to ours have been presented in literature (Albanese et al., 2015; Lansdorp et al., 2013; Messerges, 2006). Some models do not include mechanical ventilation scenarios, but only allow for simulation of spontaneous breathing (Albanese et al., 2015). In the work of Messerges (2006), pleural pressure was simply modeled as a fraction of airway pressure. The authors are not able to model the increasing systolic pressure variation in hypovolemia. The work presented by Lansdorp et al. (2013) is most similar to ours, since the authors also investigated *ppv*. But their model only allows for simulations during mechanical ventilation. Our model is unique, since we are able to model spontaneous breathing and mechanical ventilation in the same subject. This can be useful for *ppv* and *svv* determination in patients on assisted modes of mechanical ventilation that allow for intermediate spontaneous breathing (Grassi et al., 2013). Also, our cardiovascular model is more advanced since we included non linear compliances and the one-fiber model of left and right ventricle. Most importantly, we have investigated the effect of varying blood volume and specific model parameters on the *ppv* and *svv* calculation.

3.4.3 Results

Healthy volunteer results in Figure 3.4 show that we can simulate mechanical ventilation and spontaneous breathing for the same subject. However, some experimental data raise questions. Firstly, it must be noted that experimental airway pressure data does not seem cyclic. We used a cyclic variation and tuned our ventilation scheme to reported maximal and end-expiratory pressure. Secondly, the experimental data show extremely high tidal volumes ($\approx$ 1500 ml) for the conscious volunteer group. Innes et al. (1993) note that this was due to the uncomfortable measurement setup. Notably, the measured total lung elastance E_L is 0.011 cmH_2O/ml, which is high compared to 0.005 cmH_2O/ml as reported in literature (Mittman et al., 1965). This may be due to added resistance from the experimental setup. In this study the aim was to reproduce experimental data, thus we adopted the measured lung elastance in our simulations.

For anaesthetized patients we used a lung elastance E_L that is even higher (0.023 vs. 0.05 cmH_2O/ml), based on data from Innes et al. (1993). This corresponds to other findings in literature (Rehder, 1979), where it is shown that

anesthesia results in an increased unstressed chest wall volume and chest wall elastance. Consequently, clinically expected tidal volumes were measured in the patient group ($\approx$ 600 ml).

Pleural pressure (p_{pl}) is crucial in the interaction between breathing and hemodynamics. We could not test p_{pl} directly, but we find that the imposed p_{aw} leads to a change in V_A that is comparable to experimental data (Figure 3.5E-H). Assuming that our alveolar and chest wall properties are reasonable, this suggests that p_{pl} is also predicted reasonably well. V_{rv} is profoundly affected by pleural pressure increase, since it is relatively high in relation to normal transmural pressures in the right ventricle. This effect is caused by a decrease in right ventricular preload, due to a reduction in venous return and an increase in right ventricular afterload, due to increased transpulmonary pressure. Together these effects cause a reduction in $V_{s,rv}$, which is maximal at end inspiration. Through serial and direct interaction V_{lv} is affected as well, although much less. The changes in p_{pl} are relatively small as compared to normal left ventricle pressures. The transient response in left ventricular volume during the first breathing cycles, shown in Figure 3.1, corresponds to clinical observations (Michard et al., 2000). The first positive pressure cycle causes the pulmonary volume to be pushed into the left ventricle, increasing V_{lv}. After a phase lag of a few heartbeats, the reduction in $V_{s,rv}$ leads to a decrease in left ventricle preload. This decrease finally causes a minimum of $V_{s,lv}$ at end-expiration. To separate between the initial and persistent effect of preload variation, we computed *ppv* and *svv* from the third breathing cycle onwards.

When simulating the experimental protocol in Belloni et al. (2008) we assumed that the fluid challenge of 7 ml/kg HES could be simulated with a fluid bolus of 490 ml. Thus we neglected the presence of starches in HES. On the time scale of minutes to hours, this simplification might affect vascular volume and hence *ppv* and *svv*, due to a change in transmembrane fluid transport (Rosalina et al., 2019). However, on the time scale relevant in this study, transmembrane fluid transport, which is osmotic pressure-driven, is negligible. When comparing *ppv*, *svv*, and ΔCI with experimental data, we observed a good agreement in the trends. There are some noticeable discrepancies for low *svv*. In our simulations *svv* stabilizes around 12 %, whereas the clinical data suggest a continuous decrease. In the experiments, such low *svv* values were not reached. Our sensitivity analysis suggests that expected clinical trends can be captured better when reducing pericardial stiffness.

We varied arterial, venous, and pericardial properties to demonstrate their effect on the dynamic indices. Removing the pericardial constraints affects the relationship between blood volume and *svv* for blood volumes over 4750 ml (Figure 3.6). This volume corresponds to the point where total heart volume starts to increasingly exceed the pericardial unstressed volume, causing the pericardium to come into effect. When removing the pericardium, there is no constraint to the volume increase of the heart. Then, during ventilation, stroke volume changes

more freely, resulting in a low *svv*. This result is supported by experimental studies that report a variation in $V_{s,lv}$ and $V_{s,rv}$ related to the presence or absence of pericardial constraint (Kubitz et al., 2006; Wyffels et al., 2010). In the scenario without pericardium, *ppv* is affected less than *svv*, because even though stroke volume increases, the arterial compliance decreases due to arterial stiffening. The combination of these factors leads to an increased pp_{max} and pp_{min}, and a lower *ppv*. This points to an overestimation of the pericardial stiffness in our reference model, which was taken from Smith et al. (2004). The linearization of the aorta pressure-volume relation affects *ppv* much more than *svv*, because arterial stiffening highly affects pulse pressure. Finally, the linearization of the vena cava properties seems to affect *ppv* and *svv* only slightly during hypovolemia. While this result suggests that the degree of venous collapse (quantified by $\Delta p_{sv,i} < 0$) is not so important, we must note that only a small collapse of -2 mmHg was reached in this study. More research on the effects of venous collapse is recommended.

3.4.4 Future work

Our observations hold for a specific central setting of the model parameters. It is essential to perform a structured sensitivity analysis on the model parameters to investigate whether the results hold beyond the current parameter settings. This method would also allow to investigate the effect of simultaneous variations of model parameter settings. In addition, other parameters could be varied, such as myocardial passive and active properties and alveolar and chest wall properties.

The present work can be useful for clinical decision support in fluid responsiveness in various ways. Firstly, the model can be used for hypothesis generation and testing. E.g., the effect of variation in tidal volume can possibly give insights into interpreting *ppv* and *svv* in a broader patient group. Secondly, our ability to simulate *ppv* and *svv* allows for coupling of our previously developed whole body fluid exchange model (Rosalina et al., 2019) to these clinically used indices for fluid responsiveness. The measured indices can aid in making that model more patient-specific.

3.5 Conclusion

To conclude, we developed a cardiorespiratory model simulating how mechanical ventilation results in pulse pressure variation (*ppv*) and stroke volume variation (*svv*). Both indices were found to decrease with increasing blood volume until normal filling levels, in agreement with experimental data. In hypervolemia, *ppv* continued to decrease while *svv* increased slightly initially and became constant eventually. Pericardial and aortic properties were found to affect these trends clearly, while, in the current model parametrization, venous properties had only

a minor effect during hypovolemia. These findings support the evidence-based high sensitivity of *ppv* and *svv* to blood volume and provide insight into their dependence on other patient properties.

Finally, we consider the current model to be a first step towards mathematical interpretation of *ppv* and *svv* on the basis of the underlying patient characteristics, potentially leading to a broader use of these indices in the clinical environment.

Appendix

The one-fiber model relates local behaviour (stress and strain) to global behaviour (volume and pressure) (Bovendeerd et al., 2006) for each of the ventricles, according to:

$$\Delta p = \frac{1}{3}(\sigma_{a,f} + \sigma_{p,f} - 2 \cdot \sigma_r) \cdot \ln\left(1 + \frac{V_w}{V}\right) \tag{3.27}$$

Here, Δp is the transmural cavity pressure drop in the ventricle, $\sigma_{a,f}$ is the active fiber stress, $\sigma_{p,f}$ is the passive fiber stress, σ_r is the passive radial tissue stress, V is the cavity volume and V_w is the corresponding wall volume.

For the one-fiber model, the following equations are used, in combination with parameters in Table 3.4 (taken from Bovendeerd et al. 2006). The passive fiber stress is described by:

$$\sigma_{p,f} = \begin{cases} 0 & \lambda_f \leq 1 \\ \sigma_{pf0} \cdot (\exp(c_f \cdot (\lambda_f - 1)) - 1) & \lambda_f > 1. \end{cases} \tag{3.28}$$

Here, σ_{pf0} and c_f are fitting parameters. The fiber stretch ratio (λ_f) can be approximated by:

$$\lambda_f = \left(\frac{V + \frac{1}{3}V_w}{V_0 + \frac{1}{3}V_w}\right)^{\frac{1}{3}} \tag{3.29}$$

Additionally, the radial myofiber stress is described by:

$$\sigma_r = \begin{cases} 0 & \lambda_r \leq 1 \\ \sigma_{pc0} \cdot (\exp(c_c \cdot (\lambda_r - 1)) - 1) & \lambda_r > 1. \end{cases} \tag{3.30}$$

Here, σ_{pc0} and c_c are fitting parameters. The radial stretch ratio (λ_r) is described by:

$$\lambda_r = \frac{1}{\lambda_f^2}$$

Finally, active stress $\sigma_{a,f}$ is dependent on sarcomere length (l_s), time passed since activation (t_a) and sarcomere shortening velocity (v_s)

$$\sigma_{a,f}(l_s, t_a, v_s) = f(l_s)\, g(l_s, t_a)\, h(v_s) \tag{3.31}$$

with:

$$f(l_s) = \begin{cases} 0 & l_s \leq l_{sa0} \\ \sigma_{ao} \tanh^2(c_a(l_s - l_{sa0})) & l_s > l_{sa0}. \end{cases} \tag{3.32}$$

$$g(t_a) = \begin{cases} 0 & t_a < 0 \\ sin^2(\frac{\pi t_a}{2\tau_r}) & 0 \leq t_a \leq \tau_r \\ 1 - sin^2(\frac{\pi(t_a-\tau_d)}{2\tau_d}) & \tau_r \leq t_a < \tau_r + \tau_d \\ 0 & t_a \leq \tau_r + \tau_d \end{cases} \tag{3.33}$$

$$\tau_r = \tau_{r1} + a_r(l_s - l_{s0}) \tag{3.34}$$

$$\tau_d = \tau_{d1} + a_d(l_s - l_{s0}) \tag{3.35}$$

$$h(v_s) = \frac{1 - (v_s/v_0)}{1 + c_v(v_s/v_0)} \tag{3.36}$$

Table 3.4: Parameter settings, units and references used in the one-fiber model taken from Bovendeerd et al. (2006).

Symbol	*Value*	*Unit*	*Equation*	*Symbol*	*Value*	*Unit*	*Equation*
a_d	400	ms/μm	3.30	l_{s0}	1.9	μm	3.32
a_r	100	ms/μm	3.30	v_0	0.01	μm/ms	3.36
c_a	1.2	-	3.30	τ_{d1}	240	ms	3.33
c_c	9	-	3.30	τ_{r1}	140	ms	3.33
c_f	12	-	3.28	σ_{a0}	1504	mmHg	3.28
c_v	0	-	3.28	σ_{pf0}	6.77	mmHg	3.28
l_{sa0}	1.5	μm	3.32	σ_{pc0}	1.50	mmHg	3.30

Bibliography

Albanese, A. et al. (2015). "An integrated mathematical model of the human cardiopulmonary system: Model development". *American Journal of Physiology - Heart and Circulatory Physiology* 310, H899–921.

Backer, D. D. and Fagnoul, D. (2014). "Intensive care ultrasound: VI. Fluid responsiveness and shock assessment". *Annals of the American Thoracic Society* 11.1, pp. 129–136.

Belloni, L. et al. (2008). "Assessment of fluid-responsiveness parameters for off-pump coronary artery bypass surgery: a comparison among LiDCO, transesophageal echochardiography, and pulmonary artery catheter". *Journal of Cardiothoracic and Vascular Anesthesia* 22.2, pp. 243–248.

Bovendeerd, P. H. et al. (2006). "Dependence of intramyocardial pressure and coronary flow on ventricular loading and contractility: A model study". *Annals of Biomedical Engineering* 34.12, pp. 1833–1845.

Brandstrup, B. (2006). "Fluid therapy for the surgical patient." *Best Practice & Research. Clinical Anaesthesiology* 20.2, pp. 265–283.

Cannesson, M. et al. (2011). "Assessing the Diagnostic Accuracy of Pulse Pressure A "Gray Zone" Approach". *Anesthesiology* 115.2, pp. 231–241.

Cecconi, M, Singer, B, and Rhodes, A (2011). "The fluid challenge". *Annual Update in Intensive Care and Emergency Medicine 2011* 1, pp. 332–339.

Cecconi, M. et al. (2015). "Fluid challenges in intensive care: the FENICE study". *Intensive Care Medicine* 41.9, pp. 1529–1537.

Chiew, Y. S. et al. (2011). "Model-based PEEP optimisation in mechanical ventilation". *BioMedical Engineering Online* 10, pp. 1–16.

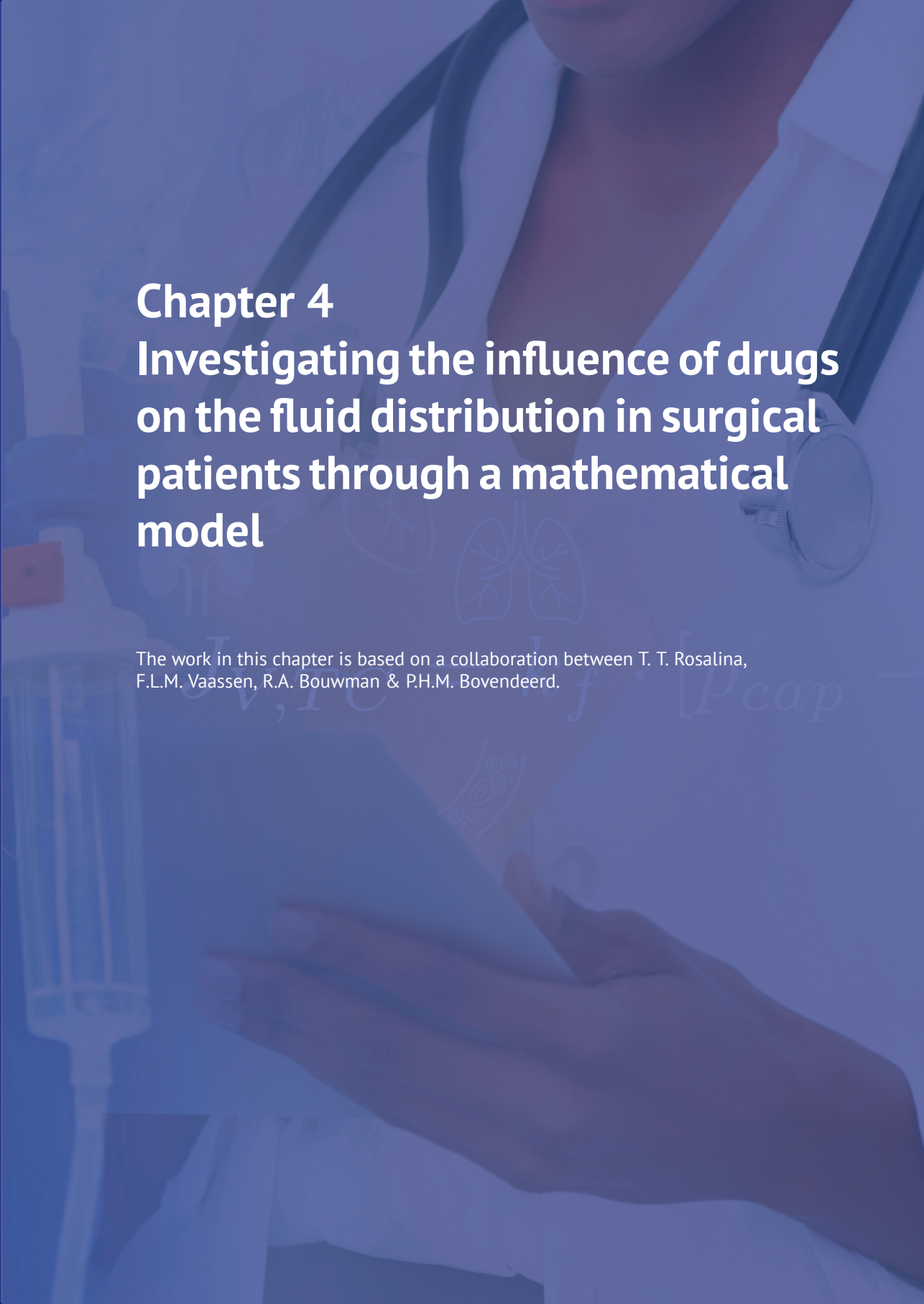
Chiew, Y. S., Poole, S. F., and Redmond, D. P. (2014). "Time-Varying Respiratory Elastance for Spontaneous Breathing Patients". *IFAC Proceedings Volumes* 47.3, pp. 5659–5664.

Cox, L. G. et al. (2009). "A mathematical model to evaluate control strategies for mechanical circulatory support". *Artificial Organs* 33.8, pp. 593–603.

Daudel, F. et al. (2010). "Pulse pressure variation and stroke volume variation during increased intra-abdominal pressure: An experimental study". *Critical Care* 14.1, R122.

Feihl, F. and Broccard, A. F. (2009). "Interactions between respiration and systemic hemodynamics. Part I: Basic concepts". *Intensive Care Medicine* 35, pp. 45–54.
Feissel, M. et al. (2004). "The respiratory variation in inferior vena cava diameter as a guide to fluid therapy". *Intensive Care Medicine* 30.9, pp. 1834–1837.
Frank, O. (1895). "Zur dynamik des herzmuskels". *Zeitschrift fur Biologie* 32, pp. 370–447.
Grassi, P. et al. (2013). "Pulse pressure variation as a predictor of fluid responsiveness in mechanically ventilated patients with spontaneous breathing activity: a pragmatic observational study". *HSR Proceedings in Intensive Care and Cardiovascular Anesthesiology*.
Holte, K., Sharrock, N., and Kehlet, H. (2002). "Pathophysiology and clinical implications of perioperative fluid excess". *British Journal of Anaesthesia* 89.4, pp. 622–32.
Innes, J. A. et al. (1993). "Within breath modulation of LV function during normal breathing and PPV in man". *Journal of Physiology* 460, pp. 487–502.
Kubitz, J. C. et al. (2006). "The influence of positive end-expiratory pressure on stroke volume variation and central blood volume during open and closed chest conditions". *European Journal of Cardiothoracic Surgery* 30.1, pp. 90–95.
Langewouters, G. J., Wesseling, K. H., and Goedhard, W. J. (1984). "The static elastic properties of 45 human thoracic and 20 abdominal aortas in vitro and the parameters of a new model". *Journal of Biomechanics* 17.6, pp. 425–435.
Lansdorp, B. et al. (2013). "A mathematical model for the prediction of fluid responsiveness". *Cardiovascular Engineering and Technology* 4.1, pp. 53–62.
Latta, T. (1832). "Malignant cholera". *Lancet* ii, pp. 45–274–7.
Marik, P. E. et al. (2009). "Dynamic changes in arterial waveform derived variables and fluid responsiveness in mechanically ventilated patients: A systematic review of the literature". *Critical Care Medicine* 37.9, pp. 2642–2647.
Messerges, J. (2006). "Modeling systolic pressure variation due to positive pressure ventilation". *Annual International Conference of the IEEE Engineering in Medicine and Biology - Proceedings*, pp. 1806–1809.
Michard, F. and Teboul, J. L. (2000). "Using heart-lung interactions to assess fluid responsiveness during mechanical ventilation". *Critical Care* 4.5, pp. 282–289.
Michard, F., Chemla, D., and Teboul, J.-L. (2015). "Applicability of pulse pressure variation: how many shades of grey?" *Critical Care* 19.1, pp. 15–17.
Mittman, C. et al. (1965). "Relationship between chest wall and pulmonary compliance and age". *Journal of Applied Physiology* 20.6, pp. 1211–1216.
Müller, L. O. and Toro, E. F. (2014). "A global multiscale mathematical model for the human circulation with emphasis on the venous system". *International Journal for Numerical Methods in Biomedical Engineering* 30.7, pp. 681–725.
Rehder, K. (1979). "Effect of anaesthesia-paralysis and mechanical ventilation". *Canadian Anaesthesiology Society Journal* 26.6, pp. 451–459.
Rosalina, T. T. et al. (2019). "A mathematical model to investigate the effects of intravenous fluid administration and fluid loss". *Journal of Biomechanics* 88, pp. 4–11.

Shapiro, A. H. (1977). "Steady Flow in Collapsible Tubes". *Journal of Biomechanical Engineering* 99.3, pp. 126–147.
Shoukas, A. A. (1975). "Pressure-Flow and Pressure-Volume Relations in the Entire Pulmonary Vascular Bed of the Dog Determined by Two-Port Analysis". *Circulation Research* 37, pp. 809–818.
Smith, B. W. et al. (2004). "Minimal haemodynamic system model including ventricular interaction and valve dynamics". *Medical Engineering and Physics* 26.2, pp. 131–139.
Starling, E. and Visscher, M. (1926). "The regulation of the energy output of the heart". *Journal of Physiolology* 62, pp. 243–261.
Sun, Y et al. (1997). "A comprehensive model for right-left heart interaction under the influence of pericardium and baroreflex." *The American Journal of Physiology* 272.3 Pt 2, H1499–515.
Wyffels, P. A. H., Sergeant, P., and Wouters, P. F. (2010). "The value of pulse pressure and stroke volume variation as predictors of fluid responsiveness during open chest surgery". *Anaesthesia* 65.7, pp. 704–709.



Chapter 4
Investigating the influence of drugs on the fluid distribution in surgical patients through a mathematical model

The work in this chapter is based on a collaboration between T. T. Rosalina, F.L.M. Vaassen, R.A. Bouwman & P.H.M. Bovendeerd.

Abstract

Fluid administration in surgical patients is necessary to compensate for bleeding, evaporation, perspiration and urine production. Unfortunately, administration of the correct amount of fluid is difficult, due to the lack of applicability and sensitivity of clinically available measurements, while direct measurements are not available. This may leave patients at risk of becoming hypo- or hypervolemic. In previous work, we developed a mathematical model to predict the fluid (re-) distribution in the human body, and evaluated it on the basis of experimental data obtained in healthy volunteers. In the current study we aim to test this model for use in surgical patients. For this purpose, we extended our model with pharmacokinetic and - dynamic models to describe the effect of anesthesia, inotropes and vasopressors. We simulated three intra-operative patient scenario's, and compared measured and model predicted blood pressure and heart rate signals. Additionally, we investigated the effect of anesthesia, inotropes and vasopressors on the final fluid distribution. The results show that the effect of anesthesia should be taken into account for predicting fluid distribution at the end of surgery, whereas the effect of inotropes and vasopressors is negligible.

4.1 Introduction

During surgery, patients lose fluid through bleeding, evaporation, perspiration, and urine production. To avoid complications related to hypovolemia, anesthesiologists administer intravenous fluid (Latta, 1832). However, administration of too much fluid has the risk of causing hypervolemia, manifested as fluid build-up in the interstitial space (Holte et al., 2002). This build-up may lead to complications such as microvascular compression, decreased renal function, and severe discomfort. Avoiding these complications is hard due to the limited sensitivity of clinically available measures, while the lack of direct measurements of fluid status are lacking.

Arterial blood pressure is one of the clinical measurements most used as a surrogate for fluid status (Cecconi et al., 2015). Indeed, arterial blood pressure depends strongly on vascular filling, but it is also affected by neurohumoral control and the effect of drugs. Additionally, vascular filling is not a good indicator of interstitial fluid status. It has been shown that vascular volume is well controlled by the transcapillary exchange of fluid between the vessels and the interstitium. For example, in volunteer experiments, approximately two-thirds of the administered fluid was shown to end up in the interstitial space on a time scale of about half an hour (Watenpaugh et al., 1992), while the vascular volume and arterial blood pressure returned to normal quickly. These observations show that arterial blood pressure is not an ideal measure for hypervolemia related complications. Other clinically used, indirect, measurements for fluid status and fluid responsiveness include dynamic indices pulse pressure variation (*ppv*) and stroke volume variation (*svv*). These indices are proven to be highly related to the vascular filling status (Michard et al., 2000; Marik et al., 2009), but they do not directly predict the interstitial fluid status and hypervolemia-related complications.

In our research, we aim to develop a clinical decision support model for fluid administration, combining vascular and interstitial fluid status. First, we developed a cardiovascular fluid exchange model and tested this model for fluid redistribution after saline infusion in healthy volunteers (Rosalina et al., 2019). Next, we included cardiorespiratory interactions to simulate clinically used indices, *ppv* and *svv*. In this chapter, we present a pilot study on the role of drugs in surgical patients.

Drugs will affect blood pressure. Vasopressors and inotropes like phenylephrine, ephedrine and noradrenaline increase blood pressure. Anesthesia, induced for example by propofol or sevoflurane, reduces blood pressure directly as well as the action of the baroreflex, that controls arterial blood pressure (Sellgren et al., 1994). The extent of this reduction is unclear. Changes in blood pressure directly influence the fluid balance by changing capillary pressure and the fluid exchange rate (Rosalina et al., 2019). Indirectly, drugs influence the fluid balance since the changes in blood pressure are used as a clinical guide to adapt the infusion protocol.

To investigate the first effect, we extend our model with the effect of drugs on blood pressure and subsequently, on the fluid status. We describe the hemodynamic effect of anesthetics, inotropes and vasopressors with pharmacokinetic and -dynamics models. Whereas these models are commonly accepted and easily implemented, the patient-specific estimation of the model parameter values, especially pharmacodynamic parameters, is cumbersome. In particular, patients may respond quite differently to the same drug treatment. In clinical decision support modeling, the balance between model complexity and output uncertainty is one to be constantly evaluated. To evaluate this balance, we investigated which, if any, drugs should be taken into account to predict the fluid distribution at the end of surgery accurately.

In our approach, we coupled previously published pharmacokinetic and pharmacodynamic models (Marsh et al., 1991; Wissing et al., 2000; Hengstmann et al., 1982; Kazama et al., 1999; Nygren et al., 2006) to our cardiovascular fluid exchange model (Rosalina et al., 2019). To test the predictive capabilities of the model, we perform a pilot study with simulations of three perioperative patients. Firstly, we model all three patients using generic values for the pharmacokinetics and -dynamics model parameters. We compare simulated blood pressure and heart rate to the measurements and calculate the fluid distribution in these patients. Secondly, parameters are manually tuned to better approximate blood pressure measurements for each patient. We expect that these patient-specific simulations better capture the fluid distribution.

Thirdly, to investigate the effect of vasopressors and inotropes, we simulate the patient with only a model for anesthesia. We hypothesize that the driving force for fluid exchange is the average pressure during surgery, which is driven by anesthesia. To test this hypothesis further, we perform additional simulations without any effect of drugs. Here, only the effect of fluid administration and fluid loss contributes to the change in blood pressure. To investigate the effect of baroregulation, we perform the simulations without any drugs with and without regulation. Based on these results, we analyze the effect of drugs on the fluid distribution at the end of surgery.

4.2 Methods

The cardiovascular and fluid exchange model is extensively described in Rosalina et al. (2019). In short, we combined the cardiovascular system, including the heart, systemic circulation, and baroregulation, with a description for urine production, and fluid exchange. In this chapter, we extend the model with pharmacokinetics and - dynamics models for perioperative drugs, anesthetics, inotropes and vasopressors.

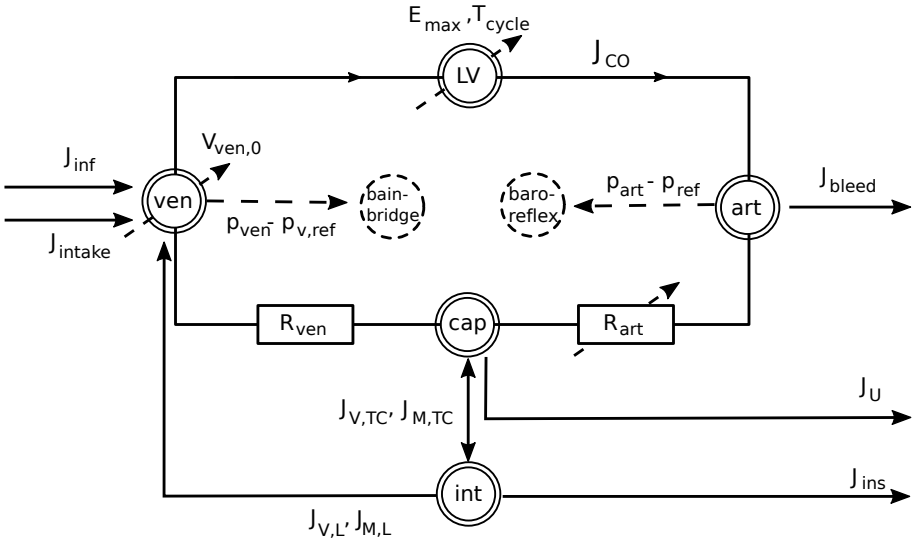


Figure 4.1: Schematic overview of the cardiovascular fluid exchange model: the left ventricle (*LV*) generates a blood flow (J_{CO}) that passes through the arteries (*art*), capillaries (*cap*) and veins (*ven*) facing a total resistance that is composed of an arterial and a venous part (R_{art} and R_{ven}). The baroregulation responds to the deviation of the mean arterial pressure (p_{art}) from a reference pressure (p_{ref}), and affects R_{art}, venous unstressed volume ($V_{ven,0}$), heart contractility (E_{max}) and cardiac cycle time (T_{cycle}). The Bainbridge reflex responds to the deviation of the mean venous pressure (p_{ven}) from the venous reference pressure ($p_{v,ref}$) and affects T_{cycle}. The fluid exchange with the environment is determined by a basal fluid intake (J_{intake}), fluid infusion (J_{inf}), bleeding (J_{bleed}), urine production (J_U) and insensible losses (J_{ins}). The fluid exchange between the vascular compartment and the interstitium (*int*) consists of transcapillary fluid flow ($J_{V,TC}$) and lymphatic fluid ($J_{V,L}$). These fluid flows are related to corresponding transcapillary ($J_{M,TC}$) and lymph protein flows ($J_{M,L}$).

4.2.1 Cardiovascular fluid exchange model

Our cardiovascular fluid exchange model (Rosalina et al., 2019) is shown schematically in Figure 4.1. It includes a cycle-averaged model for left ventricular function. The pressure is determined by a linear relationship between pressure and volume, described by the maximal and passive elastances of the left ventricle (E_{max} and E_{pas}). The arterial and venous pressure are determined by compliances and unstressed volumes. Capillary pressure is calculated with cardiac output and peripheral resistance.

Arterial pressure is regulated by baroregulation and the Bainbridge reflex (Jongen et al., 2016; Rosalina et al., 2019). This regulation works through a response of four cardiovascular effectors; the cardiac contractility (E_{max}) and cardiac cycle time (T_{cycle}), precapillary peripheral resistance (R_{art}), and venous unstressed volume ($V_{ven,0}$).

The fluid exchange model describes the intake of fluid, through intravenous infusion (J_{inf}) and basal intake (J_{intake}), the loss of fluid, through bleeding, (J_{bleed}), perspiration (J_{per}), and urine production (J_U), and the exchange of fluid (subscript *V*) and proteins (subscript *M*) between the vascular and interstitial space, through transcapillary (subscript *TC*) exchange ($J_{V,TC}$, $J_{M,TC}$), and lymph (subscript *L*) flow ($J_{V,L}$, $J_{M,L}$). The balance between hydrostatic and osmotic pressure is the driving force for transcapillary fluid exchange, moving volume and proteins in between the vascular (V_{PL}, M_{PL}) and interstitial compartment (V_I, M_I).

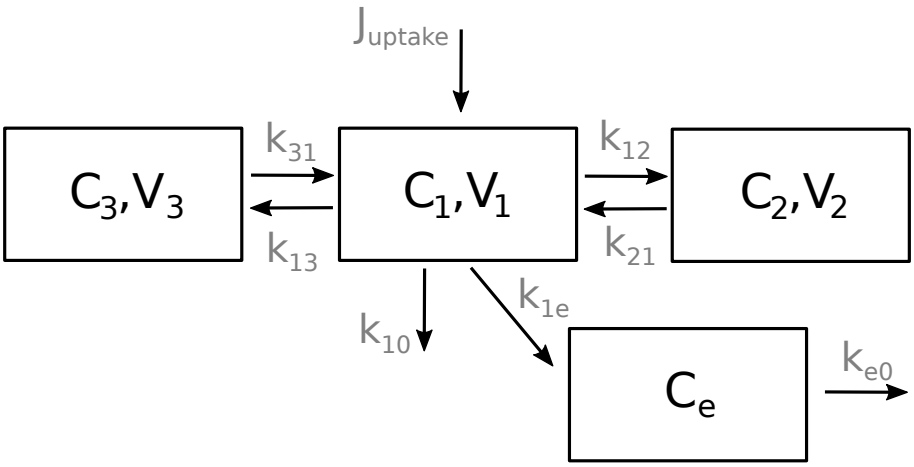


Figure 4.2: General three-compartment model used to the simulate the pharmacokinetic drug pathway with effect-site compartment. C_1 and V_1 are the plasma concentration and volume, C_2 and V_2 are the tissue concentration and volume, C_3 and V_3 are the deep tissue concentration and volume, C_e is the effect-site concentration, J_{uptake} is the infusion rate, k_{12} and k_{21} are the exchange rate between plasma and tissue, k_{13} and k_{31} are the exchange rate between plasma and deep tissue, k_{10} is the elimination rate from the plasma compartment, and k_{1e} and k_{e0} are effect site intake and elimination rates, respectively.

4.2.2 Pharmacokinetics

Pharmacokinetics describes the uptake, distribution, and elimination of drugs by the body. The distribution is generally modeled by a 3-compartment model with an effect site (Marsh et al., 1991; Kazama et al., 1999), shown schematically in Figure 4.2. The basic compartments are the central blood compartment, with drug concentration C_1 in mg/l and volume V_1 in l, a tissue compartment, with concentration C_2 in mg/l and volume V_2 in l, and a deep tissue compartment, with concentration C_3 in mg/l and volume V_3 in l. Uptake J_{uptake} in mg/min can occur through intravenous infusion or inhalation (Section 4.2.3). Elimination occurs through drug metabolism, described through a rate constant k_{10} in min^{-1}. Exchange between compartments is determined with rate constants k_{12}, k_{21}, k_{13} and k_{31} in min^{-1}.

The corresponding mass balance equations are as follows:

$$V_1 \cdot \frac{dC_1}{dt} = J_{uptake} - k_{12} \cdot V_1 \cdot C_1 + k_{21} \cdot V_2 \cdot C_2 - k_{13} \cdot V_1 \cdot C_1 + k_{31} \cdot V_3 \cdot C_3 - k_{10} \cdot V_1 \cdot C_1 \tag{4.1}$$

$$V_2 \cdot \frac{dC_2}{dt} = k_{12} \cdot V_1 \cdot C_1 - k_{21} \cdot V_2 \cdot C_2 \tag{4.2}$$

$$V_3 \cdot \frac{dC_3}{dt} = k_{13} \cdot V_1 \cdot C_1 - k_{31} \cdot V_3 \cdot C_3 \tag{4.3}$$

Finally, the concentration C_e in mg/l, that actually induces the effect, is related to the concentration in the blood compartment (C_1), according to Kazama et al. (1999):

$$\frac{dC_e}{dt} = C_1 \cdot k_{1e} - C_e \cdot k_{e0}, \tag{4.4}$$

with the rate constants for transport from blood compartment to the effect compartment (k_{1e}) and for effect elimination (k_{e0}), in min^{-1}.

4.2.3 Administration pathways

Perioperative drugs can be administered through intravenous or inhalation pathways. The intravenous pump infusions are modeled through a constant rate (J_{uptake}) in mg/min, determined by the concentration (C_{drug}) in mg/ml and infusion speed (q_{drug}) in ml/min:

$$J_{uptake} = q_{drug} \cdot C_{drug}. \tag{4.5}$$

For intravenous bolus infusions, we use a Dirac delta function $\delta(t)$, multiplied with the infusion speed (q_{drug}) in ml/min and drug concentration (C_{drug}) in mg/ml. Hence,

$$J_{uptake} = \delta(t) \cdot q_{drug} \cdot C_{drug}. \tag{4.6}$$

The pharmacokinetic pathway of inhalation drugs occurs through uptake via the lungs. Through mechanical ventilation, air with a concentration of anesthetics reaches the alveoli, where gas exchange with the blood takes place. We assume a steady state situation, in which the blood concentration (C_1) is proportional to alveolar concentration (ρ_{alv}). To determine ρ_{alv} in mol/m^3, we use the ideal gas equation:

$$\rho_{alv} = \frac{C_{alv} \cdot P_{atm}}{R \cdot T}. \tag{4.7}$$

Here, C_{alv} is the alveolar concentration in %, P_{atm} is the atmospheric pressure in Pa, R is the ideal gas constant in J/mol $\cdot$ K, T is the temperature in K. The blood concentration (C_1 in mg/l) is obtained from:

$$C_1 = \lambda_{BG} \cdot \rho_{alv} \cdot M_{drug} \cdot 1000, \tag{4.8}$$

with the unitless blood-gas partition coefficient (λ_{BG}) and molar mass for a specific drug (M_{drug}) in mg/mol.

4.2.4 Pharmacodynamics

Pharmacodynamics describes the relationship between the effect site concentration (C_e), as derived by the kinetics model, and the observed value of an effector (E). In this study, we investigate the effect of drugs on blood pressure. Firstly, these drugs act through cardiovascular effectors, indirectly affecting blood pressure. Specifically, these effectors are the venous unstressed volume ($V_{ven,0}$), peripheral resistance (R_p) and cardiac cycle time (T_{cycle}). Secondly, anesthesia reduces, but not completely blocks, the baroreceptor reflex (Sellgren et al., 1994). This effect is modelled through k_{baro}, representing a change in reference effector gain k_{eff}.

For propofol we use a sigmoidal model for the relationship between effect E and effect-site concentration C_e (Derendorf et al., 1999):

$$E = E_0(1 + k_{max} \cdot \frac{C_e^\gamma}{C_{50}^\gamma + C_e^\gamma}) \tag{4.9}$$

where E_0 is the reference setting of the effector, k_{max} is the maximal relative change of the effector value, C_e is the concentration at the effect site, C_{50} is the concentration of the drug that produces half of the maximal effect, and γ is the steepness parameter.

For other drugs, we assume a linearisation around an empirical reference concentration:

$$E = E_0 \cdot (1 + k_{ref} \cdot \frac{C_e}{C_{ref}}). \tag{4.10}$$

where k_{ref} is a reference change of the effector value, obtained at reference concentration (C_{ref}). Our baroregulation model was described in Chapter 2 (2.28).

We model the change in baroregulatory control due to anesthesia as a reduction in reference effector gain (k_{eff}) by a dimensionless factor k_{baro}. The new equations for the receptor-to-effector signal are as follows:

$$E = E_0 \cdot (1 + k_{baro} \cdot k_{eff} \cdot r(t)), \tag{4.11}$$

where $r(t)$ is the baroreflex signal, k_{eff} is the relative change of the effector without anesthesia, and k_{baro} represents the relative reduction of this effect due to anesthesia. We assume a linear reduction of the baroreflex sensitivity with the anesthesia effect site concentration (C_e) to a minimum ($k_{baro,min}$):

$$k_{baro} = \begin{cases} (k_{baro,min} - 1) \cdot \frac{C_e}{C_{ref}} + 1 & \text{for } C_e \leq C_{ref} \\ k_{baro,min} & \text{for } C_e > C_{ref} \end{cases} \tag{4.12}$$

4.2.5 Parameter estimation

Cardiovascular parameters

The parameter settings for the cardiovascular system were tuned to yield initial conditions for each patient such as arterial blood pressure and cardiac output, obtained from the data (Section 4.2.6). Heart rate was expected to be higher than normal at the beginning of surgery, due to stress. Therefore, initial conditions were tuned to preoperative data in rest. Total blood volume (V_{bl}) was determined by an empirical equation (Drobin et al., 1999):

$$V_{bl} = \alpha_1 \cdot w + \alpha_2 \cdot h^3 + \alpha_3 \tag{4.13}$$

where w is the weight in kg, h is the height in m, and empirical parameters (α_1 = 32.19 ml/kg, α_2= 366.9 ml/m^3 and α_3= 604.1 ml).

The total blood volume is divided over the arteries (17.5 %), microcirculation (5 %) and veins (77.5 %). The total venous unstressed volume is 70% of V_{bl} (Feihl et al., 2009) and divided over the vessels accordingly. Settings for most parameters in the fluid exchange model are taken from (Xie et al., 1995). Since urine production is reduced during surgery, J_{UN} was adapted to 0.5 ml/kg/h (Gupta et al., 2016). Remaining parameters k_f, $J_{L,N}$, PS and J_{intake} were computed to satisfy steady state conditions (Rosalina et al., 2019).

Propofol

Propofol is an anesthetic drug that induces a decrease in blood pressure through a decrease in peripheral resistance and venous unstressed volume (Sullivan et al., 2010). Weight dependent pharmacokinetic rate constants were taken from (Marsh et al., 1991). We use the full three-compartment model with an effect

compartment as described by the authors (Table 4.1). Since there is no information available on the change of the effectors separately, the cumulative change in blood pressure is used to determine parameter settings. Kazama et al. (1999) describe the total effect of propofol on blood pressure, characterised by C_{50}, k_{max} and γ. Pharmacodynamic parameters are taken from this study and k_{max} is determined with

$$k_{max} = (p_{art,max} - p_{ref,max})/p_{art,max}. \tag{4.14}$$

In our study, we assume $p_{art,max}$ is 150 mmHg and $p_{ref,max}$ is 80 mmHg. We simulate this cumulative effect through the underlying sigmoidal model (4.9) for R_p and $V_{ven,0}$ (Table 4.2). Finally, there is an effect on the baroregulation, that is modeled through (4.12). Since there is little quantitative data on the effect of anesthesia on the baroregulation, the reference concentration (C_{ref}), is determined from manual tuning to patient A. $k_{baro,min}$ is tuned so a maximal reduction to 20 % of the baroregulation strength can be achieved (Table 4.3).

Sevoflurane

Sevoflurane is an anesthetic inhalation drug with similar effect on blood pressure as propofol. This drug is modeled using a two-compartment model with an effect site compartment, adapted from (Wissing et al., 2000). Pharmacokinetic rate constants are taken from Wissing et al. (2000) and λ_{bg} is taken from Ghimenti et al. (2013). Due to a lack of data on the effect of sevoflurane on blood pressure, k_{e0} was manually tuned to patient A. The pharmacodynamic parameters in the linear model (Equation 4.10), were determined from patient A as well. The concentration at maximal blood pressure drop is labeled C_{ref}. Subsequently, k_{ref} was taken from literature (Ciofolo et al., 1999) In our study, we simulate the pharmacodynamic effect with our linear model (4.10) for R_p and $V_{ven,0}$. Finally, the effect on the baroregulation is modeled through Equation (4.12). Since there is little quantitative data on the effect of anesthesia on the baroregulation the reference concentration C_{ref}, is determined from tuning to patient A. $k_{baro,min}$ is tuned so a maximal reduction to 20 % of the baroregulation strength can be achieved.

Phenylephrine and ephedrine

Phenylephrine and ephedrine are both drugs that induce a quick increase in blood pressure. They are modeled by a 2-compartment model with an additional effect site, based on the work by Hengstmann et al. (1982). Pharmacokinetic parameters are taken to be the same for both drugs. The injection of these drugs leads to an increase in blood pressure by an increase in vascular resistance and decrease of venous unstressed volume. Ephedrine has an additional effect, reducing cardiac cycle time. For phenylephrine, the relative change of R_p for a reference concentration (C_{ref}) is taken from Nygren et al. (2006). We assume that there is an equal

relative change in $V_{ven,0}$ (Magder, 2016). For ephedrine, no reference pharmacodynamic data were found. Therefore, C_{ref} and E_{ref}, in our linear pharmacodynamic relationship (4.10), are manually tuned to patient A. Here, we assume the maximal effect site concentration is achieved, taken from the pharmacokinetic results in patient A, and this can be related to a change in R_p. From Nygren et al. (2006) the maximal increase of R_p through ephedrine is taken to be 9%. An equal relative change in $V_{ven,0}$ and T_{cycle} is assumed (- 9%).

Noradrenaline

Noradrenaline is also a vasopressor, inducing a quick increase in blood pressure. This drug is characterised by a short elimination half time of 2.5 minutes (Farmacokinetisch Compas, 2019). It is modeled through a one-compartment model, and thus without effect-site. In this model, effect-site concentration (C_e) is substituted by plasma concentration (C_1). The elimination rate from the plasma compartment is calculated with:

$$k_{10} = \frac{\ln(2)}{t_{1/2}}. \tag{4.15}$$

In the study by Nygren et al. (2006), the change in R_p is given for C_{ref}, and we assume the pharmacodynamic effect can be described by the linear model (4.10).

Table 4.1: Pharmacokinetic constants for intravenous and inhalation drugs. Rate constants (k) are given in min^{-1}, volumes (V) are given in l, *scaled for 70 kg patient.

Symbol	k_{10}	k_{12}	k_{21}	k_{13}	k_{31}	k_{1e}	k_{e0}
Propofol	0.119	0.112	0.042	0.055	0.0033	0.149	0.119
Sevoflurane	0.105	0.117	0.007	-	-	0.12	0.096
Phenylephrine	0.0512	0.0922	0.0139	-	-	0.30	0.30
Ephedrine	0.0512	0.0922	0.0139	-	-	0.30	0.30
Noradrenaline	0.277	-	-	-	-	-	-

Symbol	V_1	V_2	V_3
Propofol	15.96*	32.41*	202.51*
Sevoflurane	7.95	12.25	-
Phenylephrine	41.2	298.8	-
Ephedrine	41.2	298.8	-
Noradrenaline	-	-	-

Table 4.2: Generic pharmacodynamic constants for intravenous and inhalation drugs. Concentrations (C_{50}, C_{ref}) are given in mg/l, change of effect (k_{max}, k_{ref}) and steepness parameter (γ) are dimensionless.

Sigmoidal model	*Effector*	C_{50}	k_{max}	γ
Propofol	R_p	3.18	-0.46	1.86
	$V_{ven,0}$	3.18	0.46	1.86
Linear model	*Effector*	C_{ref}	k_{ref}	
Sevoflurane	R_p	92.25	-0.34	
	$V_{ven,0}$	92.25	0.34	
Phenylephrine	R_p,	0.006	0.46	
	$V_{ven,0}$	0.006	-0.46	
Ephedrine	R_p,	0.125	0.09	
	$V_{ven,0}$	0.125	-0.09	
	T_{cycle}	0.125	-0.09	
Noradrenaline	R_p	0.0041	0.40	
	$V_{ven,0}$	-	-	

Table 4.3: Pharmacodynamic parameters for k_{baro}, concentration (C_{50}) is given in mg/l, change of effect ($k_{baro,min}$) is dimensionless.

Linear model	*Parameter*	C_{50}	$k_{baro,min}$
Propofol	k_{baro}	4.5	0.2
Sevoflurane	k_{baro}	101.2	0.2

4.2.6 Clinical data

A retrospective dataset was obtained from patients during elective abdominal surgery at Catharina Hospital Eindhoven. Inclusion criteria were a surgery including anesthesia, patients above 18 years old and a complete dataset available. Exclusion criteria were heart or kidney failure or peripheral vascular disease. The study was approved by the Medical Research Ethics Committees United (study ID:non-WMO W17.165). The study was classified as non-WMO, and informed consent was not deemed necessary as it entails a retrospective study. All data were analyzed anonymously.

Several data were retrieved from the electronic patient information system (EZIS test, Chipsoft ®, Amsterdam, The Netherlands) and the electronic anesthesia archive (AIMS, AnStat ®, Carepoint, Ede, The Netherlands). Firstly, we obtained continuous intraoperative data such as blood pressure waveforms, heart frequency, and respiratory settings. Secondly, periodical measurements such as hematocrit measurements, infusion boluses, blood, and urine loss were obtained. Thirdly, patient characteristics such as age, height, and weight were obtained. Additionally, annotations were imported and used to interpret perioperative data. In this pilot study, three patients from the dataset are analyzed (measurements

are shown in black, Figures 4.3-4.5). Patient A was used for parameter tuning, since there are little interventions, no blood loss and limited drug administration during surgery. Patient B received similar drugs and interventions as the previous, with the addition of noradrenaline infusion through a continuous pump. Additionally, the measurements are more dynamic. Total blood loss of 300 ml was recorded. Patient C is the most complex, with more dynamic changes in blood pressure and heart rate. Additionally, this dataset is different from the first two because only propofol was used to induce and maintain anesthesia, opposed to maintenance through sevoflurane inhalation. Total blood loss of 1200 ml was recorded.

4.2.7 Simulations performed

The model was implemented in MATLAB 2014b. Differential equations are solved by an Euler forward integration scheme with a time step of 0.1 s. In the *generic model* all three patients were modeled using generic parameter settings for the pharmacokinetics and -dynamics model. As described in section 2.5, generic reference concentrations for propofol, sevoflurane, and ephedrine were determined using data from patient A. Computed and measured mean arterial blood pressure and heart rate were compared. Additionally, we calculated the fluid (re-) distribution.

For each of the patients, a *patient-specific model* was created by manually tuning k_{max} for propofol, and k_{ref} for sevoflurane, phenylephrine, ephedrine and noradrenaline, to match computed and measured blood pressure and heart rate per patient (Table 4.4). Notably, for patient B & C, a better match was found by adding noradrenaline feedback on $V_{ven,0}$. The corresponding volume distribution was calculated.

In the *anesthesia-only model* the effect of the inotropes and vasopressors was omitted, but the generic pharmacokinetic and -dynamic models for propofol and sevoflurane were still included. With this model we solely evaluate the role of anesthesia on the blood pressure and heart rate during surgery and volume distribution at the end of surgery. Lastly, in the *no-drug model* the effect of all drugs was excluded. The simulations were performed with and without baroregulation. Thus, in this scenario blood pressure and heart rate are only affected by fluid administration.

Table 4.4: Patient-specific pharmacodynamic constants for intravenous and inhalation drugs. Parameters for the change of effect (k_{max}, k_{ref}) are dimensionless.

		Effector	k_{max}	k_{ref}
Propofol	Patient A.	R_p	-0.92	-
		$V_{ven,0}$	0.92	-
	Patient B.	R_p	-0.69	-
		$V_{ven,0}$	0.69	-
	Patient C.	R_p	-0.92	-
		$V_{ven,0}$	0.92	-
Sevoflurane	Patient B.	R_p	-	-0.34
		$V_{ven,0}$	-	0.34
Phenylephrine	Patient A.	R_p	-	0.69
		$V_{ven,0}$	-	-0.69
Ephedrine	Patient B.	R_p	-	0
		$V_{ven,0}$	-	0
Noradrenaline	Patient B.	R_p	-	0.4
		$V_{ven,0}$	-	-0.16
	Patient C.	R_p	-	0.4
		$V_{ven,0}$	-	-0.16

4.3 Results

4.3.1 Patient A

Hemodynamic measurements

Interventions, drug and fluid administration, measured mean arterial blood pressure, and heart rate for patient A are shown in Figure 4.3 (black). For this patient, anesthesia is induced by a bolus of 130 mg propofol (Figure 4.3A) and maintained with sevoflurane inhalation (Figure 4.3B). In the first 14 minutes, these drugs result in an initial blood pressure drop from 118 to 60 mmHg (Figure 4.3C), and heart rate drop from 110 to 63 bpm (Figure 4.3D). At 14 and 21 minutes two boluses of ephedrine, of 10 mg, and phenylephrine, of 0.1 mg, are given, each associated with a small blood pressure increase ($\approx$ 10 mmHg) followed by small increases in heart rate ($\approx$ 12 bpm). Blood pressure and heart rate stabilize at an average of 72 mmHg and 68 bpm until the end of surgery, respectively. At 88 minutes, an additional bolus of ephedrine of 5 mg is administered, followed by a temporary increase in blood pressure. At 126 and 141 minutes, additional blood pressure increases were measured, of 9 and 20 mmHg respectively, however, these are not associated with fluid or drug administration.

Simulations of blood pressure & heart rate

The model predictions for blood pressure and heart rate are shown in Figure 4.3C & D, respectively. In the *generic model* (Figure 4.3, dark blue), the propofol-induced pressure drop is underestimated (Δp_{art} = -21 vs. -58 mmHg at 14 minutes) in the beginning of surgery. At the same time, heart rate increases from 65 to 83 bpm, in contrast to the experimental data where blood pressure decreases steeply. At 14 and 21 minutes, the model predicts a blood pressure increase of $\approx$ 4 mmHg in response to ephedrine and phenylephrine infusion. Heart rate slowly decays and stabilizes at 73 bpm, higher than the measured data. In the long term, the average blood pressure, driven by sevoflurane, corresponds to the measured data. At 88 minutes, the response of blood pressure to the ephedrine bolus is delayed, but the increase in pressure corresponds to the measured data. Some discrepancies between the simulation and measurements occur at 125 and 140 minutes, where blood pressure change was not related to fluid or drug administration. At the end of surgery, the removal of sevoflurane administration causes a rise in the modeled arterial blood pressure (from 70 to 118 mmHg).

For the *patient-specific model* (Figure 4.3, red), the adapted model parameters are reported in Table 4.4. In comparison to the *generic model*, the propofol-induced pressure drop is better matched to the measurements (-68 mmHg vs. -58 mmHg). Heart rate increases more strongly, to 100 bpm. The increase in blood pressure at 14 and 21 minutes, in response to ephedrine and phenylephrine is more pronounced. From 40 minutes onwards, the average blood pressure and heart rate correspond to the generic simulation results.

In the *aneasthesia-only model*, (Figure 4.3, light blue) arterial blood pressure slowly decays to 68 mmHg in the first 40 minutes, close to average measured blood pressure. The temporary vasopressor-induced increases in pressure and heart rate, at 14, 21, and 88 minutes, disappear. Heart rate is similar to that in the generic model results.

In the *no-drug model* blood pressure remains higher compared to the previous simulations throughout the surgery. In the simulation with active baroregulation arterial blood pressure decreases from 118 to 117 mmHg, and heart rate increases from 65 to 67 bpm, at the beginning of surgery. After that, blood pressure increases gradually to 123 mmHg, and heart rate decreases gradually to 61 bpm, at the end of surgery. Without baroregulation, heart rate remains constant at 65 bpm throughout the surgery. Blood pressure increases gradually to 137 mmHg at the end of surgery.

Simulations of volume distribution

During surgery, a total of 2 liters of fluid is administered to the patient (Figure 4.3E). According to the *generic model*, this fluid contributes to an increase of

plasma volume from 2.55 to 2.8 l from beginning to end of surgery (Figure 4.3F), of interstitial volume from 6.2 to 7.1 l (Figure 4.3G) and of urine volume from 0 to 0.6 l (Figure 4.3H). Notably, a steep decrease in plasma volume occurs as a result of the increased blood pressure, from 175 to 200 minutes.

In the *patient-specific model*, simulations volumes at the end of surgery are not affected. However, between 20 and 40 minutes, there is an increase in plasma volume ($\approx$ 200 ml) due to the lower arterial pressure. Correspondingly, the interstitial volume is temporarily reduced ($\approx$ 200 ml).

Similar volumes at the end of surgery are predicted with the *anesthesia-only model*. However, in the first 40 minutes, plasma volume increases smoother and slower, compared to the *patient-specific* simulation.

For the *no-drug model* with active baroregulation the elevated blood pressure drives more fluid into the interstitium, causing plasma volume and urine volume to be lower. However, at the end of surgery plasma volume converges to the predictions of the *generic model*, *patient-specific model*, and *anesthesia-only model*. At that moment, interstitial volume is higher (+600 ml) and urine volume is lower (-370 ml), compared to prior simulations. Volume distribution results between simulations with and without baroregulation differ by less than 30 ml.

4.3.2 Patient B

Hemodynamic measurements

Interventions, drug and fluid administration, non-invasively (stars) and invasively (line) measured mean arterial blood pressure, and heart rate for patient B are shown in Figure 4.4 (black). For this patient, anesthesia is induced by a bolus of 200 mg propofol (Figure 4.4A) and maintained with sevoflurane inhalation (Figure 4.4B). These drugs result in an initial blood pressure drop from 119 to 58 mmHg (Figure 4.4C), and heart rate drop from 75 to 49 bpm (Figure 4.4D). At the beginning of surgery, ephedrine and phenylephrine are given through four boluses of 5 mg (Figure 4.4B), with no clear blood pressure increase observed in the data. Therefore, a noradrenaline infusion pump (0.1 mg/ml) was connected at 90 minutes (Figure 4.4B), causing a blood pressure increase of about 30 mmHg. Subsequently periods of noradrenaline infusion at 200 and 231 minutes, cause a blood pressure increase of about 30 and 40 mmHg, respectively. Although no interventions were recorded from 120 to 200 minutes, oscillations in blood pressure and heart rate are measured. Blood pressure remains at an average of 82 mmHg until the end of surgery. Heart rate continuously increases to 69 bpm at the end of surgery. Notably, there are steep changes in blood pressure and increases in heart rate from 185 to 200 minutes and 267 to 278 minutes. These are not associated with fluid or drug administration, and possibly associated with bleeding. The increase in HR suggests some baroreflex activity.

Simulations of blood pressure & heart rate

The model predictions for blood pressure and heart rate are shown in Figure 4.4C & D, respectively. With the *generic model* (Figure 4.4, dark blue), at the beginning of the surgery, the propofol-induced pressure drop is underestimated, as was also the case in patient A (-10 mmHg vs. -49 mmHg at 46 minutes). The model shows responses to the ephedrine boluses at 37, 47, 79, and 86 minutes, whereas the patient did not respond to the boluses. Notably, when starting noradrenaline infusion, the increase in blood pressure seems quicker than the measured response. At the end of surgery, blood pressure and heart rate increase, as was also the case in patient A. On average, blood pressure stabilizes around 75 mmHg, corresponding closely to the measured blood pressure.

For the *patient-specific model* (Figure 4.4, red), the adapted model parameters are reported in Table 4.4. Here, the propofol-induced pressure drop (-55 mmHg vs. - 49 mmHg) is better matched to the measurements. At 91 minutes, there is a better correspondence of blood pressure during noradrenaline infusion compared to the *generic model* results. In the long term, average blood pressure remains the same as for the *generic model*. Interestingly, at 200 and 231 minutes, the administration of noradrenaline causes a more pronounced increase in blood pressure as compared to the *generic model*, along with minor drops in heart rate.

In the *anesthesia-only model*, (Figure 4.4, light blue) arterial blood pressure slowly decays to 55 mmHg and heart rate increases to 69 bpm. Similar to patient A, the temporary increases in blood pressure, associated with ephedrine and noradrenaline infusion, disappear.

In the *no-drug model* with active baroregulation arterial blood pressure remains high, comparable to patient A. Blood pressure is increased from 119 to 125 mmHg at the end of surgery. Heart rate remains constant at 55 bpm. Again, arterial blood pressure is highly affected when baroregulation is turned off. In this case, at the end of surgery, pressure has increased from 119 to 149 mmHg, and heart rate gradually decreased to 50 bpm.

Simulations of volume distribution

During surgery, a total of 3 liters of fluid is administered to the patient and 0.3 liters of blood loss is recorded (Figure 4.4E). According to the *generic model*, this fluid contributes to an increase in plasma volume from 3.5 to 4.3 l from beginning to end of surgery (Figure 4.4F), interstitial volume from 10.3 to 10.6 l (Figure 4.4G) and urine volume from 0 to 1.6 l (Figure 4.4H).

In the *patient-specific model* simulations volumes at the end of surgery are not affected, similar to the results of patient A. Still, between 20 to 40 minutes, there is a temporary increase in plasma volume ($\approx$ 200 ml), and decrease in interstitial volume ($\approx$ 200 ml).

For the *anesthesia-only model* similar volumes, to the previous model, at the end of surgery are found.

In the *no-drug model*, plasma volume converges towards volumes predicted in the previous simulations at the end of surgery. However, during surgery, this volume is again lower than the previous simulations. This underestimation leads to a similar increased interstitial volume and decreased urine volume, as in patient A. Turning off the baroregulation affects the volume distribution by less than 100 ml.

4.3.3 Patient C

Hemodynamic measurements

Interventions, drugs and fluid administration, non-invasively (stars) and invasively (line) measured mean arterial blood pressure, and heart rate for patient C are shown in Figure 4.5 (black). For this patient, anesthesia is induced by a bolus of 280 mg propofol (Figure 4.5A), and maintained with a target-controlled infusion pump of propofol with concentration 10 mg/ml (Figure 4.5B). In the first 50 minutes, these drugs result in an initial blood pressure drop from 109 to 62 mmHg (Figure 4.5C), and heart rate drop from 82 to 48 bpm (Figure 4.5D). At 28 and 31 minutes two boluses of phenylephrine of 0.05 mg are given. At 55 minutes, an ephedrine bolus of 7.5 mg is given and simultaneously the noradrenaline pump (0.1 mg/ml) is started. Together, these inotropes and vasopressors result in a blood pressure increase from 74 to 108 mmHg, and heart rate increase from 63 to 87 bpm, as a result of ephedrine administration. Another ephedrine bolus is given at 99 minutes, followed by phenylephrine boluses, of 0.05 mg, at 115 and 240 minutes. The effect of this can be seen in the blood pressure fluctuations. In the long term, blood pressure is 83 mmHg on average, and heart rate increases until 81 bpm at the end of surgery.

Simulations of blood pressure & heart rate

The model predictions for blood pressure and heart rate are shown in Figure 4.5C & D, respectively. With the *generic model* the propofol-induced pressure changes on the short term- (-17 vs. -49 mmHg at 26 minutes) and long term (+4 vs. -30 mmHg) are greatly underestimated (Figure 4.5, dark blue). Average blood pressure is higher compared to the measured pressure (110 vs. 83 mmHg) until the end of surgery. Heart rate corresponds to the measured data from 25 to 125 minutes, but it is underestimated by 12 bpm until the end of surgery.

For the *patient-specific model* (Figure 4.4, red), the adapted model parameters are reported in Table 4.4. Here, the propofol-induced pressure drop (-62 mmHg vs. -49 mmHg) corresponds better to the measurements. At the same time, the in-

crease in heart rate is overestimated. Until 150 minutes, average blood pressure (90 mmHg) is better matched to the measurements. After 150 minutes, there is an overestimation in blood pressure of $\approx$ 15 mmHg. Heart rate is underestimated by $\approx$ 12 bpm until the end of surgery.

The *anesthesia-only model* predicts blood pressure and heart rate comparable to *generic model* results, without the temporary blood pressure increases created by infusion of phenylephrine, ephedrine, and noradrenaline.

Finally, for the *no-drug model* simulations with active baroregulation, blood pressure remains higher compared to previous simulations. At the end of surgery, blood pressure is increased from 109 to 117 mmHg, converging with previous simulation results. Heart rate remains constant at 60 bpm. Arterial blood pressure is highly affected when baroregulation is turned off. At the end of surgery, pressure has increased from 109 to 145 mmHg. Heart rate was gradually decreased to 54 bpm.

Simulations of volume distribution

During surgery, a total of 5 liters of fluid is administered to the patient and 1.2 liters of blood loss is recorded (Figure 4.5E). According to the generic model simulations, this fluid contributes to an increase in plasma volume from 2.5 to 2.9 l from beginning to end of surgery (Figure 4.5F), interstitial volume from 7 to 10.4 l (Figure 4.5G) and urine volume from 0 to 1.5 l (Figure 4.5H).

In the *patient-specific model* volumes at the end of surgery are slightly affected ($\pm$ 100 ml). Between 20 and 100 minutes, there is an increase in plasma volume (200 ml) related to the lower arterial pressure. Correspondingly, the interstitial volume is temporarily reduced by 200 ml.

For the *anesthesia-only model* simulations similar volumes are predicted at the end of surgery. In the first 40 minutes, plasma volume increases smoother and slower, compared to the patient-specific simulation.

In the *no-drug model*, plasma volume converges to plasma volume as predicted in the previous simulations at the end of surgery. However, a similar increased interstitial volume and decreased urine volume, as in patient A & B are observed. Turning off the baroregulation affects the volume distribution by less than 100 ml.

4.4 Discussion

In our research, we aim to develop a clinical decision support model for fluid administration during surgery. First, we developed a cardiovascular fluid exchange model and tested this model for fluid redistribution after saline infusion in healthy volunteers (Rosalina et al., 2019). In this chapter, we extended the model with the effect of drugs, to enable simulation of the fluid status in surgical patients. In particular, we investigated which, if any, drugs should be taken into account in our mathematical model to accurately predict the fluid distribution at the end of surgery. The results of this pilot study show that we were able to reproduce intraoperative blood pressure with our *patient-specific model*. However, if the aim is to predict long term fluid distribution, one can make due with a model only including models for pharmacokinetics and -dynamics of anesthesia.

4.4.1 Model setup

The model consists of our previously published cardiovascular fluid exchange model, coupled to drugs through a pharmacokinetic and -dynamics model. We chose a lumped parameter representation for the systemic circulation, assuming we can neglect the right heart and pulmonary circulation. In our 0-D modeling approach, we neglected spatial dimension (Shi et al., 2011). We considered this approach allowed, in view of the difference in time scale between the quick convective transport and mixing of the drugs in the cardiovascular circulation, as compared to the slow pharmacokinetic and - dynamic processes.

The compliances and resistances of the cardiovascular system were tuned to yield steady state hemodynamics for each patient characterised by preoperative p_{art}, weight and height. Notably, in all perioperative results heart rate was measured to be higher than expected in rest. The measured heart rate is assumed to be high due to stress before surgery. Therefore, our initial conditions for heart rate are taken from preoperative measurements instead of from the surgical measurements.

We included pharmacokinetics and -dynamics models for anesthesia (propofol and sevoflurane) and vasopressors and inotropes (noradrenaline, phenylephrine and ephedrine). The distribution of these drugs has been extensively studied in the past (Marsh et al., 1991; Wissing et al., 2000; Hengstmann et al., 1982). For the pharmacokinetic model structure and parameters, we rely on these studies. Since we had no information on the pharmacokinetics of ephedrine, we assume this is similar to that of phenylephrine. Therefore, the same parameter settings are be used for these drugs. Volumes (V_1, V_2, V_3) are taken from literature as well. It is important to note that these are volumes are model entities that and do not represent physical volumes. For sevoflurane, little experimental data about the effect-site concentration for blood pressure are available. Therefore we manually tuned k_{e0} to the available patient data.

The pharmacodynamic setup, if available, was adopted from literature as well (Table 4.2). However, there are little published data on pharmacodynamic models regarding the effects on the cardiovascular effectors. E.g., studies on the effect of sevoflurane and propofol are mostly focussed on achieving unconsciousness. The experimental comparison of this pharmacodynamic part of the model is hard to perform, and the patient variability is extensive (Bibian et al., 2006). In most models, a sigmoidal relationship between concentration and effect is used. For propofol we adopted this model from Kazama et al. (1999). However, for sevoflurane, phenylephrine, ephedrine and noradrenaline we assume that the effect on blood pressure can be linearised around their working points. We assume this approach is sufficient for this pilot study. In the patient-specific simulations pharmacodynamic parameters were manually tuned. A structured fitting procedure can be performed to investigate if unique solutions for parameters can be found, increasing the reliability of the results.

No model was found in literature for the effect of propofol and sevoflurane on baroregulation either. However, it is known that there is a reduction in baroreflex intensity by these drugs. Based on clinical observations, we assumed a linear relationship with maximal reduction to 20 % of the original effector gains. Experimental data to confirm this exact value is hard to obtain. However, our simulations without drugs and with and without baroregulation show that not much variation in output should be expected, thus baroregulation may be fully neglected in anesthetized patients.

4.4.2 Data limitations

We tested our model on a retrospective dataset of three intraoperative patients. These data contain discrete registrations for intravenous fluid administration, and fluid loss, through bleeding and urine production. The exact rate of infusion is unknown, only the connection of a new infusion bag is registered. Therefore, we assume that fluid infusion is continuous from connection of one bag until a new bag. Similarly, for bleeding and urine production only discrete datapoints are available. Bleeding is included in the model as a continuous flow, based on discrete measurements. Data on urine production were sparse and unreliable at times. Therefore, these are not used in the simulations.

While the surgical data contain enough information for clinical decision making, they sometimes lack the more detailed quantitative information, needed in our model. E.g., for patient B, no cardiovascular interventions were recorded from 120 to 200 minutes, whereas oscillations in the blood pressure tracings are present. These might have been caused by unregistered interventions such as movement or extra surgical stress, such as incisions. Additionally, some patient-specific responses to the drugs can be observed. E.g., in patient B, there are two boluses of ephedrine given, followed by a continuous infusion of noradrenaline. The patient did not respond to the first two boluses, leading to the noradrenaline

pump to be connected. These patient-specific responses were deduced visually from our retrospective data. Additionally, events such as intubation, incision and changes of position, as well as previously mentioned pain and analgesia may have affected hemodynamics. Modeling these factors was outside the scope of this study, contributing to some unexplained hemodynamic discrepancies between the data and model results.

4.4.3 Model results

Hemodynamics

With our extended model, we simulated three scenario's of perioperative patients, comparing predicted and measured arterial blood pressure and heart rate, and predicting volume distribution. Firstly, for all three patients in the *generic model* there is a short term overestimation of blood pressure after administration of a propofol bolus. In patient C, this overestimation of simulated blood pressure remains on the long term. In patient A & B, this is not the case, since k_{e0} and k_{max} for sevoflurane are manually tuned leading to good agreement between simulated and measured blood pressure. The pharmacodynamic parameters of propofol, controlling the effect on blood pressure, were taken from Kazama et al. (1999). Their experimentally measured effect does not seem to correspond to our observations. As shown by (4.14), Kazama et al. (1999) measured the effect of propofol on blood pressure, and describe the effect as deviation of maximal blood pressure ($p_{art,max}$) from a reference blood pressure ($p_{ref,max}$). For our patients these values were taken to be constant, and the effect on our cardiovascular effectors is assumed to be similar to that on the blood pressure. The parameter settings taken from Kazama et al. (1999) are not enough to capture the change in blood pressure in our patient datasets. More research, including model improvement and sensitivity analysis, is needed to analyze these differences.

Secondly, in all three patients, blood pressure is temporarily affected by inotropes and vasopressors. From the data we can conclude that there is a large patient-variability for the response to these drugs. Distinguishing the effect of each vasopressor or inotrope (noradrenaline, ephedrine and phenylephrine) is hard, since different drugs may be given simultaneously. However, with our *generic model* we are able to simulate the trends of temporary blood pressure increase in each patient.

Simulating these patients with the *patient-specific model* in stead of the *generic model*, presents the best correspondence between simulated and measured blood pressure. Especially, the effect of propofol was tuned for all patients such that blood pressure drop after induction, and maintenance for patient C, correspond to measurements. Table 4.4 shows that a large variation in k_{max} is needed to simulate these three patients. Additional confirmation of the importance of anesthesia is given by comparing the simulations performed with the *anesthesia-only*

model and *no-drug model*, which show that average blood pressure is controlled by propofol or sevoflurane.

In the *no-drug model* we also investigated the effect of baroregulation. As expected, turning the baroregulation on and off results in a difference in arterial blood pressure and heart rate. Although, average blood pressure is similar for both cases and remains much higher compared to all previous simulations. This is mainly because of the omission of anesthesia.

Fluid distribution

Finally, our goal was to investigate the effect of these drugs on the fluid distribution in these patients. Unfortunately, our dataset does not contain information available on the plasma and interstitial volume. Therefore, we manually tuned pharmacokinetic and -dynamic parameters (Table 4.4) to the blood pressure data in the *patient-specific model* simulations. Assuming our fluid exchange model is correct, this gives us an indication of the actual fluid distribution in the patients. The results show that per patients, the plasma volumes at the end of surgery converge to the same level in all models. For the *generic model*, *patient-specific model* and *anesthesia-only model* there are small temporary differences ($\approx$ 100 ml) that do not affect the plasma volume on the long term. The *no-drug model* results in higher blood pressures ($\approx$ +25 mmHg) which affects capillary pressure. By extension, this results in lower plasma volume during surgery through fluid exchange (Rosalina et al., 2019).

The close correspondence between arterial blood pressure and plasma volume was expected from the Starling equation. This regulatory mechanism shows that for patient and volunteers with normal capillary permeability, vascular volume is strictly regulated. Determining fluid status (modeled as interstitial volume) based on plasma volume or arterial blood pressure alone is therefore unreliable.

Interstitial and urine volume are affected by the long-term plasma volume. Going back to our fluid exchange model, based on conservation of mass, the administered volume is distributed between perspiration, urine or storage in plasma and interstitium. Since we observed plasma volume to be regulated, and perspiration is modeled as a constant value, the administered volume can lead to an increased urine or interstitial volume. Since anesthesia affects the long term plasma volume, the pharmacodynamic effects of anesthetics must be included in the model in order to reasonably predict the long term fluid balance. Ideally, the model for fluid distribution has the least amount of parameters to be estimated. When only interested in long term fluid distribution, one can make due with a model only including models for pharmacokinetics and -dynamics of anesthesia. Temporary anesthetics, inotropes and vasopressors are not as crucial for long term fluid predictions. However, they may have a considerable impact on short-term predictions that may be used for intraoperative decision making.

4.4.4 Model limitations

It is important to note that this is a pilot study. As discussed above, the choice of the drug models and the associated parameter settings was not without problems. In addition, the model was evaluated by simulating only three patients. Still, we believe this study serves as a relevant proof-of-concept.

In our model we neglected the effect of pain-associated responses as well as the effects of analgesia (e.g., morphine and fentanyl), administered for pain management. Since the experience of pain is highly subjective and patient-specific, including these effects is outside the scope of our research. Some discrepancies between measured and modeled heart rate can be attributed to this, since pain is a large surgical influences on heart rate.

One of the major model limitations is that we adopted our fluid exchange model parameters from our healthy volunteer study. However, it is known that inflammation and surgical stress may result in different parameter settings such as membrane permeability (k_f), reflection coefficient (σ) and permeability coefficient-surface area (PS). These parameters highly influence the fluid and protein exchange between vascular and interstitial space, affecting the results and conclusions of this study. More research is necessary to assess the quantitive effects in possible inflamed patients.

There are some similar studies to ours available in literature, mostly physiology based commercial software tools (such as Biogears, Pulse Physiology Engine, SimMan 3G). These software tools have coupled pharmacokinetic and -dynamic models to the cardiovascular circulation. However, the main goal of these products is to provide a comprehensive overview of the full body physiology. To the best of our knowledge, these models are not intended for clinical decision support. The novelty in our study is that we are comparing our model directly with clinical data and showing it's clinical applicability.

4.4.5 Future work

There are still many steps to be taken before we can use this work as a clinical decision support model. Many parameters were introduced by adding pharmacokinetic and -dynamic model descriptions for drugs. Fortunately, only anesthesia seems relevant for predicting the fluid status at the end of the surgery. A structured sensitivity analysis, for submodels of sevoflurane and propofol, could be performed to confirm these findings and eventually could be used to fix and prioritize model parameters (Eck et al., 2015). Since, the model contains many parameters which could be tuned it is still an open question if finding a unique solution is possible.

Another solution for reducing the uncertainty caused by parameter estimation, may be to use our model in combination with (real-time) measured data

for blood pressure and heart rate. If a combination between measurements and model predictions can be made, there is a possibility of significant model simplification and parameter reduction. Still, with our model results, some preliminary conclusions can be made.

4.5 Conclusion

In conclusion, we extended our previously published cardiovascular fluid exchange model with the effect of drugs and evaluated it on a retrospective dataset of three perioperative patients. This pilot study showed that to model exact intraoperative blood pressure anesthesia, inotropes and vasopressors must all be included in our model. However, if one is only interested in an average blood pressure during surgery, necessary for good predictions of fluid distribution at the end of surgery, vasopressors and inotropes can be omitted. This reduces the model complexity. The results in this study can form the basis for a more structured prospective study where our cardiovascular fluid exchange model is extended with only with only pharmacokinetic and - dynamic models for anesthesia.

4.6 Acknowledgements

This chapter is based on the MSc Thesis 'Clinical application of a model for perioperative fluid exchange' by Femke Vaassen. We thank her for her contribution to the literature review, data collection and model development. Additional thanks to the surgical and ICT staff at Catharina Hospital Eindhoven for their support and interest in the work. This work was performed within the IMPULS II perioperative monitoring framework in collaboration with Philips Eindhoven and Catharina Hospital Eindhoven.

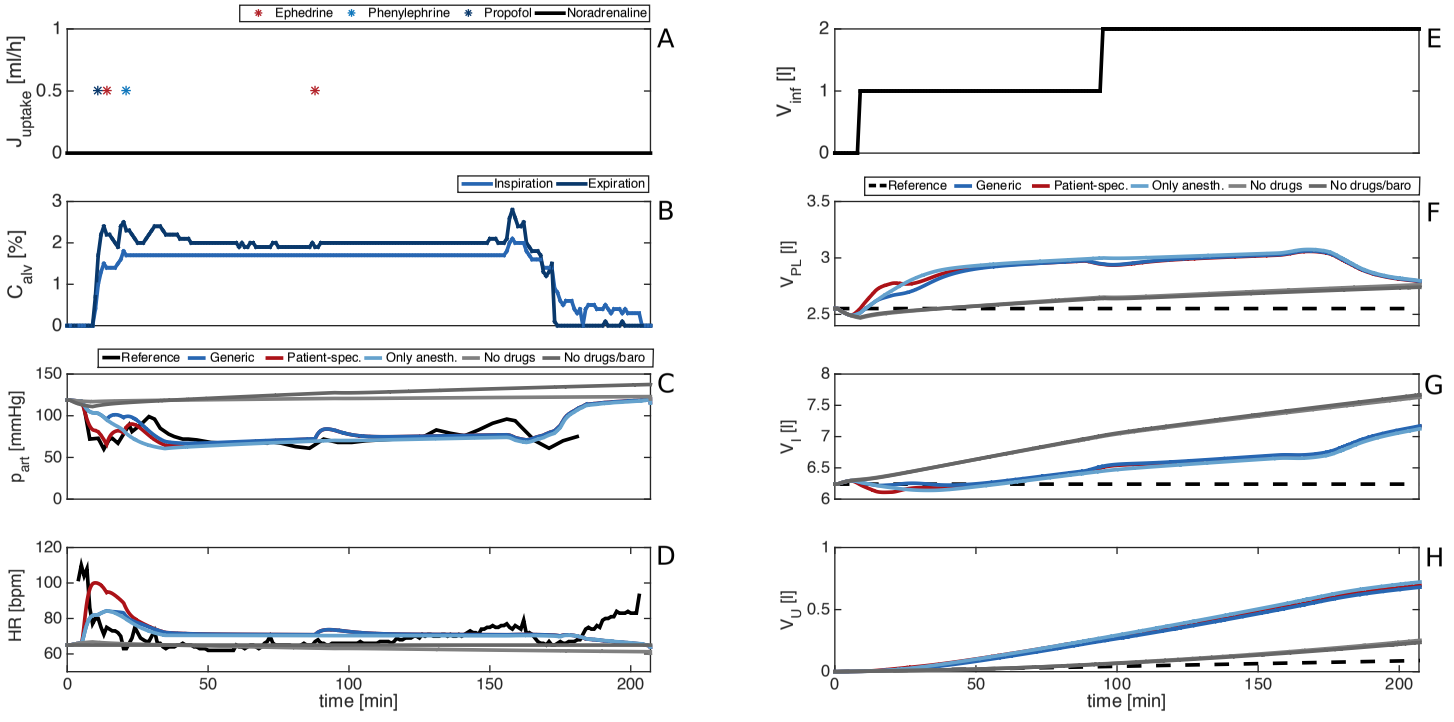


Figure 4.3: Perioperative measurements and model predictions for Patient A, with (**A**) drug administration rate (J_{uptake}), (**B**) sevoflurane concentration (C_{alv}) for in- and expiration, (**C**) mean arterial blood pressure (p_{art}) and (**D**) heart rate (HR). Also shown are, (**E**) infused volume (V_{inf}), (**F**) plasma volume (V_{PL}), (**G**) interstitial volume (V_I), and (**H**) urine volume (V_U), compared to the reference volume (- - -). Panels (**C**)-(**H**) show measured data in black, and model results obtained with the *generic model* (d. blue), the *patient-specific model* (red), the *anesthesia-only model* (l. blue), and the *no-drug model* with (l. grey) and without (d.grey) baroregulation.

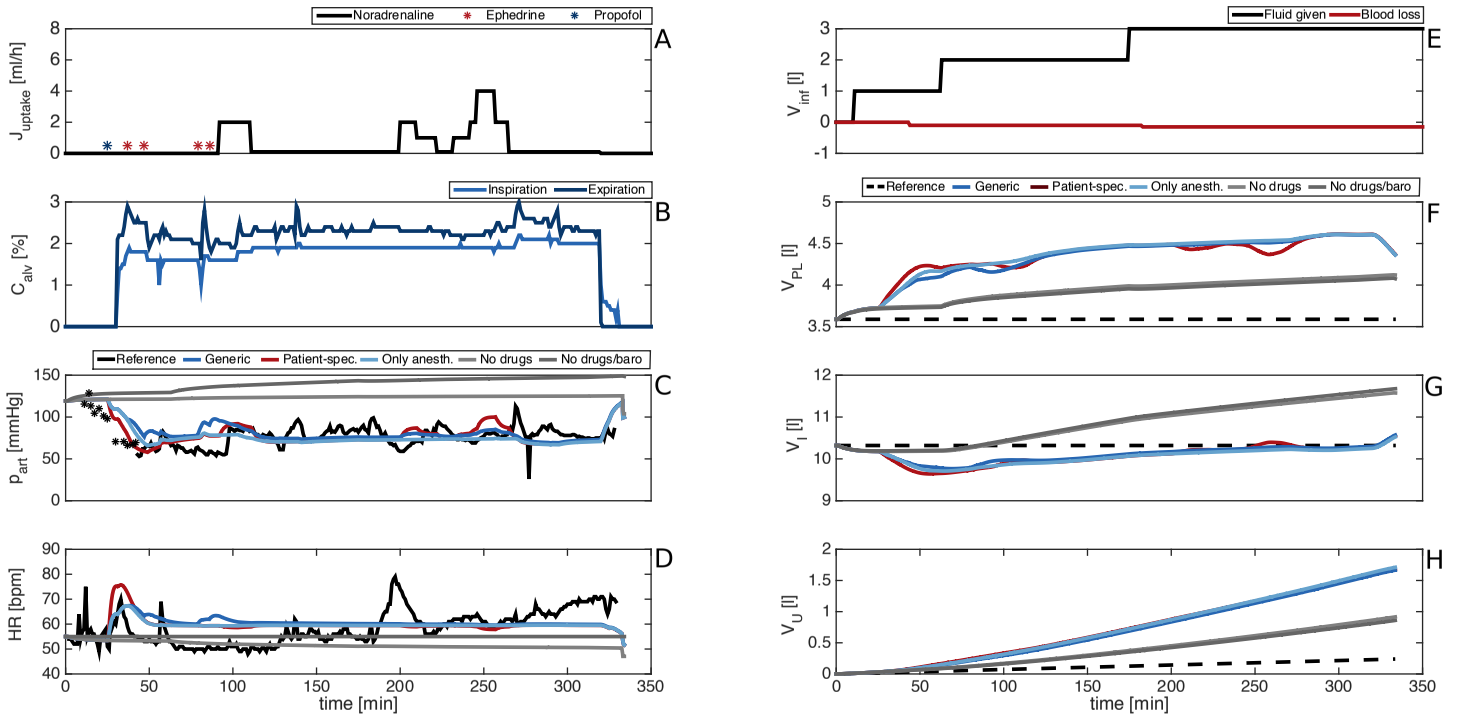


Figure 4.4: Perioperative measurements and model predictions for Patient B, with (**A**) drug administration rate (J_{uptake}), (**B**) sevoflurane concentration (C_{alv}) for in- and expiration, (**C**) mean arterial blood pressure (p_{art}) and (**D**) heart rate (HR). Also shown are, (**E**) infused volume (V_{inf}), (**F**) plasma volume (V_{PL}), (**G**) interstitial volume (V_I), and (**H**) urine volume (V_U), compared to the reference volume (- - -). Panels (**C**)-(**H**) show measured data in black, and model results obtained with the *generic model* (d. blue), the *patient-specific model* (red), the *anesthesia-only model* (l. blue), and the *no-drug model* with (l. grey) and without (d.grey) baroregulation.

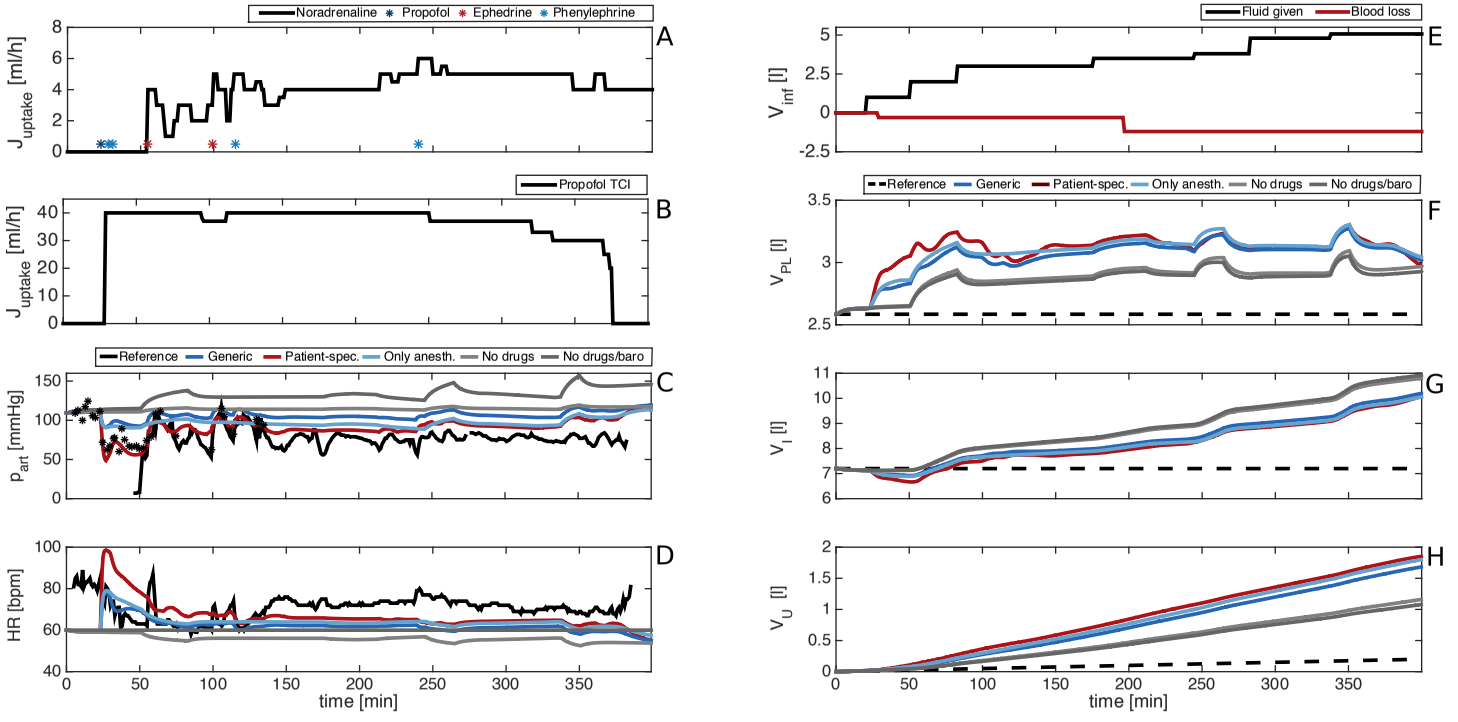


Figure 4.5: Perioperative measurements and model predictions for Patient C, with (**A**) drug administration rate (J_{uptake}), (**B**) propofol target-controlled infusion rate (J_{uptake}), (**C**) mean arterial blood pressure (p_{art}) and (**D**) heart rate (HR). Also shown are, (**E**) infused volume (V_{inf}), (**F**) plasma volume (V_{PL}), (**G**) interstitial volume (V_I), and (**H**) urine volume (V_U), compared to the reference volume (- - -). Panels (**C**)-(**H**) show measured data in black, and model results obtained with the *generic model* (d. blue), the *patient-specific model* (red), the *anesthesia-only model* (l. blue), and the *no-drug model* with (l. grey) and without (d.grey) baroregulation.

Bibliography

Bibian, S. et al. (2006). "Patient variability and uncertainty quantification in anesthesia: Part 1 - PKPD modeling and identificaion". *Proc. of the 2006 IFAC Symposium on Modelling and Control in Biomedical Systems*.

Cecconi, M. et al. (2015). "Fluid challenges in intensive care: the FENICE study". *Intensive Care Medicine* 41.9, pp. 1529–1537.

Ciofolo, M. J. and Reiz, S. (1999). "Circulatory effects of volatile anesthetic agents". *Minerva Anestesiologica* 65, pp. 232–238.

Derendorf, H. and Meibohn, B. (1999). "Modeling of Pharmacokinetic/ Pharmacodynamic (PK/PD) Relationships: Concepts and Perspectives". *Pharmaceutical Research* 16.2, pp. 176–185.

Drobin, D. and Hahn, R. (1999). "Volume Kinetics of Ringer's Solution in Hypovolemic Volunteers". *Anesthesiology* 90, pp. 81–91.

Eck, V. G., Donders, W. P., and Sturdy, J. (2015). "A guide to uncertainty quantification and sensitivity analysis for cardiovascular applications". *International Journal for Numerical Methods in Biomedical Engineering*, e02755.

Feihl, F. and Broccard, A. F. (2009). "Interactions between respiration and systemic hemodynamics. Part I: Basic concepts". *Intensive Care Medicine* 35, pp. 45–54.

Ghimenti, S. et al. (2013). "Post-operative elimination of sevoflurane anesthetic and hexafluoroisopropanol metabolite in exhaled breath: Pharmacokinetic models for assessing liver function". *Journal of Breath Research* 7.3.

Gupta, R. and Gan, T. (2016). "Peri-operative fluid management to enhance recovery". *Anaesthesia* 71, pp. 40–45.

Hengstmann, J. H. and Goronzy, J. (1982). "Pharmacokinetics of 3H-Phenylephrine in Man". *European Journal of Clinical Pharmacology*, pp. 335–341.

Holte, K., Sharrock, N., and Kehlet, H. (2002). "Pathophysiology and clinical implications of perioperative fluid excess". *British Journal of Anaesthesia* 89.4, pp. 622–32.

Jongen, G. J. et al. (2016). "A mathematical model to simulate the cardiotocogram during labor. Part A: Model setup and simulation of late decelerations". *Journal of Biomechanics* 49.12, pp. 2466–2473.

Kazama, T., Ikeda, K., and Morita, K. (1999). "Comparison of the Effect-site k_{e0}s of Propofol for Blood Pressure and EEG Bispectral Index in Elderly and Younger Patients". *Anesthesiology* 90, pp. 1517–27.
Latta, T. (1832). "Malignant cholera". *Lancet* ii, pp. 45–274–7.
Magder, S. (2016). "Volume and its relationship to cardiac output and venous return". *Critical Care* 20.1, pp. 1–11.
Marik, P. E. et al. (2009). "Dynamic changes in arterial waveform derived variables and fluid responsiveness in mechanically ventilated patients: A systematic review of the literature". *Critical Care Medicine* 37.9, pp. 2642–2647.
Marsh, B. et al. (1991). "Pharmacokinetic model driven infusion of propofol in children". *British Journal of Anaesthesia* 67.1, pp. 41–48.
Michard, F. and Teboul, J. L. (2000). "Using heart-lung interactions to assess fluid responsiveness during mechanical ventilation". *Critical Care* 4.5, pp. 282–289.
Nygren, A., Thorén, A., and Ricksten, S. E. (2006). "Vasopressors and intestinal mucosal perfusion after cardiac surgery: Norepinephrine vs. phenylephrine". *Critical Care Medicine* 34.3, pp. 722–729.
Rosalina, T. T. et al. (2019). "A mathematical model to investigate the effects of intravenous fluid administration and fluid loss". *Journal of Biomechanics* 88, pp. 4–11.
Sellgren, J. et al. (1994). "Sympathetic Muscle Nerve Activity, Peripheral Blood Flows, and Baroreceptor Reflexed in Humans during Propofol Anethesia and Surgery". *Anesthesiology* 80.3, pp. 534–544.
Shi, Y., Lawford, P., and Hose, R. (2011). "Review of Zero-D and 1-D Models of Blood Flow in the Cardiovascular System". *BioMedical Engineering Online* 10.
Sullivan, K. R., Cammarano, W. B., and Wiener-Kronish, J. P. (2010). "Analgesics, Tranquilizers, and Sedatives". *Cardiac Intensive Care*. Ed. by A. Jeremias and D. L. Brorn. 2nd ed. Philadelphia: Saunders. Chap. 41, pp. 504–515.
Watenpaugh, D. E. et al. (1992). "Role of atrial natriuretic peptide in systemic responses to acute isotonic volume expansion". *Journal of Applied Physiology* 73.4, pp. 1218–1226.
Wissing, H. et al. (2000). "Pharmacokinetics of inhaled anaesthetics in a clinical setting: Comparison of desflurane, isoflurane and sevoflurane". *British Journal of Anaesthesia* 84.4, pp. 443–449.
Xie, S. et al. (1995). "A model of human microvascular exchange". *Microvascular Research* 49, pp. 141–162.

Chapter 5
Implementing the fluid exchange model in the intensive care: a pilot study

The work in this chapter is based on a collaboration between T. T. Rosalina, J.W. Sels & P.H.M. Bovendeerd.

Abstract

Fluid administration in surgical patients is necessary to compensate for bleeding, evaporation, perspiration and urine production. Determining the correct amount of fluid to be administered is important, since fluid overloading is associated to negative patient outcome. Unfortunately, administration of the correct amount of fluid is difficult, due to the lack of applicability and sensitivity of indirect measurements, while direct measurements are not available. In previous work, we developed a mathematical model to predict the fluid (re-) distribution in the human body, and tested it with surgical patient data. In the current study we aim to test this model for use in intensive care patients, because hypervolemia-related complications often occur in the intensive care. For this purpose, we obtained a prospective dataset of four patients after cardiac surgery and performed simulations with our mathematical model to predict changes is plasma, interstitial and urine volume. The results show that we can simulate the trends of fluid buildup after fluid administration with our current model. Our simulation results confirm that the interstitial volume works as a buffer after fluid administration. Finally, with our generic model we are able to predict global trends in fluid buildup.

5.1 Introduction

Fluid administration is an important intervention in the intensive care (ICU) unit to increase cardiac output, and maintain volume balance in patients. To determine which patient needs fluid administration, fluid responsiveness is an important concept in the ICU. After surgery, critical patients are often in need of fluid administration. However, patient-specific fluid administration is extremely difficult, since there are no direct or indirect measurements that are specific and sensitive enough to assess fluid responsiveness and distribution. Determining the correct amount of fluid to be administered is important, since fluid overloading has been shown to be associated to negative patient outcome. Too much administration of fluid has the risk of causing hypervolemia, manifested as fluid build-up in the interstitial space (Holte et al., 2002). This may lead to complications such as microvascular compression, decreased renal function, severe edema-related discomfort and longer recovery time.

To test if a patient will benefit from fluid administration, i.e., whether cardiac output increases, multiple fluid challenges have been proposed. Unfortunately, the use of these fluid challenges is not standardised, (Cecconi et al., 2015) and these fluid challenges only give information on the intravascular volume. However, administered fluid can move from the vascular to interstitial volume where it may lead to fluid build-up, which is associated with a higher complication rate (Holte et al., 2002; Brandstrup, 2006).

In this thesis, we developed a cardiovascular fluid exchange model, based on physics and physiology. This framework captures hemodynamic variables (pressures, flows and heart rate), fluid loss (urine production, hemorrhage and perspiration), exchange of fluid between vascular and interstitial volume (transcapillary exchange and lymph flow), and lung mechanics. The development and initial testing of this model has been described in the previous chapters. In Chapter 2, our model was presented and tested on its capabilities to describe changes in the fluid status of three healthy volunteers undergoing fluid administration. In Chapter 3 we extended the model to simulate mechanical ventilation and calculate dynamic indices for fluid responsiveness. In Chapter 4 a first step towards patient-specific modeling was made by including models for commonly used medication (anesthetics, inotropes and vasopressors). There the predictive capability of the model was tested for three patients in a retrospective surgical dataset. From the results we concluded that including a model for anesthesia, which affects long term average blood pressure, is key for accurate fluid distribution predictions. Also, boluses or short term pumps of vasopressors have little influence on the fluid distribution.

The goal of our current study is to test the predictive capabilities of the model regarding plasma and interstitial volume in an intensive care setting. We set up a prospective study for patients after cardiac and vascular surgery, and recorded hemodynamic variables and fluid infusion and losses. Additionally we obtained

retrospective surgical data. Firstly, we present the data of four patients and simulate the subjects with our *generic-model* of cardiovascular fluid exchange (presented in Chapter 4). Next, to move towards better patient predictions, we examine our *generic-model* assumptions, by performing several model variations are performed for one representative patient. Firstly, we exclude the urine production model by replacing the output of urine model by actually measured output (*prescribed-urine model*). Secondly, we replace our complete fluid exchange model by a simple model, based on the hypothesis that blood volume is always regulated in the longterm and can therefore be taken as constant (*constant-blood-volume model*). Thirdly, we increased and decreased membrane permeability (k_f) ten-fold. Based on these results, we aim to provide insight into what further steps may be needed to translate our pilot model to a clinical decision support model.

5.2 Methods

5.2.1 Generic model

Our cardiovascular fluid exchange model is extensively described in Rosalina et al. (2019). The cardiovascular model represents the systemic circulation and includes a cycle-averaged model for the cardiac left ventricle. The pressure is determined by a linear relationship based on the maximal and passive elastances of the left ventricle (E_{max} and E_{pas}). The mean arterial (p_{art}) and venous pressure (p_{ven}) are determined by compliances (C), unstressed volumes (V_0) and total blood volume (V_{bl}). Mean capillary pressure (p_{cap}) is calculated with cardiac output and peripheral resistance (R_p).

Capillary pressure is an important link between the cardiovascular hemodynamic state and whole body fluid distribution since it is one of the driving forces for fluid exchange between the vessels and the interstitium. The fluid exchange model describes the intake of fluid, through intravenous infusion (J_{inf}) and basal intake (J_{intake}), the loss of fluid, through bleeding, (J_{bleed}), insensible losses (J_{ins}), and urine production (J_U), and fluid exchange through transcapillary exchange($J_{V,TC}$), and lymph fluid flow ($J_{V,L}$). The balance between hydrostatic (p_{cap} and p_I) and osmotic pressure (π_{cap} and π_I) is the driving force for transcapillary fluid exchange, moving volume from the vascular (V_{PL}) to interstitial compartment (V_I). Urine production (J_U) is assumed to be linearly dependent on plasma volume with a normal urine production rate ($J_{U,N}$) (Rosalina et al., 2019). Insensible losses are assumed to be constant.

In surgical patients, arterial pressure is also affected by medication. In this chapter, we only modeled propofol (anesthesia) and noradrenaline (vasopression) administration, based on the findings in Chapter 4. Bolus administrations of vasopressors and analgesia are not included, because they have a limited effect on fluid distribution. For the distribution of propofol, we use a three-compartment

pharmacokinetic model with an effect-site compartment as described by Marsh et al. (1991). For the action of propofol, we use a pharmacodynamics model with a sigmoidal relationship (4.9) between cardiovascular effect and effect-site concentration C_e (Derendorf et al., 1999). For the noradrenaline we use a one-compartment pharmacokinetic model without effect-site. The pharmacodynamic effect is described by a linear model (4.10).

5.2.2 Clinical data

A prospective dataset was obtained from seven patients that underwent open-heart surgery at Maastricht University Medical Center. Exclusion criteria were advanced chronic kidney disease (CKD 4) or patients that need dialysis, and known inflammatory diseases. The study was approved by the local Medical Research Ethics Committees United (study ID: non-WMO METC 2018-0414). The study was classified as non-WMO, since readily available measurements are collected. Informed consent was deemed necessary, and obtained for all included patients. All data were analyzed anonymously.

Firstly, patient characteristics such as age, height, and weight were obtained from the electronic patient information system (PDMS, Patient Data Management Systeem, Chipsoft ®, Amsterdam, The Netherlands). Secondly, retrospective periodical measurements were obtained during surgery, such as hematocrit, infusion boluses, blood loss, and urine loss. Thirdly, in the ICU we collected data for four hours post surgery in ten-minute intervals. These data included blood pressure, heart frequency, infusion (fluid and drugs) pump settings, blood, and urine loss, and respiratory settings from the intensive care electronic archive (ICCA, IntelliSpace Critical Care and Anesthesia everywhere, Philips, The Netherlands).

In this pilot study, four representative patients from the dataset are selected. Patient 1 received a coronary artery bypass grafting surgery. Patient 2, 3 & 4 received a mini mitral valve repair.

5.2.3 Parameter estimation

Cardiovascular parameters

The parameter settings for the cardiovascular system were tuned to match initial conditions of arterial blood pressure for each patient, obtained from the preoperative patient data. Heart rate was taken to be constant during and after surgery, since cardiovascular regulation (baroregulation and the Bainbridge reflex) is assumed to be inactive. Total blood volume (V_{bl}) for each patient was determined by an empirical equation as posed by Drobin et al. (1999):

$$V_{bl} = \alpha_1 \cdot w + \alpha_2 \cdot h^3 + \alpha_3 \tag{5.1}$$

where w is the weight in [kg], h is the height in [m], and empirical parameters (α_1 = 32.19, α_2 = 366.9, α_3 = 604.1). Hematocrit was assumed to be 36 %. The total V_{bl} is divided over the arteries (17.5 %), microcirculation (5 %) and veins (77.5 %). The total venous unstressed volume is 70% of V_{bl} (Feihl et al., 2009) and divided over the vessels accordingly.

Fluid distribution parameters

Interstitial volume (V_I) for each patient was determined by scaling parameters from Xie et al. (1995) to the patient weight. Protein initial conditions are taken from Rosalina et al. (2019). Settings for many parameters in the fluid exchange model are taken from Rosalina et al. (2019), tuned to healthy volunteer data. Settings for normal lymph flow ($J_{L,N}$) and protein permeability-surface area product of the capillary (PS) were computed, to satisfy steady state conditions (as explained in (2.32). Since urine production is reduced during surgery and intensive care period, J_{UN} was adapted to 0.5 ml/kg/h as described by Gupta et al. (2016). Insensible losses (J_{ins}) are taken to be constant at 46 ml/h from Brandstrup (2006). Infusion rate (J_{inf}) is determined from the surgery and intensive care data. Each new iv-fluid bag is registered, and J_{inf} is determined by assuming that fluid is infused linearly in time until the next bag is attached.

Pharmacokinetic and -dynamic parameters

In this model, only continuous propofol and noradrenaline pumps are included. Firstly, weight dependent pharmacokinetic rate constants for propofol were taken from Marsh et al. (1991). Kazama et al. (1999), describe the total effect of propofol on blood pressure, characterised by C_{50}, k_{max} and γ (4.9). Pharmacodynamic parameters are taken from this study and k_{max} is taken equal to estimations in Chapter 4. During surgery, there is no information on the pump speed of propofol, thus we assume a fixed infusion rate of 20 ml/h with a concentration of 10 mg/ml. During intensive care the measured pump speed is adopted as model input.

Secondly, for noradrenaline an elimination rate is calculated based on a half time of 2.5 minutes (Farmacokinetisch Kompas, 2019). The pharmacodynamic parameters are tuned based on the study by Nygren et al. (2006). Here, the change in peripheral resistance is measured for one specific concentration, and we assume the pharmacodynamic effect can be described by a linear model (4.10). During surgery, there is no information on the pump speed of noradrenaline either, thus we take a fixed rate equal to that at the admission to intensive care with a concentration of 0.1 mg/ml.

5.2.4 Simulations performed

The model was implemented in MATLAB 2014b. Differential equations are solved by an Euler forward integration scheme with a time step of 0.1 s. First, we simulated each patient scenario with our *generic model* as described in the previous sections. Model results on blood pressure, heart rate and urine production are shown and compared in the results section. Additionally, blood volume and interstitial volume are predicted.

Next, several model variations are performed for one representative patient (patient 2). First, we excluded the urine production model by replacing the output of urine model by actually measured output. This variation is investigated because of our observation in Chapter 2 that the urine production model is too simple. We analyze the difference in blood and interstitial volume and arterial blood pressure for the *generic-model* and *prescribed-urine model*

Secondly, we replace our complete fluid exchange model by a simple model, based on the hypothesis that blood volume is always regulated in the longterm and can therefore be taken as constant. In that case, changes in interstitial volume (ΔVI) can be calculated from infused volume (V_{inf}), and fluid loss through urine, based on the *prescribed-urine model* to investigate (V_U), insensible losses (V_{ins}) and bleeding (V_{bleed}).

$$\Delta V_I = V_{inf} - V_U - V_{ins} - V_{bleed} \tag{5.2}$$

The interstitial volume as predicted by this *constant-blood-volume model*, is compared to the previously predicted volumes.

Lastly, one of the major problems in fluid overloaded patients is the occurrence of sepsis. In the model we interpret this as an increase in membrane permeability (k_f). In the model, this value is increased and decreased ten-fold and the effect on interstitial and blood volume is investigated. For simplicity, here only the *prescribed-urine model* is used.

5.3 Results

5.3.1 Generic model simulations

Patient 1

Measured data

Measured data during surgery and intensive care for patient 1 are shown in Figure 5.1 in black. During surgery, from 0 to 390 minutes, propofol (10 mg/ml) administration (Figure 5.1A) is 20 ml/h. During intensive care period, propofol administration is reduced to 6.8 ml/h at 420 minutes, to 3.8 ml/h at 600 minutes

and to 0 ml/h at 650 minutes. Noradrenaline (Figure 5.1B) is administered at 6 ml/h during surgery and intensive care period (0.1 mg/ml).

During surgery, mean arterial blood pressure data is not available for this study. In the intensive care, blood pressure (Figure 5.1C, in black) rose from 66 mmHg to 111 mmHg. Heart rate data during is surgery not available either. In the intensive care (Figure 5.1D, in black) the heart is paced at 80 bpm, until 610 minutes. Thereafter, the heart rate increases to 100 bpm.

Turning to the volume measurements, during surgery 4860 ml of fluid is administered and this was increased to 6170 ml at the end of intensive care period (Figure 5.1E, solid line). During surgery, 1250 ml blood loss is recorded, this rose to 1300 ml at the end of intensive care period (Figure 5.1E, dashed line). Additionally 180 ml urine is produced during surgery, which rose to 1050 ml at the end of intensive care period (Figure 5.1G, in black).

Model results

In the model, during surgery, predicted mean arterial blood pressure (Figure 5.1C in blue) decreases from 102 mmHg to 55 mmHg. Next, during intensive care period, the model predicted that blood pressure increases continuously to 110 mmHg. This corresponds to the measured data. Since baroregulation is turned of, modeled heart rate remains at 80 bpm during the full simulation (Figure 5.1D in blue).

In the first 100 minutes of surgery, blood volume (Figure 5.1F, in red) increases from 4600 ml to 5400 ml. In the intensive care period blood volume decreases slowly to 4550 ml. The infused volume contributes to an increase in interstitial volume (Figure 5.1F, in blue) from 8120 ml to 9560 ml at the end of surgery. A further increase to 10220 ml at the end of intensive care period is observed. Lastly, the predicted urine production (Figure 5.1G, in blue) is 1750 ml at the end of surgery, and 2660 ml at the end of intensive care period. This is higher than the measured urine production.

Patient 2

Measured data

Measured data during surgery and intensive care period for patient 2 are shown in Figure 5.2 in black. During surgery, from 0 to 390 minutes, propofol (10 mg/ml) administration (Figure 5.1A) is 20 ml/h. During intensive care period, propofol administration is reduced to 7 ml/h at 420 minutes, to 0 ml/h at 540 minutes. Noradrenaline (Figure 5.2B) is administered at 8 ml/h during surgery (0.1 mg/ml). In the intensive care period this is reduced to 6 ml/h at 550 minutes, and to 5 ml/h at 590 minutes.

During surgery, mean arterial blood pressure data is not available for this study. In the intensive care, blood pressure (Figure 5.2C, in black) is around 60 mmHg. Some temporary increases to approximately 80 mmHg are observed.

Heart rate data during is surgery not available either. In the intensive care (Figure 5.2D, in black) it decreases for 107 bpm to 85 bpm.

Turning to the volume measurements, during surgery 7260 ml of fluid is administered and this was increased to 9070 ml at the end of intensive care period (Figure 5.2E, solid line). During surgery, 2150 ml blood loss is recorded, this rose to 2240 ml at the end of intensive care period (Figure 5.2E, dashed line). Additionally 2050 ml urine is produced during surgery, which rose to 2580 ml at the end of intensive care period (Figure 5.2G, in black).

Model results

In the model, during surgery, predicted mean arterial blood pressure (Figure 5.2C in blue) decreases from 67 mmHg to 40 mmHg. Next, during intensive care period, the model predicted blood pressure continuously increases to 62 mmHg. This corresponds to the measured data. Since baroregulation is turned of, modeled heart rate remains at 75 bpm during the full simulation (Figure 5.2D in blue).

In the first 120 minutes of surgery, blood volume (Figure 5.2F, in red) increased from 4600 ml to 5480 ml. Subsequently, blood volume decreases slowly to 4470 ml at the end of the intensive care period. The infused volume contributes to an increase in interstitial volume (Figure 5.2F, in blue) from 8400 ml to 10000 ml at the end of surgery. Interstitial volume continues to increase to 12000 ml at the end of intensive care period. Lastly, the predicted urine production (Figure 5.2G, in blue) is 2020 ml at the end of surgery, and 3400 ml at the end of intensive care period. This is higher than the measured data.

Patient 3

Measured data

Measured data during surgery and intensive care period for patient 3 are shown in Figure 5.3 in black. During surgery, from 0 to 330 minutes, propofol (10 mg/ml) administration (Figure 5.3A) is 20 ml/h. During intensive care period, propofol administration is reduced to 8 ml/h at 360 minutes, to 8.4 ml/h at 420 minutes. Noradrenaline (Figure 5.3B) is administered at 0.1 ml/h during surgery (0.1 mg/ml). During intensive care period it is slowly increased to 2 ml/h.

During surgery, mean arterial blood pressure data is not available for this study. In the intensive care, blood pressure (Figure 5.3C, in black) rose from 39 mmHg to 76 mmHg, with some high outliers to 113 mmHg. Heart rate data during is surgery not available either. In the intensive care (Figure 5.3D, in black) it is 80 bpm, until 450 minutes, whereafter it slowly increases to 90 bpm.

Turning to the volume measurements, during surgery 7400 ml of fluid is administered and this was increased to 9750 ml at the end of intensive care period (Figure 5.3E, solid line). During surgery, 2650 ml blood loss is recorded, this rose to 3060 ml at the end of intensive care period (Figure 5.1E, dashed line).

Additionally 1160 ml urine is produced during surgery, which rose to 2200 ml at the end of intensive care period (Figure 5.3G, in black).

Model results
In the model, during surgery, predicted mean arterial blood pressure (Figure 5.3C in blue) decreases from 72 mmHg to 52 mmHg. Next, during intensive care period, the model predicted blood pressure slowly increases to 63 mmHg. This corresponds to the measured data. Since baroregulation is turned of, modeled heart rate remains at 75 bpm during the full simulation (Figure 5.1D in blue).

In the first 143 minutes of surgery, blood volume (Figure 5.3F, in red) increased from 5600 ml to 6700 ml. In the intensive care period blood volume decreases slowly to 5540 ml. The infused volume contributes to an increase in interstitial volume (Figure 5.3F, in blue) from 10770 ml to 13000 ml at the end of surgery. Interstitial volume continues to increase to 14400 ml at the end of intensive care period. Lastly, the predicted urine production (Figure 5.3G, in blue) is 1700 ml at the end of surgery, and 3240 ml at the end of intensive care period. This is higher than the measured urine production.

Patient 4

Measured data
Measured data during surgery and intensive care period for patient 4 are shown in Figure 5.4 in black. During surgery, from 0 to 240 minutes, propofol (10 mg/ml) administration (Figure 5.4A) is 20 ml/h. During intensive care period, propofol administration is reduced to 12 ml/h at 270 minutes, to 10 ml/h at 300 minutes and to 0 ml/h at 390 minutes. Noradrenaline (Figure 5.4B) is administered at 3.1 ml/h during surgery (0.1 mg/ml). During intensive care period, the administration rate is increased to 4.1 ml/h from 300 to 430 minutes, and decreased to 0 ml/h afterwards.

During surgery, mean arterial blood pressure data is not available for this study. In the intensive care, blood pressure (Figure 5.4C, in black) rose from 73 mmHg to 91 mmHg. Heart rate data during is surgery not available either. In the intensive care (Figure 5.4D, in black) there is a slow increase in heart rate from 59 bpm to 66 bpm.

Turning to the volume measurements, during surgery 6600 ml of fluid is administered and this was increased to 8180 ml at the end of intensive care period (Figure 5.1E, solid line). During surgery, 1450 ml blood loss is recorded, this rose to 1800 ml at the end of intensive care period (Figure 5.4E, dashed line). Additionally 200 ml urine is produced during surgery, which rose to 520 ml at the end of intensive care period (Figure 5.4G, in black).

Model results
In the model, during surgery, predicted mean arterial blood pressure (Figure 5.4C in blue) varies around 75 mmHg. Next, during intensive care period, the model

predicted blood pressure slightly increases to 81 mmHg. This corresponds to the measured data. Since baroregulation is turned of, modeled heart rate remains at 75 bpm during the full simulation (Figure 5.4D in blue).

In the first 180 minutes of surgery, blood volume (Figure 5.4F, in red) increased from 5600 ml to 6600 ml. In the intensive care period blood volume decreases slowly to 5800 ml. The infused volume contributes to an increase in interstitial volume (Figure 5.4F, in blue) from 10800 ml to 14000 ml at the end of surgery. Interstitial volume continues to increase to 15000 ml at the end of intensive care period. Lastly, the predicted urine production (Figure 5.4G, in blue) is 1170 ml at the end of surgery, and 2740 ml at the end of intensive care period. This is higher than the measured urine production.

5.3.2 Model variations

Figure 5.5 shows how variations in our model assumptions affect results for a representative patient (patient 2). In solid lines, the results of the *generic-model* are shown. Simulations with the *prescribed-urine model* are shown in dotted lines. In this case, the urine output of our generic urine production model is replaced by the actual measured urine output. Urine output is 1050 ml lower than in the generic model. Of this volume, only 150 ml is stored in the blood compartment, which results in a slightly increased arterial pressure (about +9 mmHg). The remaining 900 ml are stored in the interstitium.

The simulation results of the *constant-blood-volume model* are shown in gray. Here we simply compute interstitial volume on the basis of the mass balance for the fluid entering and leaving the patient, assuming vascular volume to be constant. At the end of the simulation, the predicted interstitial volume is converged to the same volume as that in the prescribed-urine model.

Next, Figure 5.6 shows our investigation on the effect of a varying membrane permeability (k_f). In solid lines, the reference value for k_f is used, representing the *prescribed-urine model* simulation. When decreasing the membrane permeability ten-fold, the arterial pressure, blood and interstitial volume are affected (in dotted red and blue). Blood volume is increased throughout the simulation and remains elevated by about 1500 ml at the end of the simulation. Correspondingly, this leads to a lower interstitial volume. Arterial pressure is closely related to the vascular volume, it increases and ends at a higher value (about +55 mmHg) at the end of the simulation.

Increasing the membrane permeability has a much smaller effect, decreasing pressure (about -14 mmHg) and blood volume slightly (about -100 ml), and correspondingly increasing interstitial volume. The trends within these upper and lower boundaries of k_f remain the same. Namely, at the end of surgery blood volume is decreasing towards the reference level, and change in interstitial volume can vary up to 30% at the end of simulations.

5.4 Discussion

Adequate fluid administration in critical patients has been shown to be extremely difficult. A lack of specific and sensitive measurements for fluid distribution, no consensus on fluid protocols and large inter-patient variability are some of the pitfalls. Additionally, complications related to fluid buildup in the interstitial space occur on the time scale of hours, making direct evaluation of fluid administration impossible. Mathematical modeling can help in predicting the fluid shifts, based on physiology and physics. To test these long term predictions, we performed a pilot study in the intensive care.

The results of this study show that with our *generic model* we were able to simulate four patients during and after surgery. Predicted arterial blood pressure corresponded closely to the blood pressure measured in the ICU. Urine production was overestimated in all patients. Still, pilot results show that we can simulate the trends of fluid buildup after fluid administration with our current model. The model is shown to be sensitive to urine production and membrane permeability, interestingly, no matter the parameter settings, all extra fluid buildup occurs in the interstitial space. Our simulations with the *constant-blood-volume model* confirm that indeed on the long term, blood volume is well regulated and the interstitial space acts as a buffer for extra fluid.

5.4.1 General considerations

Mathematical model

Our model consists of a coupled cardiovascular fluid exchange model, coupled to drugs through a pharmacokinetic and -dynamics model. We used a 0-d lumped parameter model with cycle-averaged elastance model for the left ventricle, representing the heart. Notably, our patient population consists of cardiothoracic surgical patients. In this patient group, often large volumes are administered, making this an interesting group for our pilot study. Also, much perioperative data is available for these patients. However, their cardiac function is compromised before surgery and in all patients the heart was arrested using cardioplegia, during which the heart-lung machine was used for cardiopulmonary bypass. We did not include this bypass in our model. The cardiac function may still be recovering after cardioplegia, which may result in lower cardiac output as opposed to our assumption of a healthy heart

Additionally, the effect of baro- and bainbridge regulation is neglected in this study. For simplicity, we assume that regulatory functions are fully suppressed due to the administration of propofol. Since we did not include pain or stress either, heart rate remains constant throughout the simulations. This does explain the discrepancy between model results and clinically measured heart rate.

The assumption is allowed since previous work has shown that heart rate has a small effect on arterial blood pressure.

The fluid exchange model is extensively discussed in our earlier work (Rosalina et al., 2019). We adopted the model with the parameter settings matched to data from our healthy volunteer study. It has been shown in literature, that surgical trauma and inflammation affect the glycocalix barrier. In some cases, the glycocalix in the microcirculation may be completely destroyed, leading to increased membrane permeability (Henrich et al., 2010; Chappell et al., 2014). In our model, this effect was investigated qualitatively by inducing a variation of membrane permeability. Another option is to use the adapted Starling equation (Adamson et al., 2004), where local fluid exchange in the capillaries can be described better. This allows for local changes adaptation of the membrane permeability. For the purpose of this study we only looked at the global behavior of fluid exchange, this the orginal Starling equation is sufficient.

Experimental data

We tested our model on a semi-prospective dataset of four intra- and postoperative patients. These data contain preoperative patient characteristics, retrospective discrete data points during surgery, on infused volume, hemorrhage and urine production, and prospective intensive care data. The latter is collected for four hours post surgery in ten-minute intervals. Since the exact rate of infusion or bleeding is unknown, we assume that fluid infusion is continuous from one to the next discrete datapoint.

During surgery, arterial blood pressure, heart rate or medication data were not available for this study. We modeled the propofol and noradrenaline administration at a fixed rate. Since temporary changes in blood pressure are not important for this study, this choice is justified.

To test our model results, we only have urine production, blood loss and infused volumes available, next to standard hemodynamic monitoring. These data are deemed enough for the purpose of this pilot study, namely predicting the plasma and interstitial volume trends. Although these changes in volume cannot be quantitatively compared to experimental data, they can provide useful insights into clinically expected trends.

5.4.2 Results

Averaged over the four patients, about 8300 ml was infused during surgery and the 4 hour stay in the ICU. About 45% of the fluid infused had left the body through bleeding or urine production. Of the remaining 55%, less than 1% is expected to have left the body through insensible losses. According to all model versions evaluated, the remaining fluid is almost completely stored in the interstitium after 4 hours post surgery. This demonstrates the role of the interstitium as a fluid buffer, enabling intravascular volume to remain fairly constant. This was confirmed by our simulations with the *constant-blood-volume model*. Additional simulations showed that this buffer function is affected when endothelial permeability is increased.

The total urine production at the end of simulations is about 1000 ml higher than measured urine for each patient. In the model, urine production depends on plasma volume only. As plasma volume is fairly constant, urine production rate in our model is fairly constant as well. In reality, urine production can vary widely, but it is probably depressed, since arterial blood pressure and renal perfusion are low in the patients (Gupta et al., 2016). This means that more volume remains in the body. To test the influence of a depressed urine production, we bypassed the urine production model by prescribing actually measured urine production in our *prescribed-urine model*. This increased the amount of fluid that remains in the patients body. This extra fluid was found to be stored in the interstitium, illustrating once again how intravascular volume remains constant.

Since plasma volume is so well controlled, we performed simulations with our *constant-blood-volume model* to test if interstitial volume can be calculated as the net balance of fluid administration, bleeding, urine production and perspiration, assuming that plasma volume remains constant. From the results we can conclude that on the long term, this is the case. For real-time predictions however, the full mathematical model provides more accurate results.

The buffer function of the interstitium relies on transport across the endothelium. Amongst others, this transport depends on membrane permeability. In our model we used a value of 0.15 ml/mmHg · s, which is within the range reported in literature (0.008 - 0.34 ml/mmHg · s; Chapple et al., 1993). A ten-fold increase to 1.5 ml/mmHg · s, which is outside the reported range, did not affect the fluid distribution. However, a ten-fold reduction of the permeability to 0.015 ml/mmHg · s, which is still within the reported range, did affect the buffer function. In this case the surplus of fluid in the patients body was distributed over the vascular and interstitial compartment in a ratio 1:3. Clinically, this simulation may represent the effect of sepsis or other inflammatory diseases.

The simulations (Figure 5.6) indicate that our original estimation of membrane permeability (k_f) may have been too high, since no extra fluid buildup occurs in the *high* permeability simulation. The overestimation of urine production in the *generic model* seems to contradict this. At first glance, this overestimation may raise the question if the permeability is too low, leading to the fluid being retained in the plasma volume and excreted as urine. However, we believe that the high urine production is due to our too simple urine model. This is supported by the fact that in the *prescribed-urine model* the surplus of fluid moves toward the interstitium and does not remain in the plasma volume.

The purpose of the current chapter was to perform a pilot study, that gives an indication of possibilities for implementation of the current model in the intensive care setting. Our pilot results highlight the buffer function of the interstitial space, and the dependence of this function on membrane permeability.

5.4.3 Future work

To move towards a clinically applicable model, some improvements can be made and more clinical testing must be performed. First, to improve the model, the urine production model must be improved. Our results show that the current urine production model overestimates urine production all patients by approximately 1000 ml. Now, the urine production model is solely dependent on a change in vascular volume. However, we know that during anesthesia urine production is lower, partly due to a low blood pressure. Additionally, hormonal regulation pathways and medication affect the urine production. More research is necessary to model these effects.

Second, to determine quantitative interstitial volume changes, more investigation into estimations of membrane permeability (k_f) must be performed. Research on the glycocalix is widely performed, and may give measurement techniques that can determine k_f. Alternatively, data assimilation techniques give the possibility for inverse parameter estimation. Combining current observations with model outputs can lead to better parameter estimation, leading to better model outputs (Asch et al., 2016).

The currently studied patient population was subjected to high-impact cardiothoracic surgery, complicating the fluid balance. The benefit of this group is that there is high fluid administration and extensive data registration. To test the model in a more controlled setting, a more homogenous and larger patient group may be used. Here, it is key to obtain a good initial condition for the patients, which increases the reliability of the model results. It is especially important to obtain intra- and postoperative data of hemodynamic variables and fluid administration and loss (through bleeding, urine production and insensible losses). Ideally, we would also obtain measurements indicating the intra- and extravascular volume distribution.

This could be done with e.g., hemodilution measurements to determine plasma volume. Body weight or even impedance measurements could be used to get an indication of interstitial fluid change.

Finally, functional clinical outcome may be recorded and compared to the interstitial volume predictions. This can give a qualitative indication on the predictive model capabilities for edema-related complications.

5.5 Conclusion

In conclusion, we tested our previously developed mathematical model for fluid distribution in postoperative patients in the Intensive Care Unit. This is important, since most hypervolemia related complications occur in postoperative care. Our simulation results suggest that vascular volume is controlled well, and that the interstitial volume works as a buffer, acting as a temporary storage for the surplus of fluid administered to the patient. Interestingly, on the long term at the end of ICU, this increase can be determined directly, as the net balance of fluid administration, bleeding, urine production and perspiration.

Acknowledgements

Special thanks to the patients that generously provided their consent to contribute in this study. Additional thanks to the staff of Department F3 in Maastricht UMC+, for their interest and contributions. This work was performed within the IMPULS II perioperative monitoring framework in collaboration with Philips Eindhoven and Catharina Hospital Eindhoven.

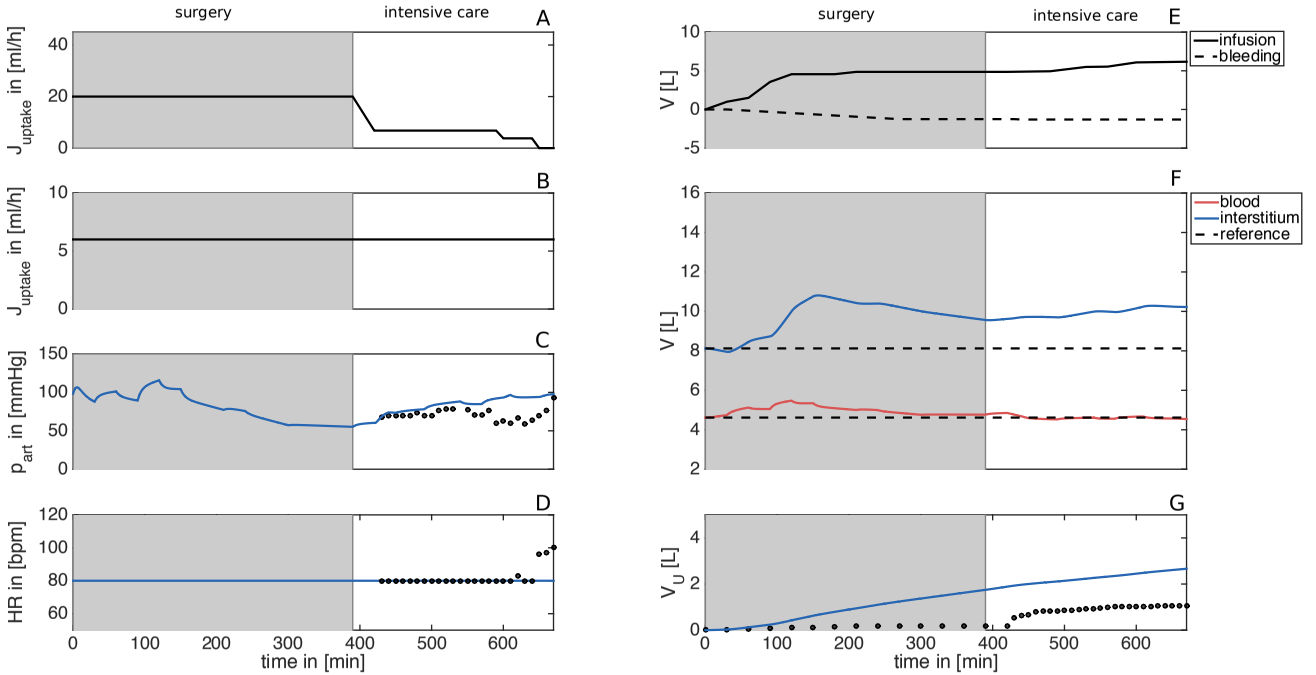


Figure 5.1: Perioperative measurements and model predictions for Patient 1, with (A) propofol and (B) noradrenaline administration rate (J_{uptake}), (C) mean arterial blood pressure (p_{art}) and (D) heart rate (HR). Also shown are, (E) infused volume (V_{inf}) and blood loss volume (V_{bleed}), (F) total blood volume (V_{bl}) in red and interstitial volume (V_i) in blue, compared to the reference volume (dashed black) and (G) urine volume (V_U). Panels show measured data in black, and model results obtained with the *generic-model* in blue and red.

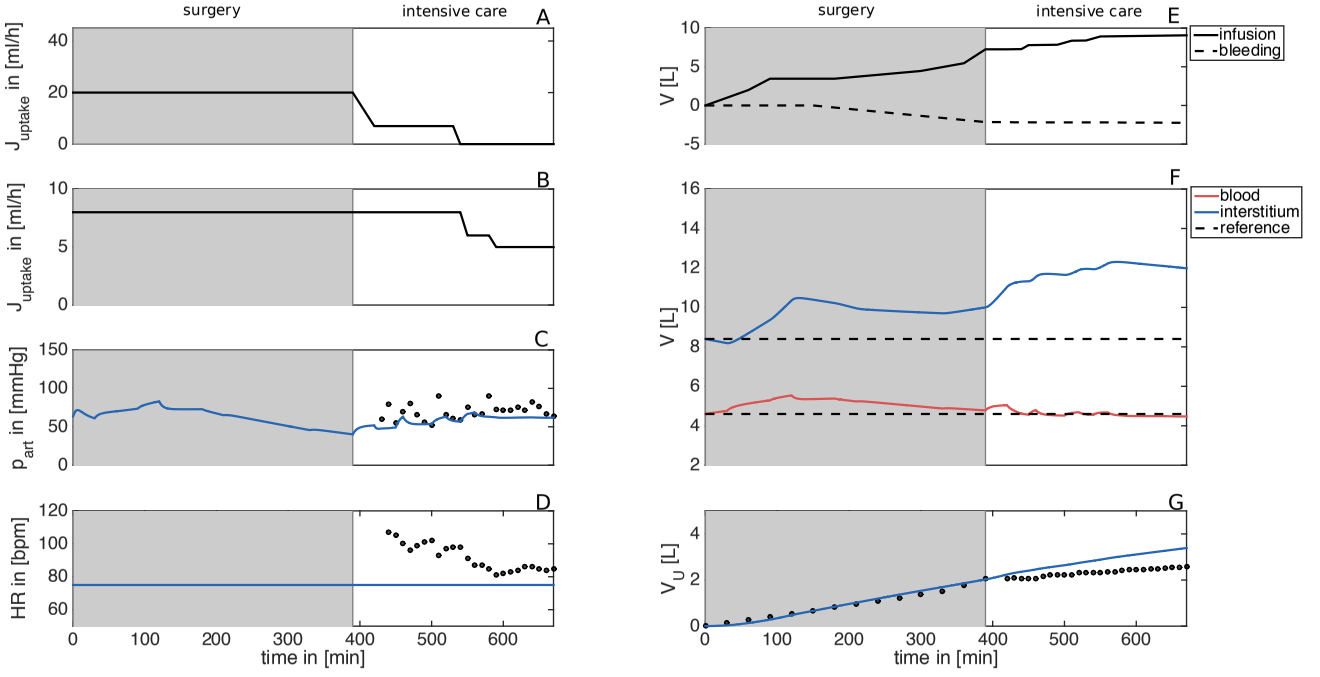


Figure 5.2: Perioperative measurements and model predictions for Patient 2, with (A) propofol and (B) noradrenaline administration rate (J_{uptake}), (C) mean arterial blood pressure (p_{art}) and (D) heart rate (HR). Also shown are, (E) infused volume (V_{inf}) and blood loss volume (V_{bleed}), (F) total blood volume (V_{bl}) in red and interstitial volume (V_i) in blue, compared to the reference volume (dashed black) and (G) urine volume (V_U). Panels show measured data in black, and model results obtained with the *generic-model* in blue and red.

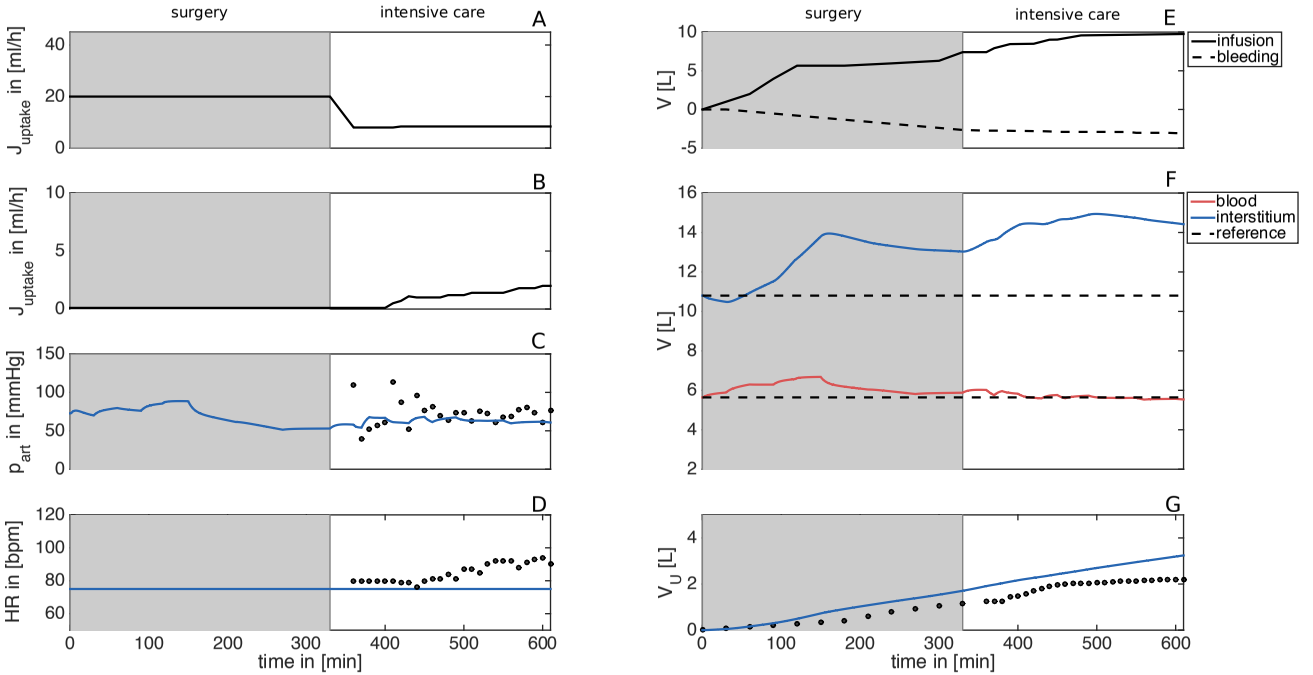


Figure 5.3: Perioperative measurements and model predictions for Patient 3, with (A) propofol and (B) noradrenaline administration rate (J_{uptake}), (C) mean arterial blood pressure (p_{art}) and (D) heart rate (HR). Also shown are, (E) infused volume (V_{inf}) and blood loss volume (V_{bleed}), (F) total blood volume (V_{bl}) in red and interstitial volume (V_i) in blue, compared to the reference volume (dashed black) and (G) urine volume (V_U). Panels show measured data in black, and model results obtained with the *generic-model* in blue and red.

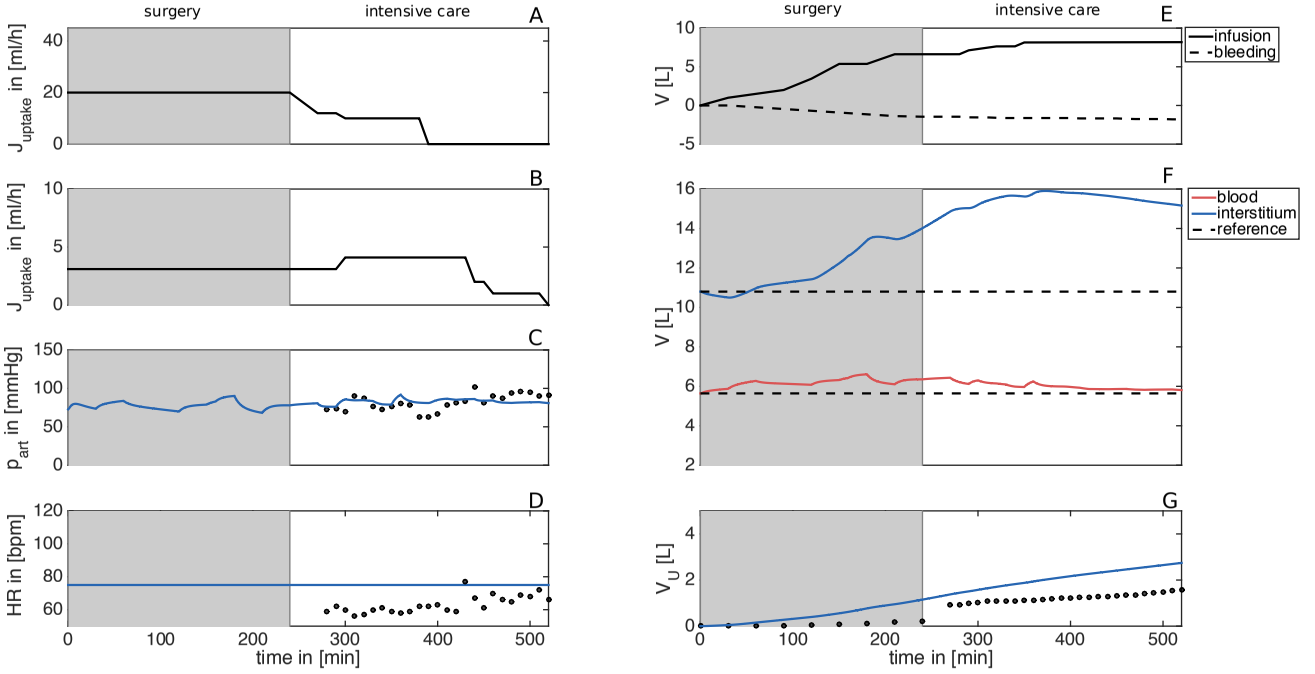


Figure 5.4: Perioperative measurements and model predictions for Patient 4, with (A) propofol and (B) noradrenaline administration rate (J_{uptake}), (C) mean arterial blood pressure (p_{art}) and (D) heart rate (HR). Also shown are, (E) infused volume (V_{inf}) and blood loss volume (V_{bleed}), (F) total blood volume (V_{bl}) in red and interstitial volume (V_I) in blue, compared to the reference volume (dashed black) and (G) urine volume (V_U). Panels show measured data in black, and model results obtained with the *generic-model* in blue and red.

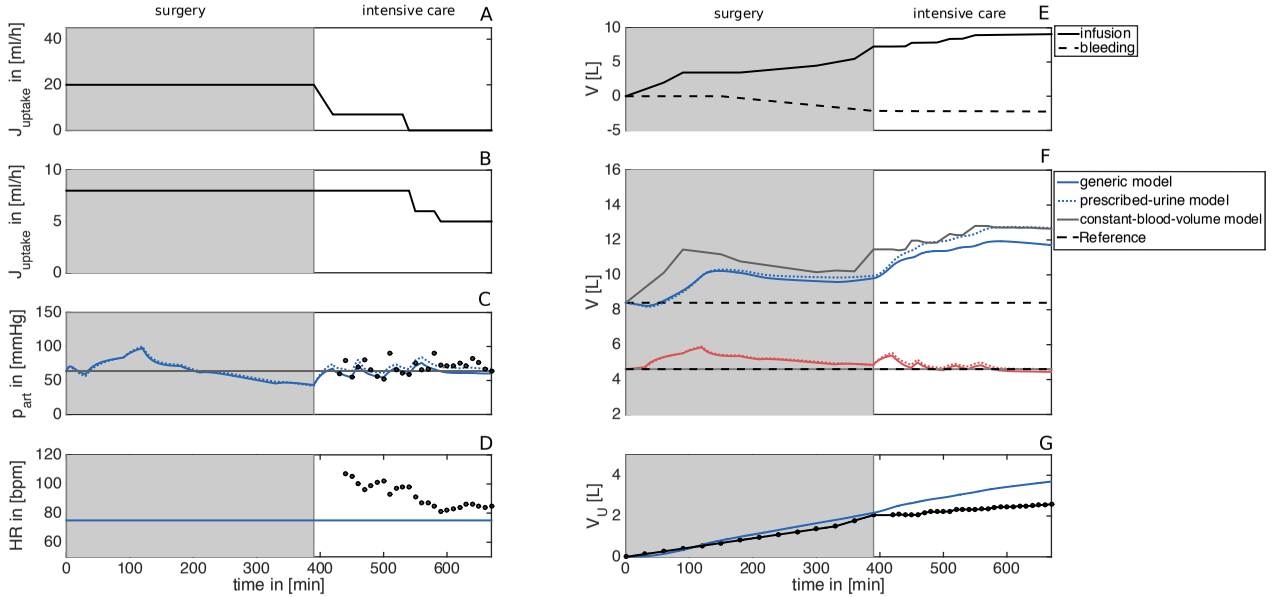


Figure 5.5: Model variations for Patient 2, with (A) propofol and (B) noradrenaline administration rate (J_{uptake}), (C) mean arterial blood pressure (p_{art}) and (D) heart rate (HR). Also shown are, (E) infused volume (V_{inf}) and blood loss volume (V_{bleed}), (F) total blood volume (V_{bl}) in red and interstitial volume (V_I) in blue, compared to the reference volume (dashed black) and (G) urine volume (V_U). Panels show measured data in black, model results obtained with the *generic-model* with solid lines, the *prescribed-urine model* with dotted lines and *constant-blood-volume model* in grey.

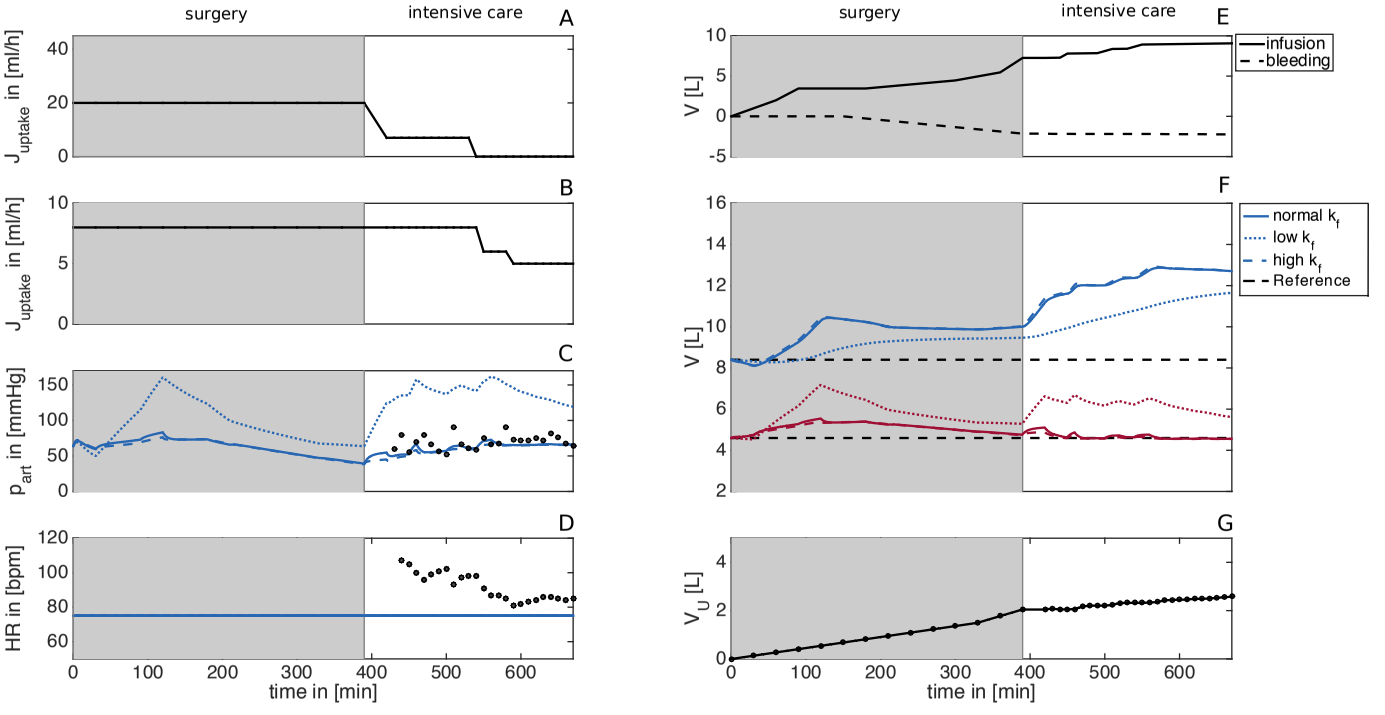


Figure 5.6: Effect of membrane permeability on model predictions for Patient 2, with (A) propofol and (B) noradrenaline administration rate (J_{uptake}), (C) mean arterial blood pressure (p_{art}) and (D) heart rate (HR). Also shown are, (E) infused volume (V_{inf}) and blood loss volume (V_{bleed}), (F) total blood volume (V_{bl}) and interstitial volume (V_I), compared to the reference volume (dashed black) and (G) urine volume (V_U). Panels show measured data in black, model results obtained with normal permeability (k_f) in solid blue and red lines, the simulations with low k_f in dotted lines, and the simulations with high k_f in dashed lines.

Bibliography

Adamson, R. H. et al. (2004). "Oncotic pressures opposing filtration across non-fenestrated rat microvessels". *Journal of Physiology* 557.3, pp. 889–907.

Asch, M., Bocquet, M., and Nodet, M. (2016). *Data assimilation: methods, algorithms, and applications*. Vol. 11. SIAM.

Brandstrup, B. (2006). "Fluid therapy for the surgical patient." *Best Practice & Research. Clinical Anaesthesiology* 20.2, pp. 265–283.

Cecconi, M. et al. (2015). "Fluid challenges in intensive care: the FENICE study". *Intensive Care Medicine* 41.9, pp. 1529–1537.

Chappell, D. and Jacob, M. (2014). "Role of the glycocalyx in fluid management: small things matter". *Best Practice & Research Clinical Anaesthesiology* 28.3, pp. 227–234.

Chapple, C. et al. (1993). "A model of human microvascular exchange: parameter estimation based on normals and nephrotics". *Computer Methods and Programs in Biomedicine* 41.1, pp. 33–54.

Derendorf, H. and Meibohn, B. (1999). "Modeling of Pharmacokinetic/ Pharmacodynamic (PK/PD) Relationships: Concepts and Perspectives". *Pharmaceutical Research* 16.2, pp. 176–185.

Drobin, D. and Hahn, R. (1999). "Volume Kinetics of Ringer's Solution in Hypovolemic Volunteers". *Anesthesiology* 90, pp. 81–91.

Feihl, F. and Broccard, A. F. (2009). "Interactions between respiration and systemic hemodynamics. Part I: Basic concepts". *Intensive Care Medicine* 35, pp. 45–54.

Gupta, R. and Gan, T. (2016). "Peri-operative fluid management to enhance recovery". *Anaesthesia* 71, pp. 40–45.

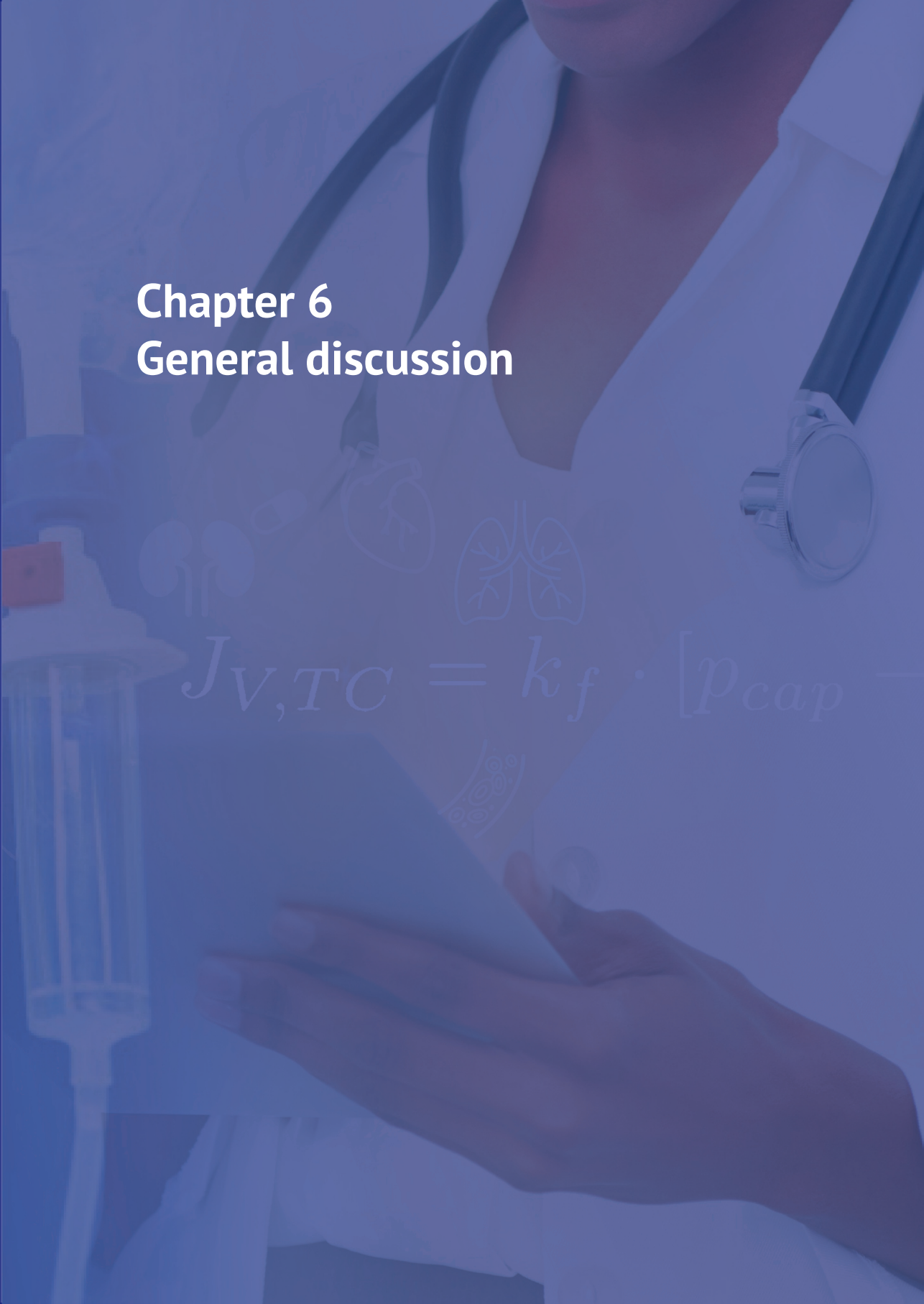
Henrich, M., Gruss, M., and Weigand, M. A. (2010). "Sepsis-induced degradation of endothelial glycocalix". *The Scientific World Journal* 10, pp. 917–923.

Holte, K., Sharrock, N., and Kehlet, H. (2002). "Pathophysiology and clinical implications of perioperative fluid excess". *British Journal of Anaesthesia* 89.4, pp. 622–32.

Kazama, T., Ikeda, K., and Morita, K. (1999). "Comparison of the Effect-site k_{e0}s of Propofol for Blood Pressure and EEG Bispectral Index in Elderly and Younger Patients". *Anesthesiology* 90, pp. 1517–27.

Marsh, B. et al. (1991). "Pharmacokinetic model driven infusion of propofol in children". *British Journal of Anaesthesia* 67.1, pp. 41–48.
Nygren, A., Thorén, A., and Ricksten, S. E. (2006). "Vasopressors and intestinal mucosal perfusion after cardiac surgery: Norepinephrine vs. phenylephrine". *Critical Care Medicine* 34.3, pp. 722–729.
Rosalina, T. T. et al. (2019). "A mathematical model to investigate the effects of intravenous fluid administration and fluid loss". *Journal of Biomechanics* 88, pp. 4–11.
Xie, S. et al. (1995). "A model of human microvascular exchange". *Microvascular Research* 49, pp. 141–162.

Chapter 6
General discussion



6.1 Finding the balance

Fluid administration is one of the most common interventions in medical care. The rationale behind fluid administration is to compensate for fluid loss, caused by bleeding, urine production and evaporation. This compensation is aimed at maintaining good tissue perfusion, and thereby oxygen delivery. Literature shows that too little or too much fluid administration can lead to severe consequences. On the one hand, too little fluid may cause hypoxia, due to low oxygen transport, which in extreme cases can eventually even lead to organ failure (Latta, 1832). On the other hand, too much fluid has the risk of causing hypervolemia, associated with complications related to fluid buildup in the interstitial space. This may lead to edema, for example, causing microvascular compression and possibly hypoxia. These two extremes show that is important to find a fluid administration protocol that balances the risks of both hypo-, and hypervolemia (Holte et al., 2002; Schrier, 2010; Vincent et al., 2006).

Due to complex underlying physiology, a critically ill patient population with inter patient differences, and the fact that the effects of (inadequate) fluid administration develop on a time scale of hours, finding this balance is not straight forward. Currently, there are no specific and sensitive direct measurements available to determine fluid responsiveness and distribution. Indirect measurements to determine if a patient may benefit of fluid administration, are available, but there is not consensus on their usability. Studies show that 50% of the patients that received fluids actually did not respond to a fluid challenge, indicating the need for better tools to asses the fluid status of the patient and decide on whether fluid administration is needed (Cecconi et al., 2015).

6.2 Main achievements

In this thesis we took the first steps towards a clinical decision support tool for fluid administration by developing models for fluid responsiveness and (re-) distribution. The ultimate goal would be to use the models to guide fluid administration and thereby reduce hypervolemia related complications in perioperative care. In Chapters 2 and 3 of this thesis we developed our mathematical model. In Chapters 4 and 5 we focused more on the clinical perspective, by implementing and testing the model with two clinical datasets.

In Chapter 2, we extended an existing fluid exchange model (Xie et al., 1995; Gyenge et al., 2003), with a regulated model of cycle-averaged cardiovascular function (Jongen et al., 2016). This combination allowed us to relate model outputs on fluid distribution in the body to measurable indices such as heart rate and arterial blood pressure, on the basis of underlying physics and physiology. The model was used to study the effects of fluid infusion and blood loss in healthy volunteers. We were able to tune specific parameters, membrane permeability (k_f),

normal lymph flow ($J_{L,N}$) and protein permeability-surface area product of the capillaries (*PS*), to correctly predict the change in plasma and interstitial volume in one experiment (Watenpaugh et al., 1992). Subsequently, we reproduced results from another experiment (Drobin et al., 1999), without additional tuning. Thus, with this model we are able to predict cardiovascular and fluid distribution changes, following fluid administration in healthy volunteers.

In Chapter 3, we aimed at predicting dynamic indices that are used for indirect estimation of fluid responsiveness in the clinic, pulse pressure variation (*ppv*) and stroke volume variation (*svv*). We converted the model of cardiovascular hemodynamics from a cycle-averaged one into a dynamic one, and extended it with models of the pulmonary circulation and lung mechanics, to simulate the effect of spontaneous breathing and mechanical ventilation on hemodynamic function. Firstly, we showed that we could obtain realistic changes in pleural pressure and alveolar volume in healthy volunteers and anesthetized patients during spontaneous breathing and mechanical ventilation (Innes et al., 1993). Secondly, we predicted realistic changes in *ppv*, *svv*, and change in cardiac index for mechanically ventilated, anesthetized patients after a fluid challenge (Belloni et al., 2008). Thirdly, the results showed that *ppv* and *svv* depend on intravascular volume, pericardial and vascular properties, in decreasing order. The developed mathematical model can be used for more advanced interpretation of *ppv* and *svv*, potentially broadening the patient group that can benefit from assessment of these indices.

In Chapter 4 we evaluated our model in the perioperative setting. Here, drugs administered to the patient affect the fluid status directly, due to a change in blood pressure, and indirectly, since blood pressure is used to guide the infusion protocol. To investigate these effects, we extended our model with the pharmacokinetic and -dynamic models for propofol, sevoflurane, phenylephrine, ephedrine and noradrenaline. In a pilot study, we compared model predictions on blood pressure and heart rate with retrospective measured data for three surgical patients. Additionally, we analyzed the predicted changes in plasma, interstitial and urine volume for different model settings, accounting for all drugs, only anesthesia or no drugs at all. From the pilot results we concluded that to model exact intraoperative blood pressure, all anesthetics, inotropes and vasopressors must be included in the model. However, to predict an average blood pressure during surgery and fluid distribution at the end of surgery, vasopressors and inotropes can be omitted.

In Chapter 5 the goal was to test the predictive capabilities of the model in an intensive care setting. We set up a prospective pilot study, recording hemodynamic variables and fluid infusion and losses, for ICU patients after major cardiovascular surgery. We tested the predictive capabilities of the model for interstitial volume, and investigated the effects of the urine production and membrane permeability on the interstitial volume model predictions. Based on our findings in Chapter 4, we neglected the effect of bolusses inotropes and vasopressors.

These results showed that we could simulate the trends of fluid buildup after fluid administration with our current model. Our simulation results confirmed that the interstitial volume works as a buffer, taking up most of the excess administered fluid and thus allowing vascular volume to remain fairly constant. Interestingly, on the long term, this increase could be determined directly, as the net balance of fluid administration, bleeding, urine production and perspiration, while assuming a constant vascular volume.

Overall, the novelty of this work lies in the development of a modeling framework that can be used to make predictions on fluid distribution, responsiveness and urine output, and allows for computation of clinical readily available measurements. The two pilot studies showed that there is potential for this model to contribute to improvement of clinical guidelines for fluid administration in critically ill patients.

6.3 Mathematical modeling perspectives

It is important to note that the findings in this thesis are mostly based on one set of parameters. While we occasionally assessed the sensitivity of model output to the settings of the model input parameters, a more structured sensitivity analysis should be preformed. This can be used to determine which model parameters are most rewarding to determine more accurately (parameter prioritization) and which models can be fixed based on population averages (parameter fixing).

In the master project by De Schipper (2018), a first sensitivity analysis was performed on the fluid exchange submodel of Chapter 2. Here, the elementary effects and variance based sensitivity analysis methods (Saltelli et al., 2004) are applied on the fluid exchange model with 16 input parameters. The results show that there are six parameters responsible for about 90 % of the variance in interstitial volume. These parameters include normal plasma and interstitial volume, normal fluid intake, the capillary pressure coefficient, the protein reflection coefficient and the fluid membrane permeability. These preliminary results give an indication that if these parameters can be estimated correctly, this reduces a large part of the uncertainty on the model output. All other parameters may be fixed, depending on the specific goal of the model. To investigate this further the sensitivity analysis must be repeated for the full model including the cardiovascular system in Chapter 2. Similarly, structured sensitivity analyses should be performed on the models presented in Chapter 3 and Chapter 4. This can be used to test the preliminary results on parameter variations as presented in this thesis.

The mathematical model presented in this thesis can be extended in a number of ways. In Chapter 2 & 5 it became clear that the urine production model is oversimplified. This can be seen in discrepancies between measured and predicted urine volumes. Our urine production model is now solely dependent on a change in vascular volume. However, we know that during anesthesia urine production is

lower, due to a low perfusion and blood pressure and a hormonal response. One of the important mechanisms is the renin angiotensin aldosterone system (RAAS). Literature review shows that there are many mathematical models available to describe the renal system. Many of these studies (Guyton et al., 1972; Ikeda et al., 1979; Keener et al., 1998) describe this system in detail. These complex models are necessary to study physiology, but have too many parameters to be used in a patient-specific model. A simpler model, with less parameters was presented by Averina et al. (2012). However, more research on the implementation should be performed.

Another possible next step in this work, is to include oxygen transport. This would allow investigation of the ultimate goal of fluid administration, to maintain oxygen supply to the tissues. Oxygen uptake and distribution models, such as presented in Jongen et al. (2016), can be added to our fluid exchange model. The resulting model could be used to investigate the effect of hemodilution on oxygen carrying capacity. It might als be used to study the effect of edema buildup on for example, pulmonary oxygen uptake, and increase of capillary resistance.

As mentioned in Chapter 1, besides water, the administered fluid contains a high amount of sodium chloride. These and other ions are distributed to the interstitial and intracellular compartments, and excreted through urine and insensible losses. The original work by Gyenge et al., (1999a, 1999b, 2003) included an ion mass balance and intracellular compartments consisting of red blood cells and tissue cells, where the transport rate depends on the transmembrane potential. Calculating this potential is computationally expensive, which may hamper clinical application of the model. However, when the interest of further studies are related to hyperosmotic solutions, the intracellular compartments should be included.

The translation of our model into the clinical workflow is a challenge. One of the major difficulties is the patient-specific parameter estimation. Since it is not possible to measure all model parameters, there is an uncertainty in the model output due to the uncertainty in the input. Therefore, it is important to find a balance between model complexity and uncertainty (Huberts et al., 2014). To assess the possibility for model reduction, and thereby reduce the amount of unknown parameters, we need to perform a full sensitivity analysis (Saltelli et al., 2004). Also, it is important to match the model complexity to the goal of each application.

6.4 Clinical perspectives

There are multiple roads forward with this work. Firstly we can use the model as an academic and research tool, secondly, as a training tool and thirdly as a clinical decision support tool. In this section, our view on the perspectives for these applications are laid out.

6.4.1 Research tool

One of the benefits of in sillico research is that well defined virtual patients can be created. This allows for specific testing of hypotheses without being compromized by inter-patient variability. Additionally, specific model parameter settings can be varied and their effects can be tested separately. Examples of generating and testing hypotheses have already been shown in this thesis.

For example, in Chapter 3 we investigated the effects of vascular volume and cardiac and vascular properties on *ppv* and *svv*. By varying parameter settings, we found that the pericardial stiffness has a great impact on stroke volume variation. This finding indicates that clinical guidelines may need to be adapted for patients after cardiac surgery, with an open pericardium. Follow up research can be used to investigate the existing guidelines. E.g., one of the guidelines specifies ventilation with a tidal volume of $\geq$ 8 ml/kg. With the model, the effect of lower ventilation can be quantified and possible new insights can be obtained. This may lead to a broader use of *ppv* and *svv* in critical patients.

Another example of parameter variation was presented in Chapter 4. Here, we compared blood pressure results obtained from *generic model* parameters to that obtained with *patient-specific model* parameters. This provides us with qualitative insight on the effects of anesthetics and vasopressors. On the one hand, the temporary effects of vasopressor boluses are shown to have little effect on the final fluid balance. On the other hand, administered fluid has a much larger and prolonged effect on the final fluid buildup. This, technically derived, insight may be of clinical use. It indicates that sometimes administering vasopressors is less harmful than administering fluids, concerning the risk of edema formation.

In Chapter 5 the effect of membrane permeability variation was shown. Since it cannot be measured, this parameter is currently estimated. The critical patient group may be septic, so there can be a large variation in membrane permeability. Our mathematical model results show the effects of a change from our normal membrane permeability. A ten-fold increase of the permeability did not affect the fluid distribution. However, a ten-fold reduction of the permeability did affect the buffer function, leading to the surplus of fluid in the patients body to be distributed over the vascular and interstitial compartment in a ratio 1:3. Model output uncertainty can be reduced if membrane permeability can be estimated precisely, however with a rough estimation general trends can still be predicted.

In Chapter 5, we also presented a model variation. In the *constant-blood-volume model* we assumed that on the long run, plasma volume is well controlled. Our simulation results confirm that, on the long run, the rule of thumb that fluid build up in the interstitial volume equals the net balance of fluid administration and loss, is reasonable. For real time predictions however, a more complex picture is painted, which is why a mathematical model is useful.

6.4.2 Training tool

Another application, moving more towards clinical use, is the development of training tools. Skills and confidence are increased by repetition, obtained by simulated conditions, or in real-life (Morgan et al., 2002). The benefit of using simulation tools in health care is that they are a way of learning without putting patients at risk or any inconvenience (Alinier, 2007). We propose two possible ways forward. Firstly, the current model can be used for virtual training in fluid administration protocols and to increase awareness on the risks of hypervolemia. This approach has been presented previously in neonatal intensive care (Meurs et al., 2018) and general cardiac care (Lumens 2014, CircAdapt). Nowadays, the CircAdapt tool is part of the curriculum for medical students at Maastricht UMC+.

Secondly, this model may be integrated into physical hands-on training tools. E.g., in patients on extracorporeal life support (ECLS), large volumes are often administered. Currently, there is ongoing work in our department (Peeters, 2019; Nievergeld, 2019) on the development of a physiologically correct patient model for ECLS evaluation and training, with a physical system for hands-on training, complemented by mathematical models (Figure 6.1). Our model (Rosalina et al., 2019) has been included to calculate volume shifts in these patients. The addition of such a model provides real-time and physiologically correct feedback as a response to clinical interventions.

6.4.3 Clinical-decision support tool

Ultimately, our model could be used as a clinical decision-support tool. In Chapter 1 a few successful examples are discussed, but there are still quite some steps to be made before the current work is at that stage.

A first step could be to use a disease-specific model (e.g., characterised by renal insufficiency or heart failure), for risk analysis and for testing of treatment protocols. When a critical patient with many comorbidities is admitted for surgery with large expected fluid administration, the model could be used to evaluate intraoperative scenarios for this class of patients beforehand. Preoperative patient data could be used to initialize the model, and simulations could be performed with the *generic model* settings for a specific disease. E.g., a lower normal urine output ($J_{U,N}$) parameter can be used in patients with renal complications.



Figure 6.1: Picture of the extracorporeal life support system, developed by Rutten et al. (Peeters, 2019; Nievergeld, 2019).

The results give an indication of trends that can be expected in a generic patient with a specific disease. These model outputs can give extra information that may be used to determine the treatment protocol. E.g., for patients with renal insufficiency, extra vasopressor administration may be preferred over large quantities of fluid administration. For patients with cardiac comorbidities, the opposite may be true. These analyses can be performed with a disease-specific model and used as extra input into the *mental model* of the responsible anesthesiologist.

In the future, complete patient-specific models may be used for real-time prediction of the fluid distribution and responsiveness. In that case, the goal is to make a *generic model* patient specific through patient-specific parameter settings. Patient-specific parameter estimation is quite complex because important model parameters, such as membrane permeability, cannot be measured. A possibility is to combine the current model with measured clinical data, data assimilation techniques and artificial intelligence (AI) software. Data science techniques, such as data assimilation and AI, are popular tools that can extract additional information or find common patterns from big datasets. Combining these techniques with our model, can lead to better patient-specific predictions.

By constantly feeding the model with intraoperatively measured data, predictions can be continuously updated. In Figure 6.2 a possible work flow is presented. In blue and grey, the normal workflow is show, and in red the additions to the work flow based on the use of our model are shown. In this workflow, first, a model of the patient baseline status is created, based on preoperative patient measurements. This model can be used to aid in surgical and anesthesia planning. In such a model, various surgical scenario's can be tested and the outcome

can be used as input for patient treatment. During surgery, real-time data processing can be used to compare model output to perioperative measurements, and adapt the model parameters to improve future predictions. After surgery, the model can be adapted to represent the postoperative patient, combining the model with data and risk predictors such as early warning scores. Possibly, this combination can be used to detect patient deterioration earlier and assist in treatment for perioperative complications. Finally, the goal is to have less fluid administration-related complications, and quicker patient recovery.

6.5 Conclusion

In conclusion, we took the first steps towards a mathematical model predicting fluid responsiveness and redistribution in critically ill patients. Next, this model must be further tested and possibly extended for patient-specific application. In the future, the model may contribute to guiding fluid administration and thereby reducing hypervolemia-related complications.

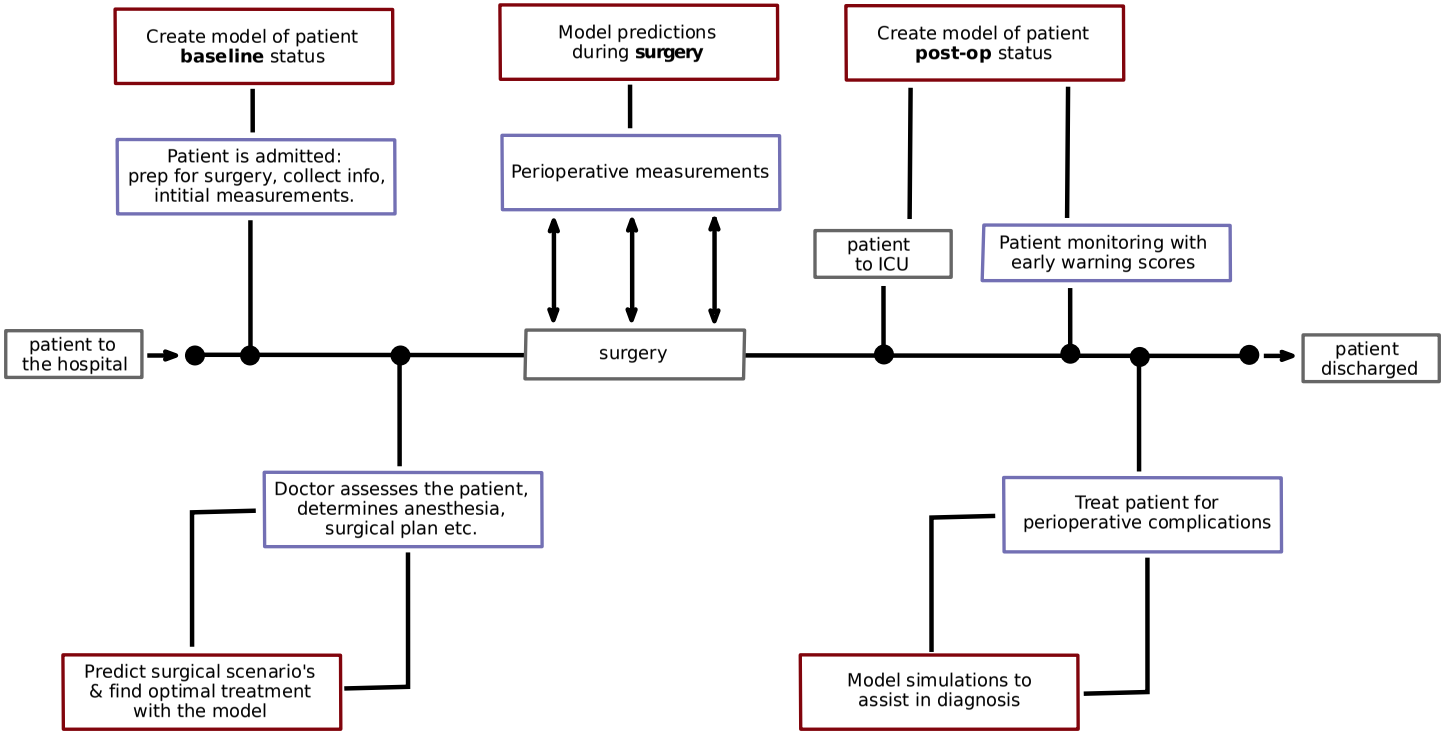


Figure 6.2: Schematic overview of possible model implementations in the clinical workflow.

Bibliography

Alinier, G. (2007). "A typology of educationally focused medical simulation tools". *Medical Teacher* 29.8, pp. 243–250.

Averina, V. a. et al. (2012). "A new conceptual paradigm for the haemodynamics of salt-sensitive hypertension: a mathematical modelling approach." *The Journal of Physiology* 590, pp. 5975–92.

Belloni, L. et al. (2008). "Assessment of fluid-responsiveness parameters for off-pump coronary artery bypass surgery: a comparison among LiDCO, transesophageal echochardiography, and pulmonary artery catheter". *Journal of Cardiothoracic and Vascular Anesthesia* 22.2, pp. 243–248.

Cecconi, M. et al. (2015). "Fluid challenges in intensive care: the FENICE study". *Intensive Care Medicine* 41.9, pp. 1529–1537.

De Schipper, P. J. (2018). "Sensitivity Analysis of a Microvascular Exchange Model". MA thesis. Eindhoven University of Technology.

Drobin, D. and Hahn, R. (1999). "Volume Kinetics of Ringer's Solution in Hypovolemic Volunteers". *Anesthesiology* 90, pp. 81–91.

Guyton, a. C., Coleman, T. G., and Granger, H. J. (1972). "Circulation: overall regulation." *Annual Review of Physiology* 34, pp. 13–46.

Gyenge, C. C. et al. (2003). "Preliminary model of fluid and solute distribution and transport during hemorrhage". *Annals of Biomedical Engineering* 31.7, pp. 823–839.

Holte, K., Sharrock, N., and Kehlet, H. (2002). "Pathophysiology and clinical implications of perioperative fluid excess". *British Journal of Anaesthesia* 89.4, pp. 622–32.

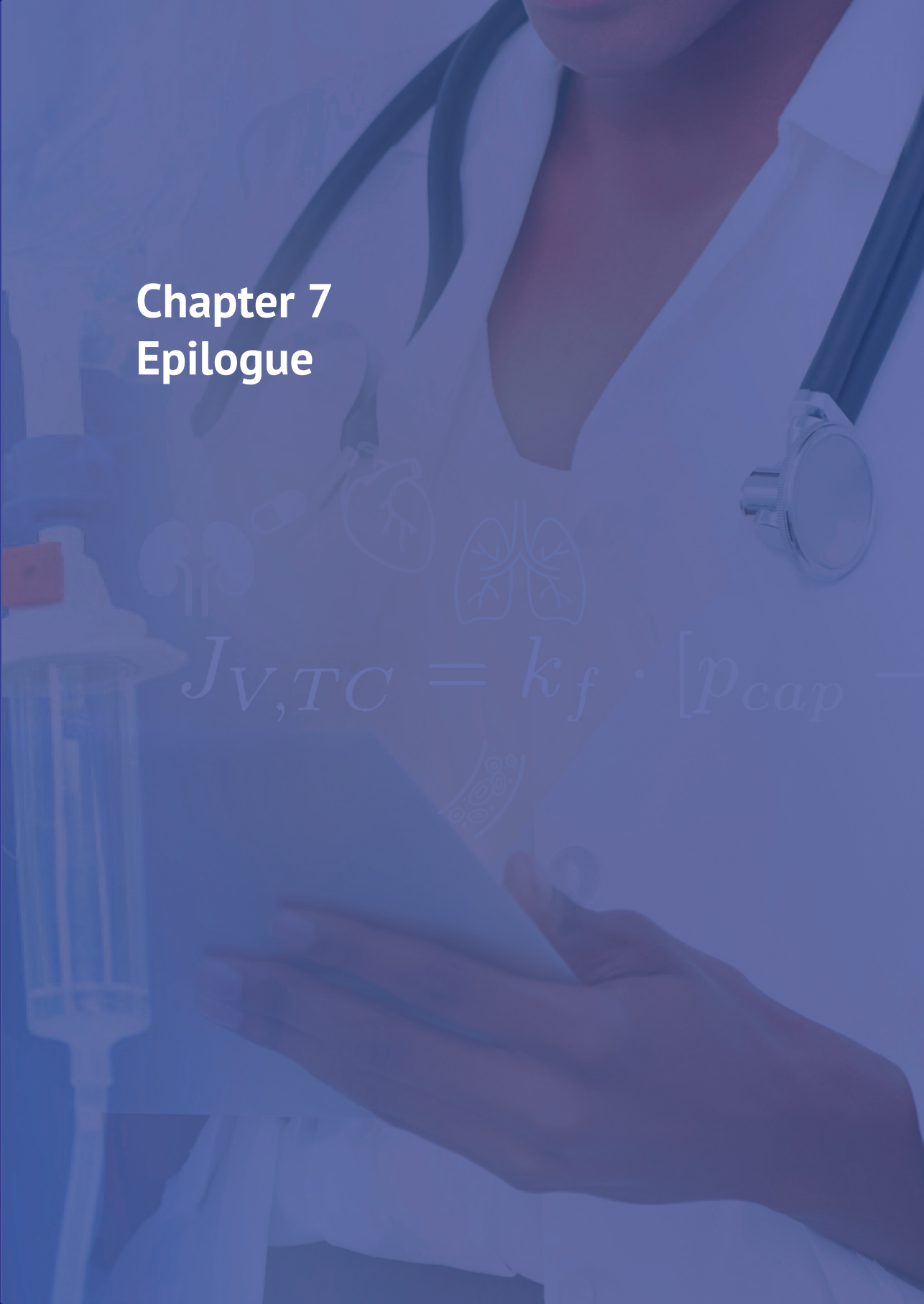
Huberts, W et al. (2014). "Applicability of the polynomial chaos expansion method for personalization of a cardiovascular pulse wave propagation model". *International Journal for Numerical Methods in Biomedical Engineering* 30.12, pp. 1679–1704.

Ikeda, N., Marumo, F., and Shirataka, M. (1979). "A model of overall regulation of body fluids". 7, pp. 135–166.

Innes, J. A. et al. (1993). "Within breath modulation of LV function during normal breathing and PPV in man". *Journal of Physiology* 460, pp. 487–502.

Jongen, G. J. et al. (2016). "A mathematical model to simulate the cardiotocogram during labor. Part A: Model setup and simulation of late decelerations". *Journal of Biomechanics* 49.12, pp. 2466–2473.
Keener, J. P. and Sneyd, J. (1998). *Mathematical physiology*. Vol. 1. Springer.
Latta, T. (1832). "Malignant cholera". *Lancet* ii, pp. 45–274–7.
Lumens, J. (2014). "Creating your own virtual patient with CircAdapt Simulator". *European Heart Journal* 35.6, pp. 335–337.
Meurs, W. W. van and Antonius, T. A. (2018). "Explanatory models in neonatal intensive care: a tutorial". *Advances in Simulation* 3.1, p. 27.
Morgan, P. J. and Cleave-Hogg, D. (2002). "A worldwide survey of the use of simulation in anesthesia". *Canadian Journal of Anaesthesia* 49.7, pp. 659–662.
Nievergeld, A. (2019). "Modeling a patient on extracorporeal life support". MA thesis. Eindhoven University of Technology.
Peeters, K. (2019). "Blood volume regulation during extracorporeal life support (ECLS) and while using an intra-aortic balloon pump (IABP) measured in a mock circulation loop (MCL)." MA thesis. Eindhoven University of Technology.
Rosalina, T. T. et al. (2019). "A mathematical model to investigate the effects of intravenous fluid administration and fluid loss". *Journal of Biomechanics* 88, pp. 4–11.
Saltelli, A. et al. (2004). *Sensitivity analysis in practice: a guide to assessing scientific models*. Wiley Online Library.
Schrier, R. W. (2010). "Fluid administration in critically ill patients with acute kidney injury". *Clinical Journal of the American Society of Nephrology* 5.4, pp. 733–739.
Vincent, J.-L. and Weil, M. H. (2006). "Fluid challenge revisited". *Critical care medicine* 34.5, pp. 1333–1337.
Watenpaugh, D. E. et al. (1992). "Role of atrial natriuretic peptide in systemic responses to acute isotonic volume expansion". *Journal of Applied Physiology* 73.4, pp. 1218–1226.
Xie, S. et al. (1995). "A model of human microvascular exchange". *Microvascular Research* 49, pp. 141–162.

Chapter 7
Epilogue



Multidisciplinary Collaborations

In this changing world, where research and industry move at the speed of light, collaboration is key to a successful project with the goal of clinical application. In the past, many projects or products have been developed within the confounds of one partner, e.g., in a university, whereafter they failed in daily use in industry or a hospital. Early collaboration with different partners is a way to prevent this 'ivory tower' phenomenon. Input of medical experts, industrial partners and scientists from different disciplines from an early research stage is very important for this. The Impuls framework (now e/MTIC) is a unique framework in the medical technology field in Eindhoven, which enables this partnership.

Finding the balance

The work presented in this thesis was performed within Impuls II, as a collaboration between Eindhoven University of Technology, Catharina Hospital Eindhoven and Philips research. This collaboration gave me easy access to the knowledge of medical professionals, and the opportunity to experience surgeries and the intensive care unit. Also, this provided me with insight into the world of technology and business at Philips Research. Without my supervisors from all three parties, this work would not have been possible.

The strength from these different partners, with their experiences and skills, can also be a pitfall. The achievements and succes of each partner is usually measured in different terms. Academics are judged by research output, quantified in journal papers and conference contributions. Industrial partners have to balance the return of investment and company-wide key performance indicators. Our clinicians have to balance their primary job of caring for patients and often personal goals for advancing the medical practice, leading to better patient care. Of course, at the end 'better patient care' is the main goal for most people involved.

The variation in short term goals, strategies and measure of succes influence the person at the center of the project. Often this role is embodied by PhD-candidates or postdocs, who have to balance the expectations from each project partner. Managing the pull to different directions is a valuable lesson and character building. In my experience, a great sense of accomplishment can be obtained when one manages to get 'everyone aligned'. I believe that the experiences and knowledge gained by previous students should be transferred to the next generation, since reinventing the wheel every time is not the most efficient way to get to the final goals of the project.

Challenges and solutions

There are some lessons to be learned from experiencing and seeing the same problems arise in projects around me. First of all, open and clear communication is one of the most important factors in life, and also in science. To me this means that when presenting one project, you may need to make three presentations. One presentation aimed at fellow technical scientists, one aimed at an industrial audience and one aimed at clinical professionals. Simple conversions of units as well as the inclusion or exclusion of details can make a big difference.

Second, in my opinion naturally formed teams, in a bottom up approach, have the highest chance to succeed. However, most important is that all partners are involved and interested in the final goal of the project. This is essential because everyone that has worked in research knows that solving a problem usually opens up multiple new doors to new questions and challenges. The investment of each person is necessary to tackle these challenges. In the case that teams are formed from a top down approach there may be an extra step needed for good results. E.g., direct communication and clear objectives must be formulated quickly and with input from all partners. A good team, with clear expectations gives rise to many more challenges to be tackled and more knowledge to be gained.

Third, it takes a village to raise a child. For 4.5 years I worked on, every word, every line of code and every figure of this thesis. This would not have been possible without the knowledge, experience and creativity of my supervisory team. Our monthly meetings have been a great source of inspiration and ensured the continuous progress of this work. Besides this team, there is another team of fellow PhD candidates who have been there for inspiration, perseverance and sharing of knowledge and sense of similarity. Daily, I had the pleasure of working alongside my colleagues at the Biomedical Engineering department. This environment was a great inspiration and brought much joy to my daily work schedule. Learning about the projects from different research fields and experiences has been valuable. Integrating PhD candidates from different projects into one office, enables easy sharing of knowledge. Also, collaborations such as MaTe are very important and should be cherished in my opinion.

Additionally, I occasionally worked together with my fellow Impuls II colleagues. The Impuls II perioperative team has seen some changes over the year. There have been formal meetings, group meetings and eventually mostly social informal meetings over the years. Each of these interactions have brought inspiration and help to each other. Making sure that these bonds are formed, tips are shared and complaints can be heard is as important as the scientific side.

Conclusion

Besides the technical and clinical part of this thesis, the organisation and multidisciplinary part has been described in this epilogue. Some of the most valuable lessons that I will carry throughout life have been learned here. The ultimate goal of every researcher is to make a contribution to the world, either by improving clinical health care, developing better transportation, or reducing global warming. The collaboration of universities with other partners is one that enables more and quicker implementation, necessary in specific projects. Let us continue to build a stronger framework with a place for every partner, working together towards one goal.

Dankwoord

Aan elk verhaal komt een einde. In dit laatste onderdeel van mijn proefschrift kijk ik met veel dankbaarheid terug op mijn promotie onderzoek. Naast de wetenschappelijke kennis en kwaliteiten die ik heb opgedaan, ben ik dankbaar voor deze unieke en bijzondere ervaring. De mensen die ik in deze jaren heb ontmoet en die hebben bijgedragen aan deze mooie tijd zullen altijd bij mij blijven.

Ten eerste, wil ik mijn promotor **prof. dr. ir. Frans van de Vosse**, en mijn copromotoren **dr. ir. Peter Bovendeerd** en **dr. Arthur Bouwman** bedanken. Jullie begeleiding heeft ervoor gezorgd dat ik met veel plezier aan dit proefschrift heb gewerkt. **Frans**, bedankt voor jouw wijde blik en altijd relevante en kritische perspectieven. Jouw kennis over het cardiovasculaire systeem en modelvorming heeft me een sterke technische basis gegeven en altijd veel inspiratie. **Peter**, bedankt voor de intensieve samenwerking afgelopen 4 jaar. Samen hebben wij het onderwerp 'Fluid administration and redistribution' mogen ontdekken en ons eigen maken. Bedankt voor de inspirerende wekelijkse overleggen, diepgaande discussies, uitgebreide (!) feedback en gezellige reisjes. Ik heb altijd op jouw eerlijke mening, steun en vertrouwen kunnen rekenen. **Arthur**, jij bent vanaf het begin betrokken geweest bij mijn onderzoek. Bedankt voor je klinische kritische blik en de toewijding aan dit onderzoek. Jouw kennis als anesthesist heeft mij nuttige sturing en praktische inzichten gegeven.

I would like to thank the members of my defence committee, **prof. Christa Boer, dr. Irene Vignon-Clémentel, prof. dr. ir. Jan Bergmans, prof. dr. ir. Natal van Riel, prof. dr. Marc van Sambeek** and **dr. Jan Willem Sels**, for their interest in my work and for reviewing the dissertation.

Marc, ook jij bent afgelopen jaren nauw betrokken geweest bij dit onderzoek. Bedankt voor de interessante discussies en jouw perspectief als vaatchirurg. **Jan Willem**, bedankt voor de samenwerking in het afgelopen jaar. Jouw enthousiasme en kennis vanuit de IC heeft een extra dimensie aan dit werk gegeven.

De kracht van dit onderzoek ligt in de velen perspectieven, vanuit de anesthesie, chirurgie en intensive care. Mijn dank gaat uit naar alle clinici in het **Catharina Ziekenhuis Eindhoven** en **Maastricht UMC+**, bij wie ik heb mogen meekijken en mijn honderden vragen heb kunnen stellen.

Kevin, your technical and practical vision as my supervisor from Philips, has been very useful. I enjoyed working with you and I am happy that you joined the team. **Wouter**, bedankt voor je begeleiding en inspiratie in het begin van mijn promotieonderzoek. **Marcel**, bedankt voor de samenwerking in de afgelopen jaren. Ik hoop dat mijn werk een mooie toevoeging zal zijn op de toekomstige ECLS patiënten zorg.

Een van de mooiste dingen in deze tijd was het begeleiden van bachelor en masterstudenten en stagiaires. **Peter** en **Femke**, het was een plezier om jullie als afstudeerders op dit project te hebben. Jullie bijdrage is zeer waardevol geweest voor het uiteindelijke resultaat. **Amy, Arjet, Daniëlle, Hans, Hilke, Lisa, Ken, Maria, Marissa, Michelle, Minette en Tessa**, bedankt voor jullie inzet en bijdrage aan dit werk tijdens jullie projecten. Ik kijk met veel plezier terug op onze samenwerkingen.

Dear colleagues, you have truly made the past years unforgettable. **Ashley, Dennis, Evelien, Ineke, Laura** and **Rick** together we were the perioperative Impuls II team. I enjoyed our discussions, learning about your PhD topics and all the beers we shared. Thanks for the support! I also want to thank everyone in the **CVB group**. I enjoyed the variety in people and research topics. I have learned something from each of you and look back with much joy on our meetings, conferences, borrels and group outings.

Of course, a big thanks goes to my dear officemates of gem-z 4.09; **Aysegul, Andrés, Bregje, Cas, Cansu, Celien, Cristina, Dewy, Emily, Germaine, Gitta, Jan Willem, Johanna, Joke, Jun, Larissa, Lorenza, Min, Priyam, Tamar, Tommaso, Valentina**. Over the years there have been many people coming and going. I want to thank you all for the most amazing work environment one can wish for. Through all our adventures, dinners, lunches, coffee breaks, parties and trips together I have gotten to know each of you so well. These memories will stay with me forever, I hope to keep seeing many of you. **Ashley**, dankjewel voor alle culturele en culinaire ontdekkingen, op nog veel meer avonturen en interessante gesprekken! **Awital**, bedankt voor de introductie aan de vegan culinaire wereld. Ik geniet van onze gedeelde passie voor koken. Dankjewel, **Gitta**, onze gezellige en interessante discussies over van alles hoop ik nog lang voort te mogen zetten. **Inge**, dankjewel voor de mooie tijd met onze gedeelde liefde voor dansen en zorgzaamheid.

Martijn, afgelopen jaren hebben wij veel met elkaar opgetrokken. Voor al mijn Latex en Matlab problemen kon ik bij jou terecht. Ook over conceptuele problemen, wijn en eten kunnen we altijd goed kletsen. Laten we dat nog heel vaak blijven voorzetten! Bedankt dat jij vandaag achter me staat als paranimf!

Dit werk is mede tot stand gekomen door mijn sociale draagvlak buiten de werkvloer. Iedereen die aan mij heeft gedacht, me verwend met chocolade, wijn en gezelligheid, dankjulliewel! **Britt**, onze weg door de academische wereld loopt zo dicht langs elkaar. Dankjewel voor de gezelligheid, steun en interesse. **Dan Jing**, dankjewel voor de vriendschap, interesse en inspiratie. Samen met **Jeroen**, wij zijn voor altijd verbonden door ons Londen avontuur. Het is altijd thuiskomen bij jullie! **Esther**, thank you for the support and sharing our love for latin cultures and food. **Moniek**, bedankt voor onze vriendschap van al bijna 10 jaar. Onze dates met gezelligheid en bijklets sessies zijn me dierbaar.

Queeninzah, danki pa bo amistad i alegría. Danki pa e support den gym i p'afo e añanan aki. **Nerissa**, maske bo ta leu, bo apoyo semper ta lagami sa ku bo ta serka. **Rozheyra**, bo ta selebrá kada echo huntu ku mi (i mas mes!). Danki pa bo apoyo i orguyo. **Stephanie**, bo tambe ta serka di yega e resultado aki! Bo positividat den bida ta inspira'mi. **Shanty**, riba mesun dia nos a kuminsá nos adventure di PhD. Danki pa kompartí tur ups and downs, huntu nos a lucha! **Tiarah**, danki pa semper bo interés i sostén. Amiga's, sa ku semper mi t'ei pa boso.

Familie Rosalina en **van de Kuilen**, bedankt dat ik altijd bij jullie terecht kan. Er kan niets op tegen de gezelligheid van familie dichtbij en ver van huis! Lieve **schoonfamilie**, de afgelopen jaren ben ik met open armen ontvangen. Bedankt voor jullie interesse in mijn werk en de steun tijdens de laatste loodjes.

Lieve **Oma**, dank je voor alle steun en liefde over de jaren heen. Er is niks vergelijkbaars met de trots van een oma. **Hila**, mi sa ku bo tambe ta orguyoso.

Lieve **Zulia**, mijn zusje, jij bent vandaag mijn paranimf, maar in werkelijkheid sta jij altijd achter me. Bedankt voor je onvoorwaardelijke steun, inspiratie en motivatie. Het is fantastisch om dit avontuur af te sluiten met een fantastische vrouw als jou aan mijn zijde. Masha masha danki!

Papa en mama, ik kan jullie nooit genoeg bedanken. Jullie hebben mij alle kansen en basis gegeven om hier vandaag te mogen staan. Mi amor pa boso ta mas grandi ku bida. Danki danki danki. **Papa**, bo a mira mi kuriosidat pa mundu for di chikitu. Danki pa kompartí bo interes pa tèknik i pùzel ku mi. Danki pa e inspirashon, bo ta un forsa di amor. **Mama**, jouw creativiteit en oplossingsgerichtheid heeft me vaak tot nieuwe inzichten gebracht. Dankjewel voor het doorgeven van jouw ontwerp kwaliteiten en voor deze mooie voorkant van mijn proefschrift. Ik voel jouw steun en liefde elke dag.

Lieve **Paul**, de afgelopen jaren was jij mijn anker. Jouw tips, positiviteit, rust en aanmoediging heeft me veel geholpen bij de laatste loodjes. Dankjewel voor je geduld, liefde, gezelligheid in de drukke maanden en je onvoorwaardelijke steun. Ik kijk uit naar alle volgende avonturen in ons mooie leven samen!

veel liefs, **Tilaï**
Eindhoven, Februari 2020

Curriculum Vitae

Tilaï T. Rosalina was born on the 14th of July 1992 in Utrecht, the Netherlands. In 1996 she moved to Curaçao with her family. She attended secondary education (VWO) at Maria Immaculata Lyceum in Curaçao, where she obtained her diploma in 2010. In the same year she started studying Biomedical Engineering at the Eindhoven University of Technology. During this time she spent 3 months at the Queen Mary University of London, following courses. After her Bachelor project on the rheology of blood clotting, for which she won the VSNU student poster award, she obtained her Bachelor degree in 2013. During her Master studies, she collaborated with AMOLF, and spent four months at the University of Pittsburgh at the department of Mathematical Engineering, where she performed a numerical study on the influence of oxygen diffusion in abdominal aorta aneurisms. For her graduation project within the group of Cardiovascular Biomechanics, she performed experiments and developed a clinical decision support model for intracoronary cooling in acute myocardial infarction, in collaboration with Catharina Hospital Eindhoven and LifeTec. In July 2015 she obtained her Master degree.

In September 2015, she started as a PhD candidate at the Eindhoven University of Technology, within the IMPULS II framework, collaborating with the Catharina Hospital Eindhoven and Philips Research. The focus of her research was on clinical decision support for intravenous fluid administration in perioperative patients. The main results of her PhD research are described in this thesis.

List of Publications

Tilaï T. Rosalina has the following publications:

Journals

Tilaï T. Rosalina, R. Arthur Bouwman, Marc R.H.M. van Sambeek, Kevin D. Lau, Frans N. van de Vosse, Peter H.M. Bovendeerd (2019), A mathematical cardiorespiratory model to simulate dynamic indices of fluid responsiveness in spontaneous mechanical ventilation, *submitted to Medical Engineering and Physics*.

Tilaï T. Rosalina, R. Arthur Bouwman, Marc R.H.M. van Sambeek, Frans N. van de Vosse, Peter H.M. Bovendeerd (2019), A mathematical model to investigate the effects of intravenous fluid administration and fluid loss, *Journal of Biomechanics*, 88, pp. 4-11.

Bettine G. van Willigen, Luuk C. Otterspoor, Marcel van 't Veer, *Tilaï T. Rosalina*, Nico H.J. Pijls, Frans N. van de Vosse (2019), A predictive computational model to estimate myocardial temperature during intracoronary hypothermia in acute myocardial infarction, *Medical Engineering and Physics*, 68, pp. 65-75.

Luuk C. Otterspoor, Lokien van Nunen, *Tilaï T. Rosalina*, Marcel van 't Veer, Sjoerd Van Tuijl, Marco Stijnen, Marcel CM Rutten, Nico H.J. Pijls (2017), Intracoronary hypothermia for acute myocardial infarction in the isolated beating pig heart, *American Journal of Translational Research*, 9 (2), pp. 558-568.

Nicholas A. Kurniawan, Thomas H. van Kempen, S. Sonneveld, *Tilaï T. Rosalina*, Bart E. Vos, K.A. Jansen, Gerrit W.Peters, Frans N. van de Vosse, Gijsje H. Koenderink (2017). Buffers strongly modulate fibrin self-assembly into fibrous networks. *Langmuir*, 33(25), pp. 6342-6352.

Congres Contributions

Tilaï T. Rosalina, Jan-Willem Sels, Arthur Bouwman, Frans N. van de Vosse, Peter H. Bovendeerd. Clinical decision support model to guide fluid administration in intensive care patients, *Computer Methods in Biomechanics and Biomedical Engineering*, August 2019, New York City, United States of America. Oral presentation.

Tilaï T. Rosalina, Arthur Bouwman, Kevin Lau, Marc van Sambeek, Frans van de Vosse, Peter Bovendeerd. A mathematical model to investigate the physiological background of pulse pressure variation. *Congress of the European Society of Biomechanics*, July 2019, Vienna, Austria. Oral presentation.

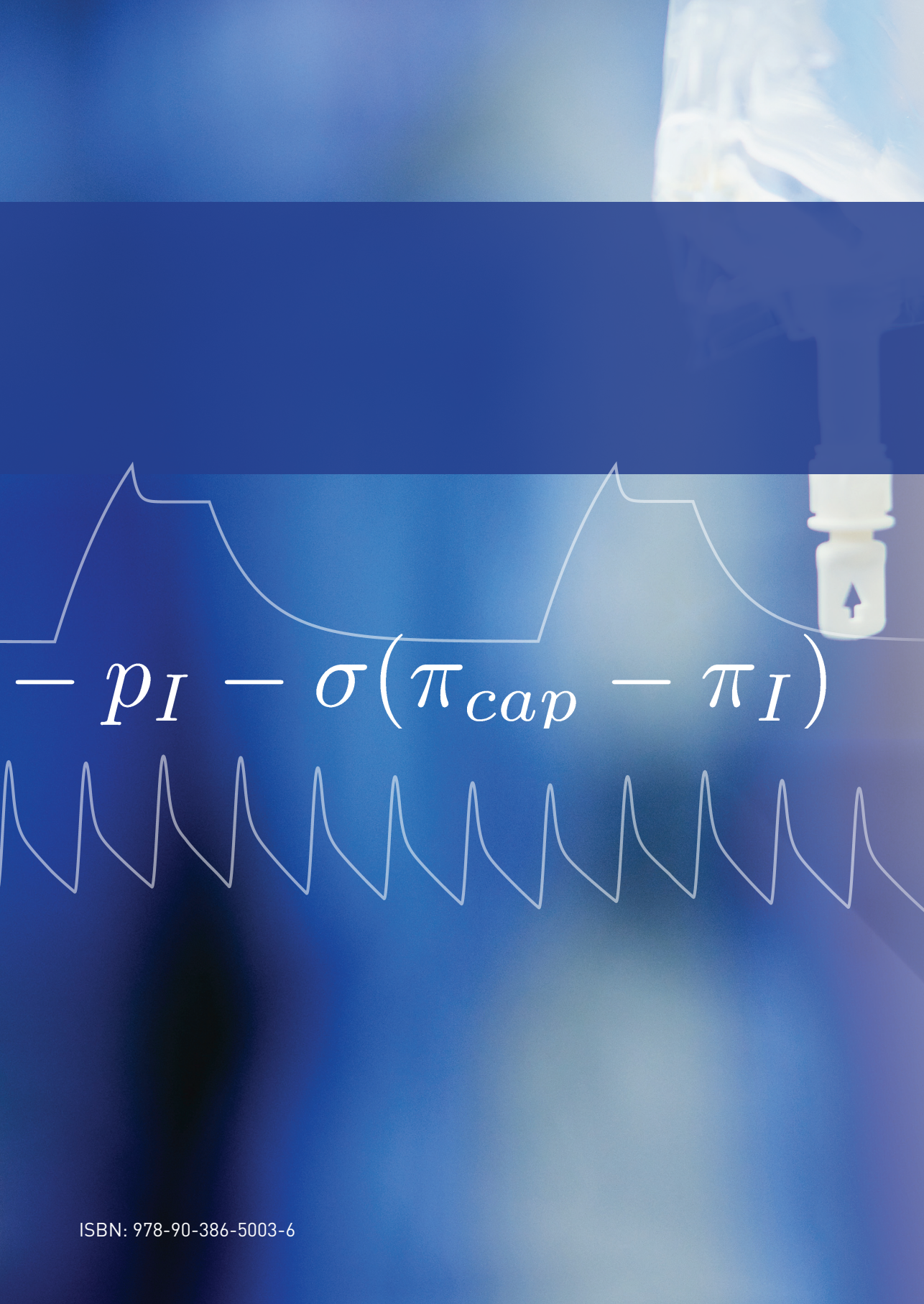
Tilaï T. Rosalina, R. Arthur Bouwman, Peter H.M. Bovendeerd. Mathematical model of the fluid status after intravenous fluid infusion: performing a structured sensitivity analysis. *Virtual Physiological Human Conference*, September 2018, Zaragoza, Spain. Oral presentation.

Tilaï T. Rosalina, R. Arthur Bouwman, Peter H.M. Bovendeerd. Mathematical model of the fluid status after intravenous fluid infusion. *World Conference of Biomechanics*, July 2018, Dublin, Ireland. Oral presentation.

Tilaï T. Rosalina, Wouter Peeters, R. Arthur Bouwman, H. Erik Korsten, Rick Bezemer, Marc R. van Sambeek, Frans N. van de Vosse, Peter H.M. Bovendeerd (2017) Perioperative volume status modelling to simulate controlled hypovolemia due to blood donation. *Applied Models in Acute Care*, October 2017, Twente, the Netherlands. Oral presentation.

Tilaï T. Rosalina, Peter H.M. Bovendeerd. Mathematical model of the fluid status after intravenous fluid infusion. *International Fluid Academy Days*, November 2017, Antwerp, Belgium. Poster presentation.

Tilaï T. Rosalina, Wouter Peeters, R. Arthur Bouwman, H. Erik Korsten, Rick Bezemer, Marc R. van Sambeek, Frans N. van de Vosse, Peter H.M. Bovendeerd. Perioperative volume status modelling to prevent hypo- and hypervolemia in major abdominal surgery, *Dutch Conference for Biomedical Engineering*, January 2017, Egmond aan Zee, the Netherlands, Poster presentation.



ISBN: 978-90-386-5003-6